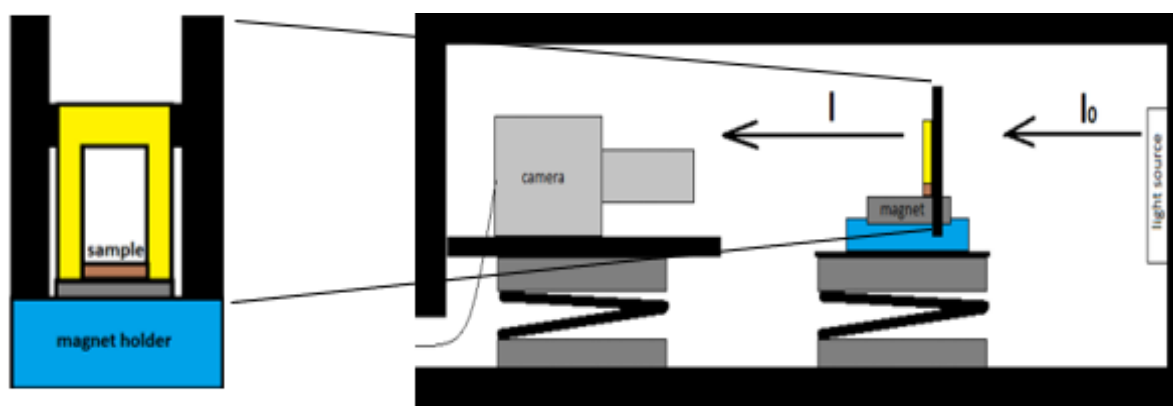# Master's thesis

Development and characterization of NIR transparent ferrofluids

Utrecht University
Physical & Colloid Chemistry

Author:
Kevin van Veen (s7449739)

Supervisors:
Dr. Alex van Silfhout
Dr. Ben Erné

Date of submission: 20-3-2023

Abbreviation list

Abbreviation	Full name
NIR	Near-infrared
YIG	Yttrium iron garnet
YAG	Yttrium aluminum garnet
VSM	Vibrating sample magnetometer
TEM	Transmission electron spectroscopy
XRD	X-ray diffraction
MSV	Magnetic sedimentation velocimetry
Son.	Ultrasonication
Cen.	Centrifugation
Abs.	Absorbance

Abstract

The aim of this master thesis project was to synthesize a yttrium iron garnet (YIG) ferrofluid with a lower absorbance coefficient in the range of (600 to 1100 nm) with comparable magnetic properties compared to conventional ferrofluids. A ferrofluid with a lower absorbance coefficient is interesting as it allows for the better study of the magneto-optical properties such as field dependent polarization of transmitted light. The ferrofluid was synthesized in 1,4 butadiol via a seeded growth method in which yttrium aluminum nanoparticles (YAG) were first synthesized before being added to the synthesis of the YIG shells. This is done in order to overcome the high nucleation barrier of yttrium iron garnet. The synthesized ferrofluid was characterized with transmission electron microscopy (TEM) in order to determine the size range of the particles, vibrating-sample magnetometer (VSM) to determine the dipole moments and to calculate the order of magnitude of the size of the particles. Furthermore X-ray diffraction analysis (XRD) was used to confirm if yttrium iron garnets was formed. Magnetic sedimentation velocimetry (MSV) was also used in order to determine the magnetophoretic velocity of sedimenting nanoparticles from which the size of nanoparticle aggregates could be calculated. Lastly UV-Vis was used in order to determine the order of magnitude of the absorbance of the synthesized ferrofluid adjusted for volume fraction which was then compared to the absorbance of a conventional ferrofluid. The XRD results confirm that the synthesized particles consist of yttrium iron garnet particles. The VSM also showed that the particles exhibited super-paramagnetism, however from the MSV measurements it became clear that the synthesized particles when exposed to an external field tents to aggregate into large clusters. Furthermore the VSM measurements showed a lower magnetization for the YIG ferrofluid when compared to conventional ferrofluids, Also the synthesized nanoparticles in the YIG ferrofluid had a lower volume fraction than the nanoparticles in the conventional fluid. When the volume fraction was normalized against the optical absorbence with UV-VIS it became apparent that the synthesized YIG ferrofluid did not exhibit a lower optical absorbance when compared to conventional ferrofluids, this is possible due to light scattering caused by large aggregation making it not yet viable as an alternative to conventional ferrofluids. Further research into surface functionalization could however substantially lower the aggregate sizes meaning that the YIG ferrofluid particles could be made to be more stable.

Contents

1. Introduction

Ferrofluids consist of colloidal dispersions of magnetic nanoparticles in a carrier liquid. These colloidal particles are single-domain magnetic particles of a few nanometers in diameter coated by a molecular layer of dispersant. In a stable ferrofluid, the magnetic particles are dispersed uniformly through the ferrofluid. The particles stay dispersed due to Brownian motion and the coating prevents aggregation (R. E. Rosensweig 1987). The behavior of ferrofluids as strongly magnetizable liquids has enabled several applications. This includes the loudspeaker industry in which ferrofluids are used as lubricants that both conduct generated heat away from the voice coil and used to dampen vibrations *(Liquids Research Limited).* It has also found its way into rotary seals as, the liquid can be held in place via magnets and constitutes a hermetic seal with low friction and very low leakage *(N. Simos at el. 2017).* Recently, ferrofluids have been applied in the recycling of waste materials through magnetic density separation, in which waste plastics which are nonmagnetic are put through a water-based ferrofluid subjected to a magnetic field. The strength of the field gradient in the process allows for the separation of the plastic granules according to their density (E.J. Bakker et al. (2009). An aspect of conventional ferrofluids (mainly magnetite and magnetite based) is the strong optical absorption, which is due to the optical properties of the material in the ferrofluid which makes them appear to be pitch-black. It would therefore be interesting to synthesize a ferrofluid which has comparable magnetic properties but has a lower optical absorbance. Previous research has shown that for yttrium iron garnet in a wavelength of 600 to 1100 nm, the absorbance coefficient in this wavelength range is lower (see figure 1).
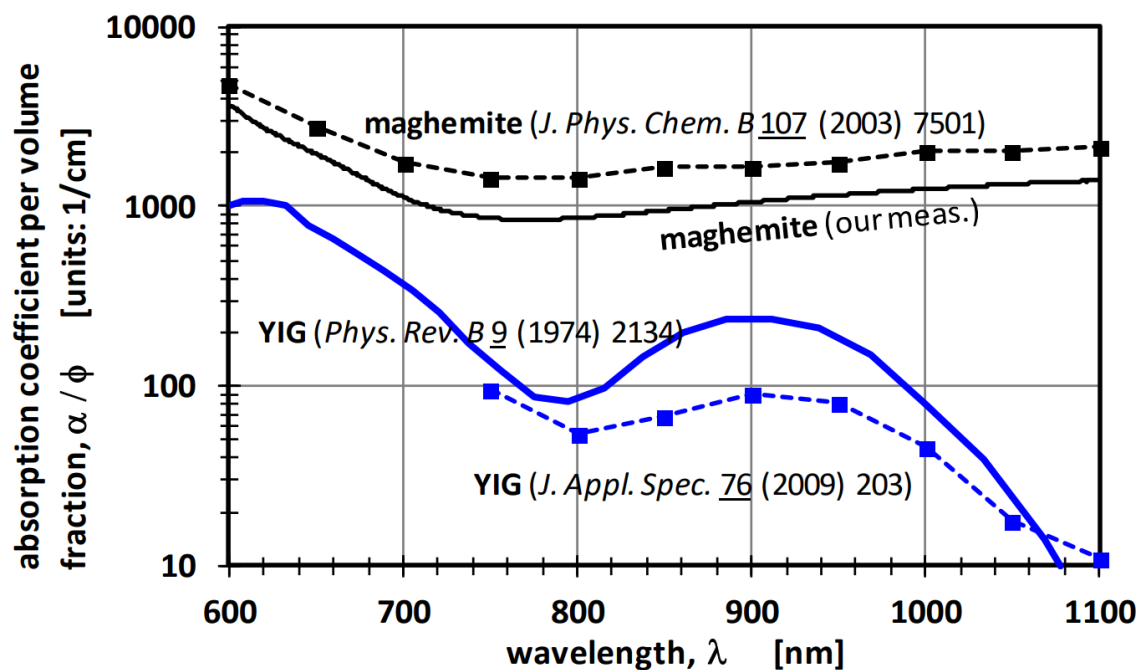

Figure 1: The absorption coefficient per volume fraction of maghemite and yttrium iron garnet in wavelength range from NIR to ultraviolet. (This figure was created by Ben Erné. (Our meas.) refers to measurements that were done by Alex van Silfhout).

1.1 Research objectives

It is the aim of this master thesis to synthesize a ferrofluid based on yttrium iron garnet (YIG) which exhibits a lower optical absorption than magnetic iron oxide while still having a stability and magnetization strength that are comparable to conventional ferrofluids. In the past, it has been found that yttrium iron garnet synthesized via a glycothermal reaction in 1,4-butanediol did not produce single phase YIG, due to the high energy barrier for nucleation. This was solved by adding small yttrium aluminum garnet (YAG) crystallites (*J. Rongjin et al. 2013*). It is this synthesis of YIG via seeded growth onto YAG nanoparticles which will be used in the formation of the ferrofluid. Transmission electron spectroscopy (TEM) will be used in order to determine the size and shape of the particles. X-ray diffraction (XRD) is utilized order to determine if yttrium iron garnets was formed. A vibrating sample magnetometer (VSM) was used in order to determine the magnetization of the ferrofluid and the magnetic and the magnetic dipole moment of particles. The colloidal stability of the ferrofluid will be determined using magnetic sedimentation velocimetry (MSV). In the case of stable ferrofluids, the magnetic particles are dispersed uniformly throughout the ferrofluid whereas in an unstable ferrofluid the magnetic particles aggregates rapidly sediment toward the bottom. This causes the ferrofluid to lose some of its ferrofluidic properties (see figure 2).
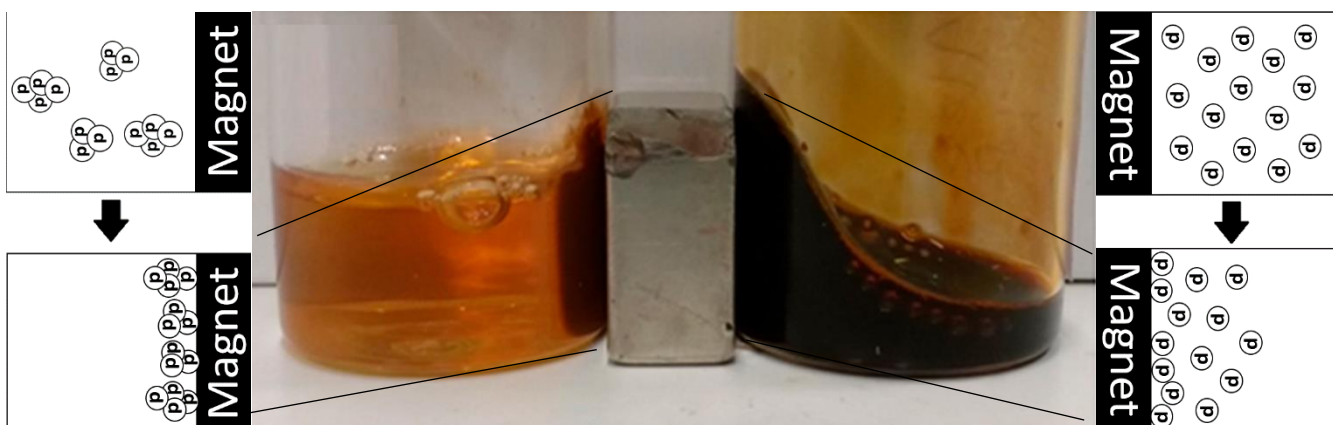
Figure 2: Effects of external magnetic field on both a stable (right) and an unstable ferrofluid (left) (picture taken by Alex van Silfhout).

MSV will be done using a custom setup, in which a capillary with ferrofluid is put onto a magnet illuminated by an uniform light source. As the magnetic particles start sedimenting towards the magnet, the camera captures the resulting difference in coloration. It is a further aim of the thesis turn this coloration difference over time into a time-dependent concentration profile according to the law of Lambert-Beer. This can then be used to determine colloidal stability of the ferrofluid.

2. Theory

The theorical section of this master thesis provides an explanation of the magnetism of ferrofluids and the difference in optical absorbance between maghemite and magnetite based ferrofluid. Magnetism will be explained in section 2.1 and optical absorbance will be explained in section 2.2. It will also provide an explanation on the mechanism behind the growth of yttrium iron garnet particles onto yttrium aluminum garnet seed crystals in section 2.3. Lastly a working principle behind the magnetic sedimentation velocimetry will be given in section 2.4.

2.1 Magnetism of ferrofluids

The magnetism of magnetic nanoparticles has its origin in the motion of the electric charge. Their motion creates (just as with an electric current through a metal wire) a magnetic field. The strength and orientation of this field is known as the magnetic moment (μ) (D. Jiles et al. 2015). On an atomic scale, the dipole moment is dependent on the orbital motion of the electrons around the nucleus and the spin of the electrons.

The total magnetic moment of an atom is dependent on its electronic configuration. An atom with no unpaired electron is set to be diamagnetic which corresponds to having no permanent magnetic dipole. Diamagnetic materials align very weakly in an external field. When atoms have unpaired electrons, their spin will contribute to the magnetic moment of the material. If a material consists of such atoms, their magnetic dipoles will react to an external field. When the atoms react individually, the material is considered paramagnetic. Paramagnetic materials align weakly to a magnetic field, due to the magnetic moment of the individual atoms being small. It is also temperature dependent as a difference in the thermal motion of the atoms will result in a difference in the alignment of the atoms to the magnetic field. *(R. Rosenweig et al. 2014).* Examples of paramagnetic materials include several metals such as gold and platinum. In order for materials to react strongly to the external magnetic field the alignment of the atoms must have coupled mutual dipole interaction with neighboring atoms which can cause them to spontaneously align their magnetic dipole moment. This magnetization is permanent as this mutual dipole moment is stronger than the thermal energy. These materials are called ferro- and ferrimagnetic and consist of magnetic domains where all atoms have aligned magnetic dipoles along a single axis. These domains exist in order to minimize field energy. The main difference between ferro- and ferrimagnetic materials is that in ferrimagnetic materials some atoms align themselves antiparallel in each crystalline unit cell. The antiparallel alignment occurs in a lower ratio to the parallel alignment, so that it still has a permanent magnetic moment albeit lower than for ferromagnetic materials. An example of ferrimagnetism are magnetite crystals (Fe_3O_4) which has paired Fe^{3+} ions and a lone Fe^{2+}. Anti-ferromagnetic materials are materials with ferromagnetic elements but also have other elements that completely cancel out all magnetic moments. This implies that the material has no magnetization at zero external field. But unlike diamagnetic materials, the ferromagnetic elements still cause a strong response when an external field is applied. Examples include MnO. Lastly, in ferromagnetic materials all the atoms in a domain align with their dipole moments. The alignment magnetic moments can only exist below the Curie temperature, above which both ferri- and ferromagnetic materials lose their permanent magnetic moment and become paramagnetic. This is due to a permanent change in direction of the magnetic moment of the material (see figure 3).

Magnetism	Examples	Magnetic behaviour	
Diamagnetism	Bi, Si, Cu, inert gases Susceptibility small and negative (-10^{-6} to -10^{-5})	$H = 0$	Atoms have no magnetic moments.
Paramagnetism	Al, O₂, MnBi Susceptibilty small and positive (10^{-5} to 10^{-3})	$H = 0$	Atoms have randomly oriented magnetic moments.
Ferromagnetism	Fe, Ni, Co, Gd Susceptibility large (generally > 100)	$H = 0$	Atoms are organized in domains which have parallel aligned magnetic moments.
Antiferromagnetism	Cr, MnO, FeO Susceptibilty small and positive (10^{-5} to 10^{-3})	$H = 0$	Atoms are organized in domains which have antiparallel aligned moments.
Ferrimagnetism	Fe_3O_4, $MnFe_2O_4$, $NiFe_2O_4$ Susceptibility large (generally > 100)	$H = 0$	Atoms are organized in domains which have a mixture of unequal antiparallel aligned moments.

Figure 3: Overview of the discussed types of magnetism (copied from R. Nisticò et al. 2020).

Beside is some rare earth metals like gadolinium and certain intermetallic compounds, all ferromagnetic materials contains cobalt, iron or nickel atoms. In the case of ferrofluids, the "ferro" refers to ferromagnetism. This makes sense as the nanoparticles in the fluid consists of ferro or ferrimagnetic particles (R. E. Rosensweig et al. 2014). However they are classified as superparamagnetic. This is due to the individual nanoparticles only possessing one magnetic domain. The individual nanoparticles react similar to dipolar atoms in paramagnetic materials, except more strongly this is due to the dipole moment of the nanoparticles being far larger than the dipolar atom in paramagnetic materials. In case of larger scale ferromagnetic material the larger crystal consist of multiple magnetic domains. These form spontaneously as it decreases the internal energy of the crystal and therefore reduces its external field making it more energetically favorable. These domains can form in different directions, the net magnetic moment of the entire crystal is calculated by the sum of all the magnetic moments of the domains. When a sufficiently strong external magnetic field is applied, the domains all align therefore removing these energy barriers. This is known as the saturation magnetization M_s. However the dis-alignment of these domains is also energetically unfavorable so the formation of these domain walls is only viable above a certain size (R. E. Rosensweig et al. 2014). It is therefore possible to create single domain particles at nanoscale. Their magnetic moment can the be calculated (see formula 1).

$$\mu_{NP} = V_{NP}\, m_s$$

Formula 1: Magnetic moment of the nanoparticles (R. E. Rosensweig et al. 2014).

In which V_{NP} is equal to the magnetic volume of the nanoparticle and m_s is equal to the bulk magnetization which is the dipole moment per unit volume or A/m

A ferrofluid is a colloidal system of single domain ferro- or ferrimagnetic particles with no longer range order which are highly mobile due to thermal motion, implying that without the presence of an external field the nanoparticles will start to randomly orientate themselves losing their magnetization which makes them superparamagnetic. The reason for the prefix ''super'' comes from

the ferrofluid particles having a much higher magnetic susceptibility (χ_m) which is a measure for how easily the spin of the electron can be oriented along a direction of an applied magnetic field H, both are used in order to calculate the magnetization M (see formula 2).

$$M = \chi_m H$$

**Formula 2:** Magnetization of the ferrofluid. (R. E. Rosensweig et al. 2014).

2.2 Optical absorbance of ferrofluids

*Information contained in this section is mainly taken from (K. Kim et al. 2002) and (W. Fontijn et al. 1997)

The conventional ferrofluids appear pitch-black which is due to their high absorbance of all wavelength of the visible light spectrum. This can be explained by applying crystal field theory for all optical transitions of the maghemite and magnetite unit cell. The chemical formula for the maghemite unit cell (Fe_2O_3) and magnetite unit cell magnetite (Fe_3O_4). In the case of maghemite the unit cell consist of two Fe^{3+} and three O^{2+} elements. Magnetite consist of two Fe^{3+} and one Fe^{2+} and four O^{2+} elements. For maghemite both the tetrahedral and octahedral sites are filled with Fe^{3+} ions (see figure 4). For magnetite Fe^{3+} in tetrahedral, octahedral is filled with either Fe^{2+} and Fe^{3+} atoms (see figure 5). Furthermore Fe^{3+} has $3d^5$ electron configuration so in ligand crystal field splitting Fe^{3+} has completely all half-filled orbitals (in high spin) whereas Fe^{2+} one orbital contained an additional spin down.
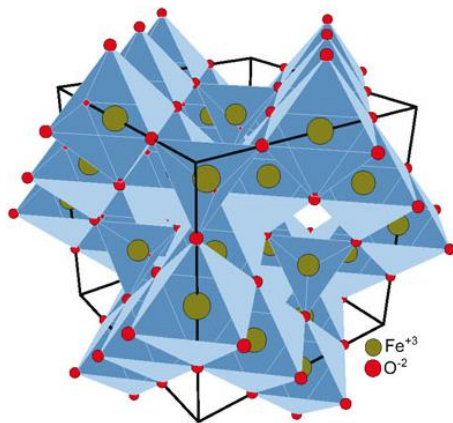

Figure 4: Structure of maghemite with representation for the tetrahedral (connected with yellow spheres) and octahedral sites (connected from red spheres) (Copied from Technical university Braunschweig).
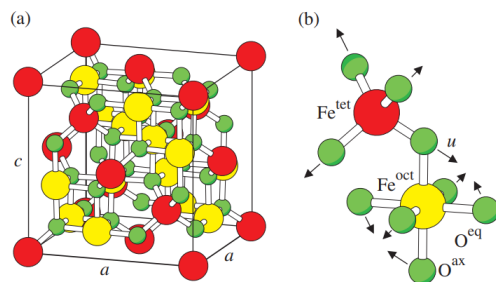
Figure 5: Face centered spinel structure of magnetite. With Fe^{tet} referring to a tetrahedral site and F^{oct} referring to an octahedral site (Copied from M. Friàk et al. 2007).

The electron configuration for Fe^{3+} and Fe^{2+} is [Ar] $3d^5$ and [Ar] $3d^6$ respectively.
Here the 3d orbital electrons will have interaction with the ligand oxygen. These d orbital electrons will split on both the tetrahedral and octahedral sites according to the crystal field splitting into T_2/E orbitals and E_g,T_{2g} respectively. Due to O^{2-} being a weak ligand, the resulting ligand field split on the iron ions is high spin. The Fe^{3+} and Fe^{2+} on the octahedral configuration are coupled via a double exchange mechanism through oxygen implying that the Fe^{3+} ions on both the octahedron and tetrahedron sites are coupled to the oxygen. The same process also holds for the Fe^{3+} ion in magnetite. The optical transition between the Fe ions on both the tetrahedral and octahedral sites will causes differences in the electronic structures (see figure 6).
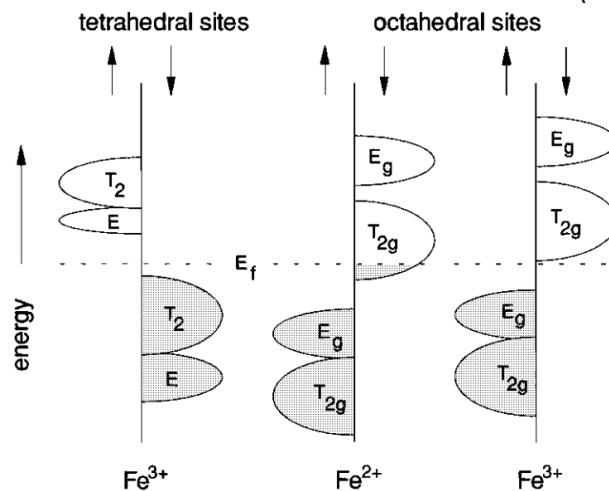

Figure 6: Electronic structure of Fe^{3+} and Fe^{2+} on both tetrahedral and octahedral sites
(copied from W. Fontijn et al. 1997)

All possible optical transition between the Fe ions can be separated into two types. Intervalence charge transfer (IVCT) meaning that an electron is optically excited from lower to higher oxidation number. Inter sublattice charge transfer (ISCT) transitions meaning that a charge is transferred between the octahedral and tetrahedral sites. Almost all of these transitions occur at energy levels which cover the entire visual spectrum.

When it comes to the crystal structure YIG ($Y_3Fe_5O_{12}$) the cell consist of Y^{3+} and O^{2-} and only Fe trivalent ions (M.A. Gilleo et al. 1958). Unlike the previously mentioned maghemite and magnetite YIG consist of a cubic garnet structure which contain besides tetrahedral and octahedra also dodecahedra sites. In YIG the tetrahedral sides are filled with three iron ions, the octahedral sides are filled with two iron ions and the dodecahedra sites are filled with three yttrium ions (see figure 7). This difference in crystal structure creates optical transitions which when synthesized as nanoparticles in YIG result in substantially lower optical absorbance (see figure 1).

Structure of maghemite with representation for the tetrahedral (connected with yellow spheres) and octahedral sites (connected from red spheres) (Copied from Technical university Braunschweig).
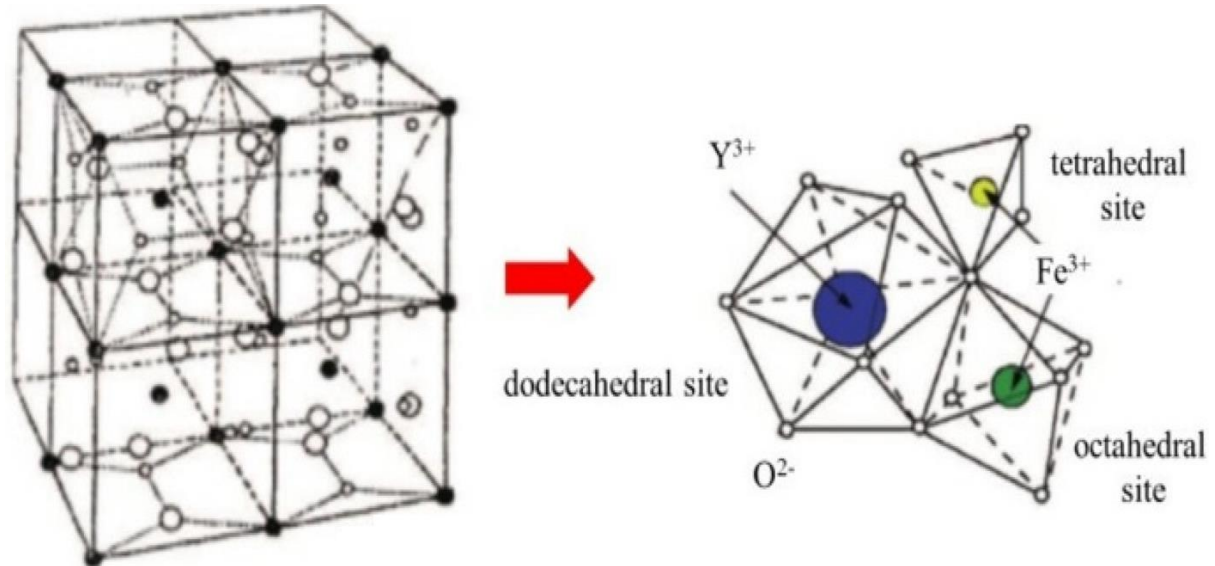
Figure 7: Unit cell of yttrium iron garnet with highlighted sub-lattices (Copied from A.Z. Arsad et al. 2023)

2.3 Colloidal system and YIG on YAG seeded growth mechanism

The aim of this master thesis is to create a ferrofluid which consist of stable colloidal YIG nanoparticles. In order to achieve this the nanoparticles must be distributed uniformly into the dispersion medium. This is challenging as with nanoparticles the surface to bulk ratio is rather large, that means that the surface forces of the nanoparticles dominate. It is therefore possible for a ferrofluid to lower their amount of free energy further by aggregating into a larger crystal. In order to prevent this, the energy of the particles must be at an energy level in which an energy barrier prevents the particles from reaching an absolute lower energy state by aggregating. This can be resolved using DLVO theory where it is explained that the Van der Waals attractive forces must be lower than the repulsive forces which is the disjoining pressure caused by the net pressure exerted by the ions in the electric double layer. Which means that particles must be charged stabilized (J. Adair et al. 2001) (see figure 8).
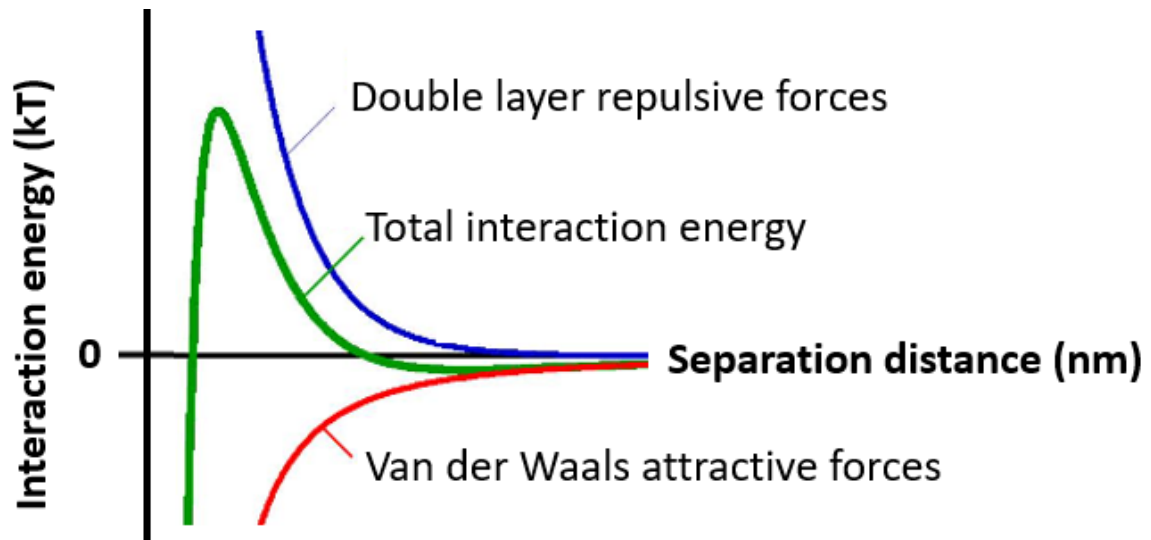
Figure 8: Diagram of the DLVO potential between two spheres (modified from University of Geneva LCSC).

It was theorized that the most optimal way to achieve stable ferrofluid particles was through a glycothermal reaction in which yttrium acetate precursors mixed in together with a second metal precursor into a binary oxide garnet structure. This done in an autoclave in order to achieve high internal temperatures necessary to create an uniform size distribution and high dispersibility in the reaction medium (M. Inoue et al. 1999). Under glycothermal conditions 1,4 butanediol acts as a homogeneous reaction medium, due to its high chemical stability. This medium aids the controlled growth of the garnets and prevents valence change of metallic ions (Y. Xiaowei et al. 2011). Previous studies have shown that signal phase yttrium aluminum particles (YAG) are synthesizable under these glycothermal conditions with 1,4 butanediol as a medium. However when the same conditions are applied to the synthesis of yttrium iron garnet particles (YIG), it does not produce single phase particles. It was found that this was due to the high homogeneous nucleation barrier of YIG. So a seeded growth method was created in which YAG particles are first synthesized before being added to the YIG synthesis. This allows the yttrium precursor to dispose during the synthesis and bind to the YAG seed particles afterwards (*J. Rongjin et al. 2013*) see figure 9.
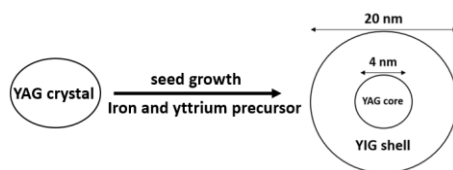

Figure 9: Mechanism of seeded growth mechanism

2.4 Magnetic sedimentation velocity

Lastly we will discuss the principle of magnetic sedimentation velocimetry. When the ferrofluid is synthesized it is important to determine if the particles are homogeneously dispersed in the mixture. Seeing as the YIG particles can aggregate during and after the synthesis it is important that the measure of aggregation is determined. An expression for the effective size of the sedimenting objects as a function of the steady-state sedimentation velocity can be obtained by equalizing the Stokes drag and the magnetic forces acting of the particles (see formula 3).

$$6\eta rv = \left(\frac{dB}{dh}\right) * r^3 * \left(\frac{4}{3}\right) * M_s$$

Formula 3: Equalized drag and magnetic forces acting on the particles A. van Silfhout et al. (2019).

**Table 1:** Variables of formula 3

Symbol	Name
η	Viscosity of solvent
r	Radius of aggregate
v	Magnetophoretic velocity
M_s	Saturation magnetization
dB/dh	Magnetic gradient

Which can be rewritten as:

$$r = \sqrt{\frac{6\eta v}{M_s * \left(\frac{4}{3}\right) * \left(\frac{dB}{dh}\right)}}$$

Formula 4: Formula 3 rewritten to calculate the radius of the particles

The saturation magnetization can be determined via VSM. And the magnetic gradient above our magnet has previously been established (A. van Silfhout et al. 2019). In order to determine the size of the aggregates the magnetophoretic velocity must be calculated. This is done through magnetic sedimentation velocimetry. The measurements consist of taken pictures of the ferrofluid in a capillary over time as the particles sediment towards the magnet (see figure 10).
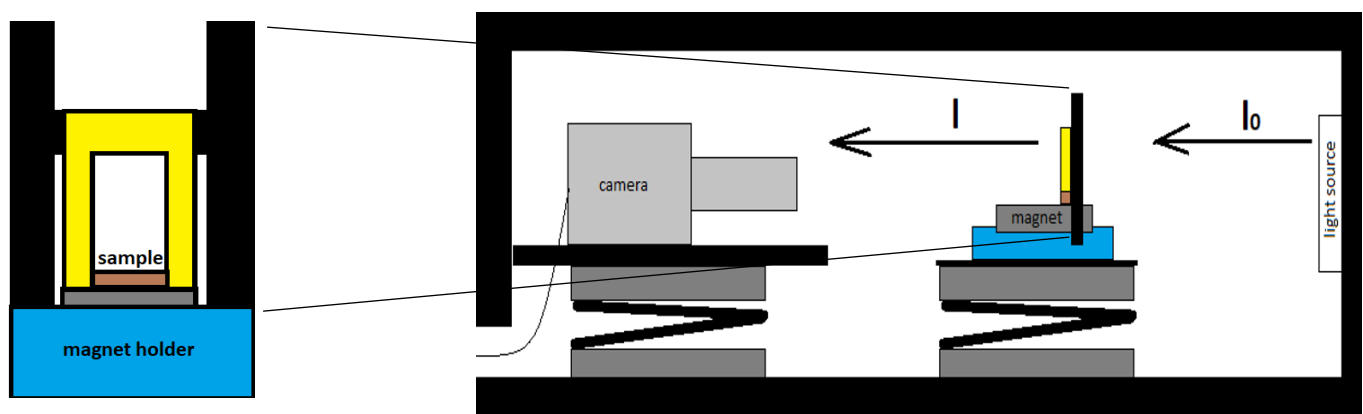
Figure 10: visual representation of the setup used for measuring magnetic sedimentation velocity

As this sedimentation occurs, the color of the ferrofluid in the capillary changes. This change can be calculated as absorbance according to the law of Lambert-Beer:

$$A = -\log(I/I_0)$$

Formula 5: Law of Lambert-Beer (D. Swinehart 1964).

Table 2: Variables of formula 5

Symbol	Name
A	Absorbance
I	Intensity of the light leaving the sample
I_0	Intensity of the light entering the sample

hydratThis means that the absorbance can be calculated from transmission measurements.

$$A = -\log(I_{sample}/I_{blank})$$

Formula 6: Law of Lambert-Beer as it relates to the optical absorbance of the sample observed during magnetic sedimenntation.

Table 3: Variables of formula 6

Symbol	Name
A	Absorbance
I_{sample}	Capillary with ferrofluid
I_{blank}	Capillary with solvent

For here it becomes possible to determine the relative difference in absorbance via A_0/A_t over height (see figure 11). Which can then be further expressed as a relative absorbance difference at different heights over time which is needed in order to calculate magnetophoretic velocity (v).
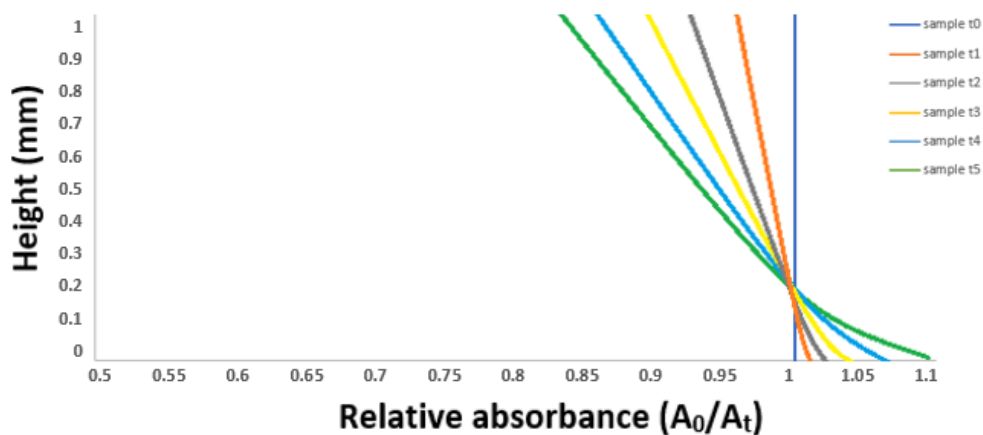

Figure 11: Expected absorbance profile of ferrofluid over time when exposed to the external field

3. Methods

This methods section consists of a synthesis section and a characterization section. The synthesis section will discuss both the yttrium aluminum nanoparticles (YAG) and the seeded growth yttrium iron garnets (YIG). The characterization section will discus the sample preparation as well as the equipment settings used for every characterization technique. The section will how the python script of the MSV technique calculates the absorbance profile.

3.1 Synthesis

The syntheses consisted of firstly synthesizing the yttrium aluminum garnet nanoparticles before adding them to the synthesis of yttrium iron garnet nanoparticles. Both were done via glycol thermal synthesis in a *Carl Roth autoclave model I (see figure 12)*.
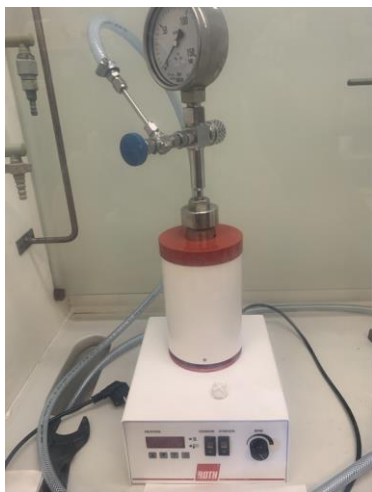
Figure 12: *Carl Roth autoclave model I.*

Yttrium aluminum garnet seed mixture synthesis

The synthesis of the yttrium aluminum particles consisted of mixing 860 milligrams (4.2115 mmol) of aluminum isopropoxide (sigma-Aldrich 98%) and 2.5269 mmol yttrium acetate (this was done by first taking 1 gram of yttrium(III) acetate hydrate (Sigma-Aldrich 99.9%) and drying it for 4 hours in an oven) with a mortar and stirrer. The mixture was added to 16.2 ml of 1,4 butanediol and 1.8 ml diethylene glycerol in a glass autoclave tube. The mixture was then stirred under nitrogen for 15 minutes. Meanwhile the metal autoclave vessel was preheated to 100 (°C) for 40 minutes. Roughly 5 ml of 1,4 butanediol was poured between the walls of the glass tube and metal vessel in order to increase thermal transfer. The mixture was then heated to 300 (°C) for 3 hours, after which the vessel was cooled to room temperature. After this the contents of the vessel were poured into a centrifugal tube. The tube was then subjected to an ultrasonic treatment of 100 W for 10 min in a Branson 8800 Series Ultrasonic cleaner, afterwards the tube subjected to a centrifugation of 3500 rpm for 15 minutes in a Beckman Coulter Allegra X-12R Centrifuge. Afterwards the supernatant layer was pipetted and stored as YAG seed crystal mixture.

Yttrium iron garnet synthesis

The method to synthesize the ferrofluid was by taking 540 milligrams of yttrium acetate (sigma-Aldrich 99.9%). And mixing it with 1200 milligrams of iron(III) acetylacetone (Sigma-Aldrich 97%) in a mortar and pestle (the molar ratio of yttrium to aluminum = (3/5). The mixture was added to 1,4 butanediol (sigma-Aldrich 99%) to act as a reaction medium. The mixture was then stirred under nitrogen for 15 minutes. Meanwhile the autoclave vessel was then preheated to 100 (°C) for 40 minutes. Before being transferred an amount of YAG particles were added which were equal to 1, 2, 3 of the mol weight of the synthesized particles which is 5,10 and 15 mg respectively. The glass tube was then transferred into the autoclave vessel. The mixture was then heated to 300 degrees for three hours after which the vessel was cooled to room temperature. Roughly 5 ml of 1,4 butanediol has been poured between the walls of the glass tube and metal vessel in order to increase thermal transfer. After this the contents of the vessel were poured into a centrifugal tube. The tube was then subjected to an ultrasonic treatment of 100 W for 10 min, afterwards the tube subjected to a centrifugation of 3500 rpm for 15 minutes. Afterwards the supernatant layer was pipetted and taken as the final product.

3.2 Characterization

VSM

VSM measurements were done on both the synthesized ferrofluid as well as the dry YIG particles. The ferrofluid measurements consisted of pipetting the ferrofluid (after homogenization via shaking) into a plastic VSM cup which was then sealed and weighted. The sample was then placed into a *Microsense Vibrating Sample Magnetometer (VSM)* with a *FCM-10 magnetic field control module.*

TEM

TEM was done on samples of every synthesized ferrofluids and consisted of diluting the YIG sample by a factor of 10^5 or 10^6 after which samples were then dried under an IR lamp on a TEM grid for roughly 4 hours. Images were recorded with a *Tecnai 20 (200 KV).-5*

UV-VIS

UV-VIS measurements were taken with a *Perkin Elmer Lambda 35 in Hellma Analytics quartz glass cuvette* with a path length of ^{10} mm. Samples were diluted to a factor of 10/20/40 depending on the absorbance recorded. This was done after the (M_{sat}) had been established

XRD

XRD measurements where done with a cobalt core XRD (*Bruker-AXS D8 ADVANCE X-ray*). Sample was obtained by drying a synthesized YIG sample on watch glasses in an oven at 130 degrees.

The iron atoms in the YIG cause fluorescence in the X-rays produced by a copper target. A solutions to lowering this background noise is using a cobalt anode due to its higher K adsorption edge (M.Mos et al. 2018).

Magnetic sedimentation velocity (MSV)

Magnetic sedimentation velocity measurements were done using a custom set up in which the synthesized ferrofluid is put in a 1 by 15 mm capillary. The capillary has been shorted from a 1 by 50 mm capillary with a wall thickness of 0.05 mm (CM scientific Cat# 5015-050) which is then glued (with Liqui Moly epoxy glue) into a sample holder. The sample was then placed onto a magnet

(cylindrical neodymium magnet of 45 mm diameter with a 30 mm thickness from Super Magnete (Gottmadingen Germany)) while a camera took pictures at set intervals. The photographs were taken with a *Nikon D7500 camera with AF-S DX NIKKOR 18-300 II VR lens* (see figure 13).

Figure 13: Picture of MSV setup

As the particles in the ferrofluid started to sediment towards the magnet the color in the ferrofluid starts to change. The change in coloration can be observed with the camera. Using a Python script (see appendix F). There are two variant of the script. One in a build in loop which calculates the absorbance profiles of every time interval. And one without a loop in which specific measurement can be loaded into manually. The second one can be used to identify/ resolve irregular measurements. The pathway of both are similar, in the script without a loop all images can then loaded, canned and cropped to heigh of the capillary (F-2 part 1), then the width boundaries are set creating a matrix. The script then generates a list of zeros for the matrices of both the ferrofluid sample as well as the blank, this list is later overwritten by the color data extracted from every pixel. The first row of pixels is set to 1 decreasing to zero by the amount of rows (this is the vertical height axis). The image is then is split in to three color channels, red (R), blue (B) and green (G), Afterwards one color channel is chosen to which the absorbance of the ferrofluid is calculated for every row of pixels according to the law of Lambert-Beer (with a failsafe that ensures all pixel values have a minimum of one(F-2 Part 2). Lastly all absorbance profiles are plotted over time into one graph (F-2) part 3). The script with the loop works similar but the loop in written in the code before the sample path is chosen. The function of both script can be expressed as a flowchart (figure 14).
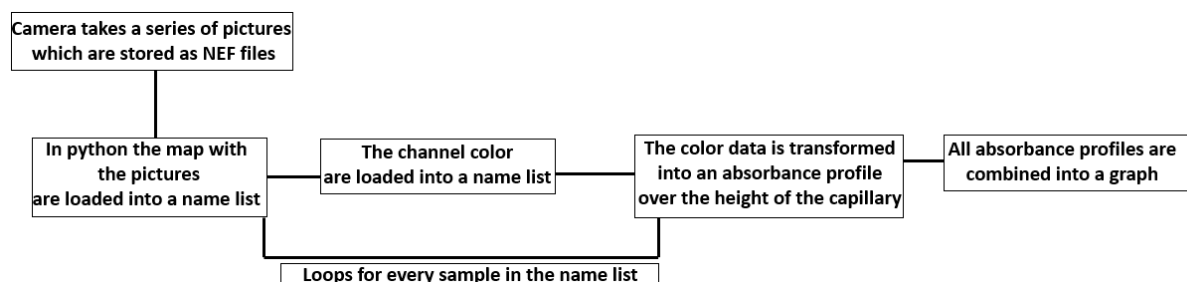

Figure 14: Flowchart of Python method

4. Results and discussion

4.1 Effects of YAG

Several synthesis were done In which the amount of YAG seed crystals added was varied, this was done in order to determine its effects on the diameter of the YIG shell. The YAG amount added was 5, 10 and 15 milligrams (this is equivalent to 1, 2 and 3 wt% of the amount of synthesizable YIG particles). The size of the particles after synthesis were measured with TEM (see figure 15).
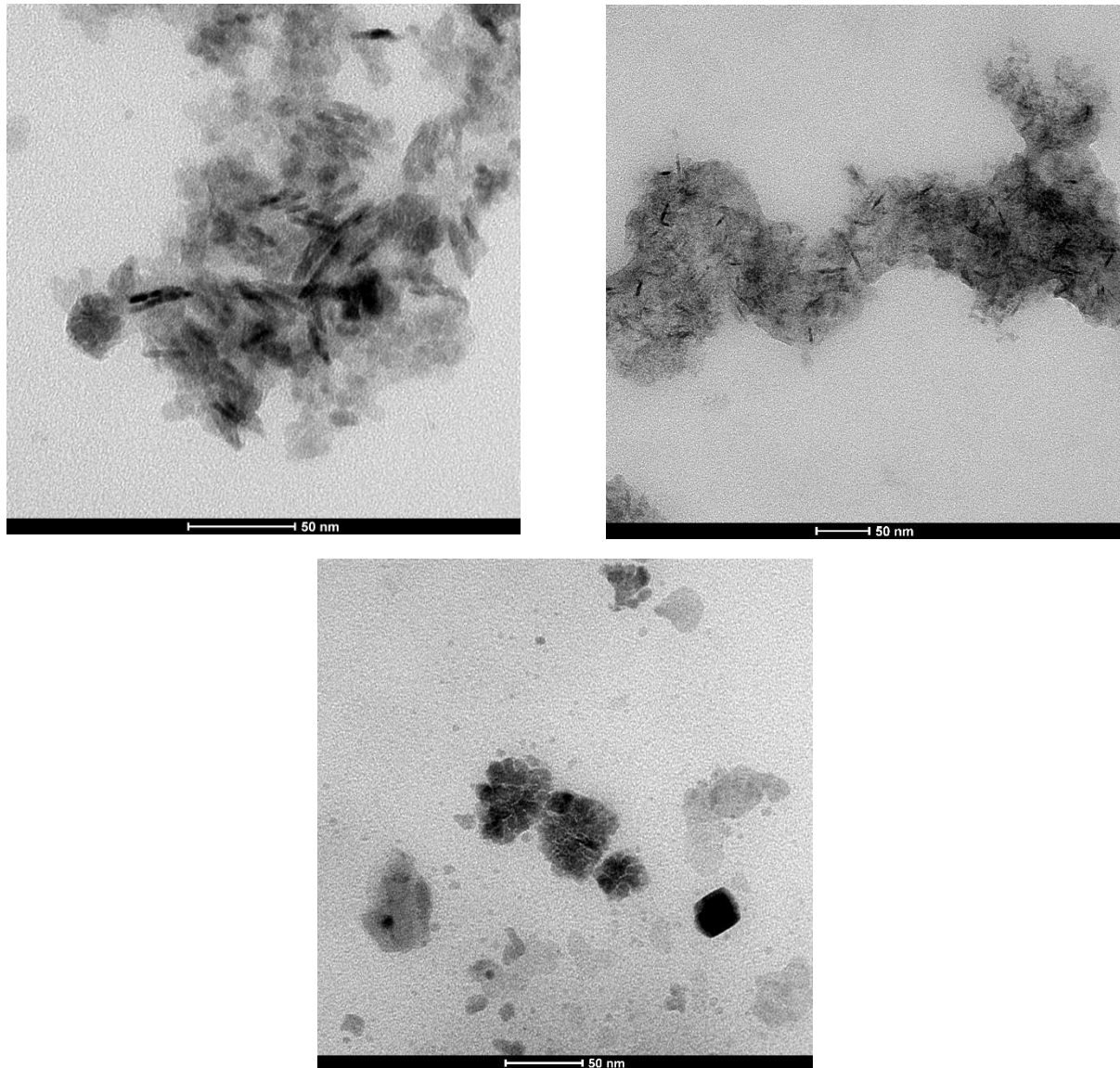
Figure 15: TEM pictures of YIG ferrofluids synthesized with (a) 5 milligrams YAG particles, (b) 10 milligrams YAG particles and (c) 15 milligrams YAG particles added.

From these pictures it becomes clear that none of the synthesized particles have a uniform size and shape. Instead the particles in most synthesized particles showed a mixture of smaller and larger particles within the 10-50 nm range. It can also be noted that both the syntheses of 5 mg YAG and 10 mg YAG added had large amount of elongated particles with a width to length ratio of 1/2 to 1/10

(see table 4). It was observed that the synthesis with the 15 mg of YAG and subsequent synthesis did not show the elongated particles meaning most likely a better core shell formation. Therefore it made sense that other variations syntheses were done with 15 mg YAG added, this is despite the still large difference in particle sizes (see A-4 to A-9 appendix A). These syntheses produced particle sizes that were within the range of 5-60 nm without the elongated particles.

Table 4: Estimated observed ranges sizes of particles from TEM

YAG concentration	Spherical particles	Elongated particles
5 mg	10-30 nm	Length 10-30 nm, width 3-6 nm
10 mg	5-20 nm	Length 5-25 nm, width 3-6 nm
15 mg	5-60 nm	Not a significant presence

The particles size seems to decrease between 5 and 10 milligrams of YAG particles added however when 15 milligrams of YAG particles are added yielded a size increases substantially. This seems counter to the assumption that an increase in the amount of bonding sites to the YIG results in smaller particles. The results seem to not be consistent with previous literature values which showed an increase in size of the particles when the amount of YAG seed crystallites is lowered (J. Rongjin et al. 2013). A possible explanation for this inconsistency found could be that current synthesis does not functionalize the surface of the particles stable enough to result in consistent particles sizes at lower YIG concentrations. Seeing as the synthesis with 15 mg of YAG added did not produce the types of elongated particles in the synthesis of 5 and 10 mg of YAG it was decided to have further syntheses variation done with 15 mg of YAG particles added. Another interesting observation is that nanoparticles in the ferrofluids that were syntheses over a longer period of time (7 to 8 hrs.) showed crystal structure that seems more well defined and more closely resemble the crystal structure seen in the reference material. This could be possible attributed to the syntheses being stirrer as supposed to reference synthesis route or possible the difference in temperature profile (see figure 16).
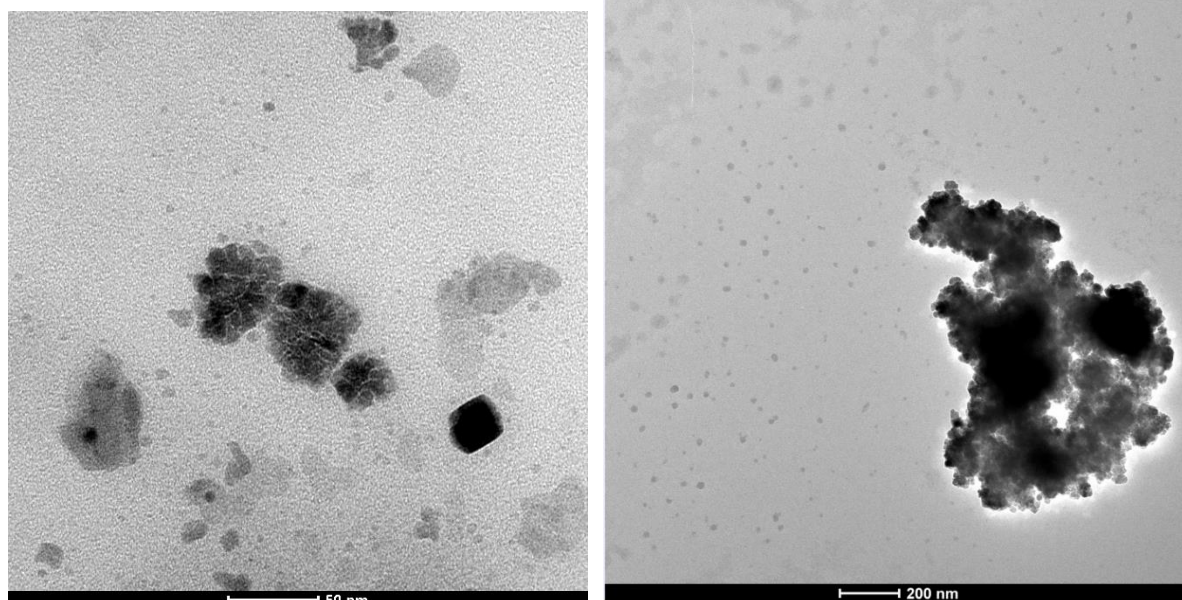

Figure 16: TEM pictures of YIG ferrofluids with 15 milligrams YAG particles added synthesized for 3 hours (left) and 8 hours (right).

4.2 Pressure evolution of synthesis

The syntheses were executed with a variation in time and pre-heating steps to determine the most optimal conditions for a highest possible internal temperature during the synthesis. A high internal temperature is preferable as it ensures the lowest possible nucleation barrier. Pressure analysis was done with a blank sample of only 1,4 butanediol and three YIG samples (see figure 17). For the YIG samples their synthesis ran for 7-8 hours, two of samples had the metal autoclave vessel preheated to 100 degrees Celsius before the reaction started the final sample was not pre-heated.

The pressures were determined by taking a picture of the pressure dial (see appendix B, B1-B8). The display of the pressure dial only shows increments of 5 bar, so in order to more accurately establish the pressure a digital protector was placed over the photo (see figures A-1 to A-4).
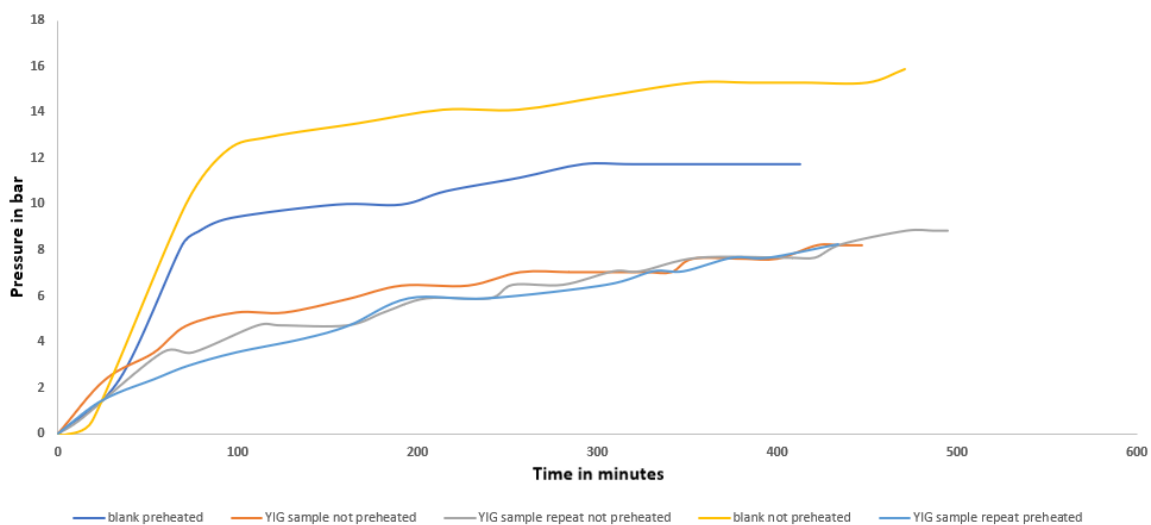
Figure 17: Pressure graph of YIG ferrofluid synthesis and the 1,4 butanediol and the blank.

From these measurements it becomes apparent that the pre-heating of the reaction tube substantially slows the build-up of pressure. This effect however seems also more pronounced between the blank and the YIG samples as it makes sense because of the endothermic reaction. It also shows a substantial difference between the pressure between the pre-heated and non-preheated samples (pre-heated referring to pre-heating the metal autoclave reaction tube to 100°C before the reaction starts). This can be explained by the Clausius Clapeyron equation (see formula 6).

$$ln\frac{P_2}{P_1} = \frac{-\Delta H_{vap}}{R}\left(\frac{1}{T_2} - \frac{1}{T_1}\right)$$

Formula 6: Clausius Clapeyron equation (L. Oliver et al 1951)

The formula allows for the determination of the internal temperature of the reaction mixture by assuming that in the vacuum of the autoclave, the temperature only depends on the balance liquid and the vapor of synthesized ferrofluid, (disregarding the nitrogen used in flushing).
This internal temperature will be determined according to the values taken in the table 5. (Vapor pressure at boiling point of 1,4 butanediol = 1atm). In the formula P_1 is the normal pressure at which the normal boiling point T_1 is measured. P_2 is the measured vapor pressure from which we can estimate the temperature T_2 in the autoclave once the highest pressure is reached.

$$T_2 - 300°\text{C} = [\frac{1}{T_1} - \frac{R*\ln\left(\frac{P_2}{P_1}\right)}{\Delta H_{vap}}]^{-1}$$

Formula 7: Clausius Clapeyron equation rewritten to determine T_2. (L. Oliver et al 1951)

Table 5: Values for Clausius Clapeyron

Symbol	Name
P_1	Vapor Pressure at t_0 = 1.01325 Bar (1 atm)
P_2	measured Vapor Pressure at t_1
ΔH_{vap}	Enthalpy of vaporization (for 1,4 butanediol = 78300 J/mol (NIST chemistry WebBook)
R	Gas constant = 8.314 J/K/mol
T_1	Temperature at t_0 (503K) (NIST chemistry WebBook)
T_2	Temperature at t_1
t_0	Time at the start of the synthesis
t_1	Time at the end of the synthesis

Table 6 presents the calculated values at the final reached pressure during the synthesis.

Table 6: Values of all synthesized ferrofluids at the end of the synthesis

Symbol	Temperature (°C)
Blank pre-heated	318.9
Blank non-preheated	308.8
YIG samples non-preheated	297.4
YIG sample repeat non-preheated	299.5
YIG sample pre-heated	297.4

Firstly the calculated temperatures of every sample were within a 5 degree margin of the temperature of the autoclave which shows that the reaction mixture reaches the temperature of autoclave during synthesis. From the pressure graph (figure 17) it becomes clear that the overall pressure difference between the samples converge around 5 hours. A drawback to this method of pressure calculation is that an one protractor degree error in the reading of the pressure results in a significant difference in the relative temperature. From the TEM data in section 4.1 it does become apparent that these differences in pressure do not have a substantial impact on the overall particle size. Possible effects of magnetization are explained in section 4.4.

4.3 Composition of the synthesized particles with XRD

In order to determine whether the synthesis successfully results in synthesized YIG nanoparticles a XRD measurement was conducted with a cobalt core (see figure 18). A cobalt core was used as the iron in the YIG would interfere with the absorption edge of other sources such as copper.
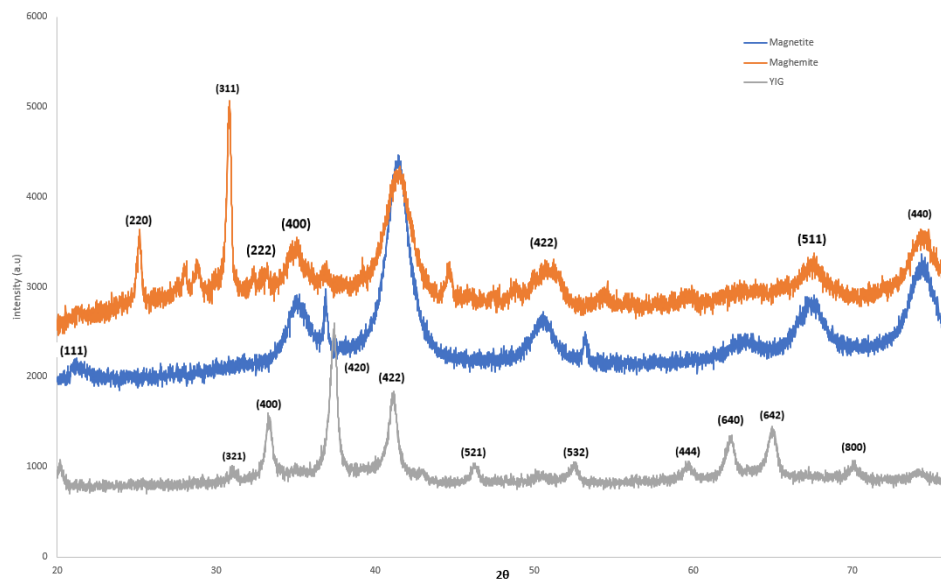
Figure 18: XRD data of synthesized magnetite, maghemite and the synthesized YIG ferrofluid

When compared to a reference spectrum of YIG it becomes apparent that all major peaks are identifiable and are consistent with Yttrium iron garnet. Meaning that the synthesis does successfully produce yttrium iron garnet nano crystals based on previous literature (D. Nguyet et al. 2012). The XRD graph also shows that synthesized conventional ferrofluids of magnetite and maghemite used for reference are consistent with the literature (M. Friàk et al. 2007). These XRD measurements also show the peaks of the synthesized YIG nanoparticles are sharper then the peaks of maghemite and magnetite which indicate that the synthesized particles are larger then the particles of the conventional ferrofluids. This is in line with expectations as the literature of the values are found to be in a size range of around 16-35 nm (J. Rongjin et al. 2013), whereas the size of the nanoparticles in conventional ferrofluids are between 5 and 10 nm (A. van Silfhout et al. 2020).

4.4 Nanoparticles size and magnetization with VSM

This section discusses the magnetization of the nanoparticles in the synthesized ferrofluid as well as the dry nanoparticles. Furthermore the VSM will also be used to determine the size of the nanoparticles and compared with TEM.

In order to determine the size of the particles, the magnetic dipole moment and the bulk magnetization of the magnetic materials must be taken in to account. The magnetic dipole moment will be determined with VSM and the bulk magnetization of magnetite, maghemite and YIG are known values (NIST webbook) (see table 8). The diameter of the individual nanoparticles will be determined with formula 7:

$$m = \pi * m_b * D^3 / 6$$

Formula 7: Calculation of magnetic dipole moment (S. Chiazumi. 1964).

Formula 7 can be rewritten in order to express the diameter of the nanoparticle (see formula 8).

Table 7: Particle size determination from VSM measurements

Symbol	Name
m	Magnetic dipole moment (A*m^2)
m_b	Bulk magnetization (A*m)
D	Diameter nanoparticle (nm)

$$D=\sqrt[3]{\frac{(m*6)}{m_b*\pi}}$$

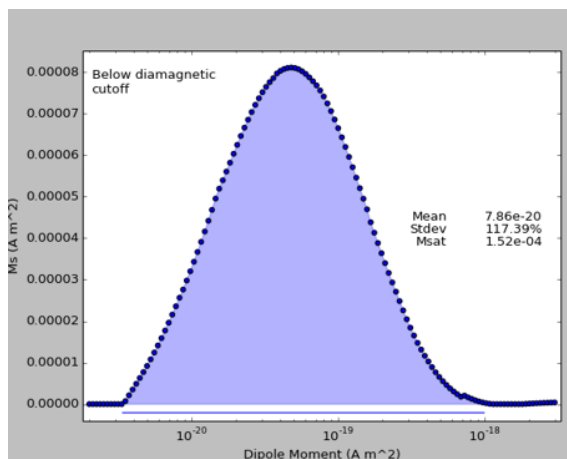**Formula 8:** Calculation to determine the diameter of the nanoparticle (S. Chiazumi. 1964).

Saturation magnetization can be calculated from the VSM hysteresis curve, this was done for all the different YAG samples as well as the pre-heated and non-preheated samples (see appendix C).

The example calculation of the particle size will be shown with the maghemite sample (see figure 19,20) this calculation was done for all other samples (see figures C-1 to C-7).
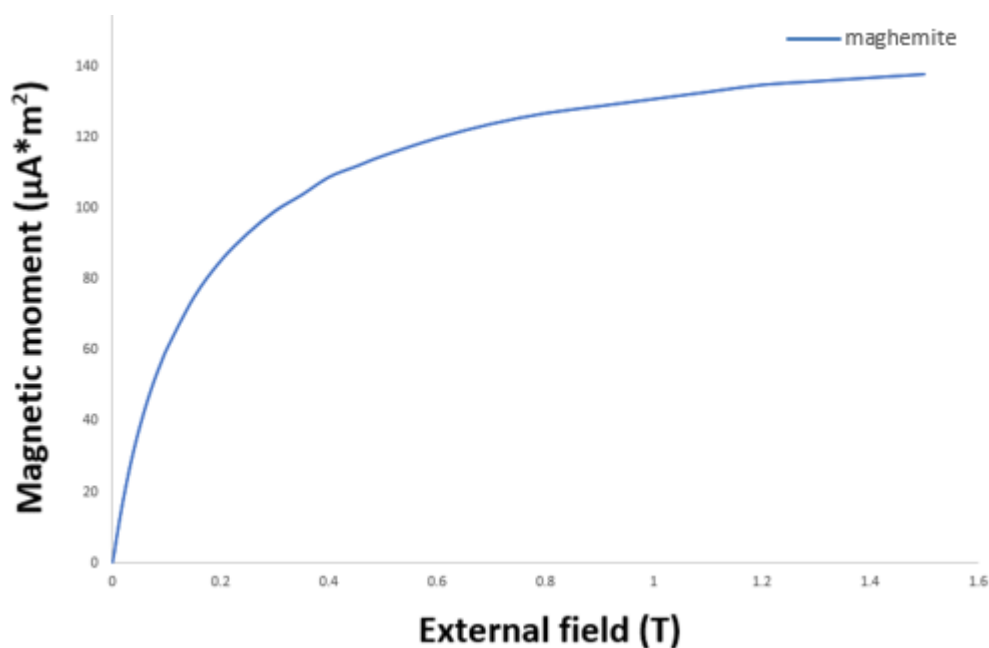
Figure 19: VSM measurement of maghemite

The VSM hysteresis loop can then be expressed as a magnetic distribution graph calculated with the Minorum program (R. van Rijssel. 2014) (see figure 20) in order to determine the dipole moment. This was also done for the other samples (see table 8).

Figure 20: Magnetic dipole moment distribution of maghemite

With this value it becomes possible to determine the particle diameter with formula 8.

$$\sqrt[3]{\frac{(7.86*10^{-20}*6)}{430000*\pi}} = 7.86 * 10^{-9} \text{ m}$$

Example calculation of the diameter of the nanoparticles of maghemite.

Table 8: Particle size determination from VSM measurements for the ferrofluids which had different amount of YAG added

Sample name	Bulk magnetization (A/m)	Saturation magnetization (A*m^2) (see appendices B1-B5)	Dipole moment (A*m^2) (see appendices C1-C5)	Particle size* (nm)
maghemite	430000 (A.Shokrollahi et al. 2017)	1.38*10^{-4}	7.86*10^{-20}±117.39%	3.52
magnetite	480000 (R.Cornell et al. 2003)	1.60*10^{-6}	1.42*10^{-19} ±144.29%	4.29
YIG with 5 mg YAG added	140000 (A. Prabhaker et al. 2009)	2.67*10^{-6}	1.13*10^{-18} ±230.85%	12.44
YIG with 10 mg YAG added	140000	1.26*10^{-6}	4.28*10^{-20} ± 127.17%	4.18
YIG with 15 mg YAG added	140000	1.47*10^{-6}	4.04*10^{-20} ±119.06%	4.10

Particle size expressed in radius (nm)

The calculations of particle size of maghemite and magnetite is consistent with the literature value (A. van Silfhout et al. 2019). The calculated particles size of YIG 10 mg is low which is consistent with TEM measurement (see table 4).

The calculated particle size of 15 mg YAG sample is relatively low when compared to the calculated particles sizes of the subsequent YIG syntheses (see table 9). This seems to indicate that a longer synthesize time results in larger magnetic core shells.

Table 9: Particle size determination from VSM measurements for the ferrofluids which differ in synthesis time and heating steps.

YIG nanoparticles	Bulk magnetization (A/m)	Saturation magnetization (A*m^2)	Magnetic dipole distribution (A*m^2)	Particle radius (nm)
Non pre-heated	140000	$1.04*10^{-5}$ $6.25*10^{-6}$	$6.79*10^{-19}\pm 52.61\%$ $5.16*10^{-18}\pm 49.7\%$	10.50 20.64
Pre-heated	140000	$1.17*10^{-5}$ $1.43*10^{-5}$	$1.37*10^{-20}\pm 100.3\%$ $1.29*10^{-18}\pm 93.69\%$	2.86 13.0

The preheated and non-preheated samples both produce particles sizes which are in range of the literature values of 16-35 nm (*J. Rongjin et al. 2013*). However the pre-heated sample seems to have a larger particle size distribution (see Appendix C, C-6 and C-7).

The magnetization of the ferrofluid can now also be expressed as magnetization divided by the weight of the nanoparticles. This can be done by taking the values of the dry nanoparticles and divide it over the weight of the ferrofluid see table 10.

Table 10: Calculated yield of the dry powder weight fraction of the pre-heated YIG ferrofluid

Average weight liquid (mg)	Average weight dry nanoparticles (mg)	Average dry powder weight fraction
$1.10 \pm 6,5*10^{-2}$	$1.67*10^{-2}\pm3.03*10^{-4}$	$1.506\%\pm7.38*10^{-2}\%$

The saturation magnetization of both the dry nanoparticles as well as the ferrofluid from the VSM (see figure 21) and dividing it over the weight of the VSM sample (or the weight of the VSM sample times the weight fraction for the ferrofluid) it becomes possible to express the weight magnetization.
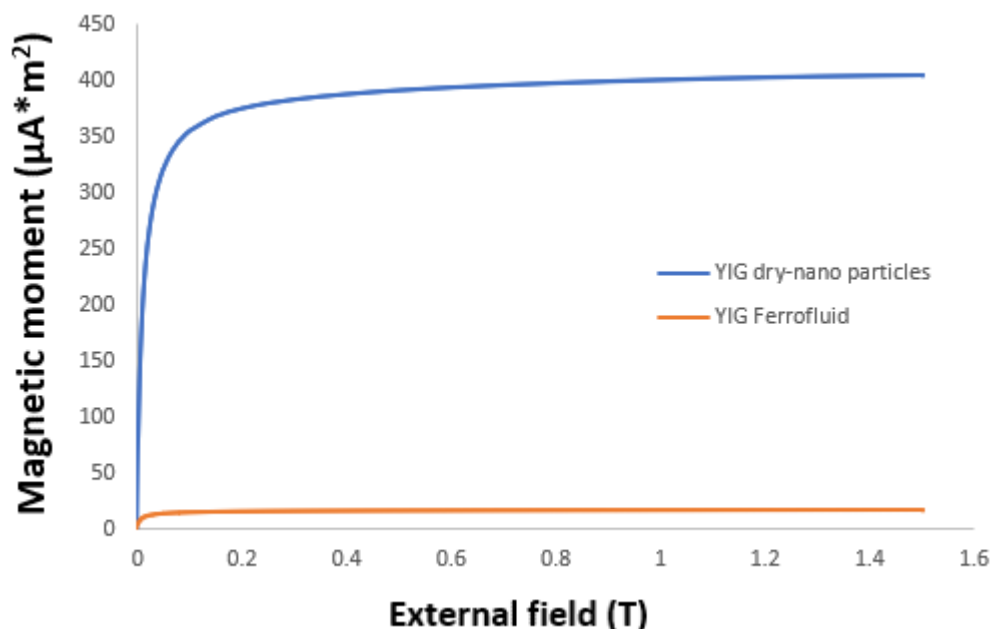
Figure 21: VSM of the YIG ferrofluid and dry nanoparticles

The saturation magnetization of samples were found to be 16.7µA/m^2 and 403.7 µA/m^2 for the ferrofluid and the nanoparticles respectively, (ferrofluid 66.41 mg, dry particles 24.63 mg).

The magnetization in (emu/g) becomes.

$$\frac{16.7}{66.41 * 0.015106} = 16.6 \; emu/g$$

$$\frac{403.7}{24.63} = 16.4 \; emu/g$$

Which shows that both the ferrofluid and the dry particles are within the order of magnitude of the magnetization found in literature 13-25 emu/g. (*J. Rongjin et al. 2013*).

Interestingly enough the dipole moment of ferrofluid and the dry YIG nanoparticles are different (see figures 22 and 23). With the ferrofluid sample showing one large peak while the dry YIG particles shows a split in the distribution. The graph of the dry samples seems to be more in line with TEM measurements which did not show an equal distribution of the size ranges. This could however still be due to artifacts of the Minorum program.
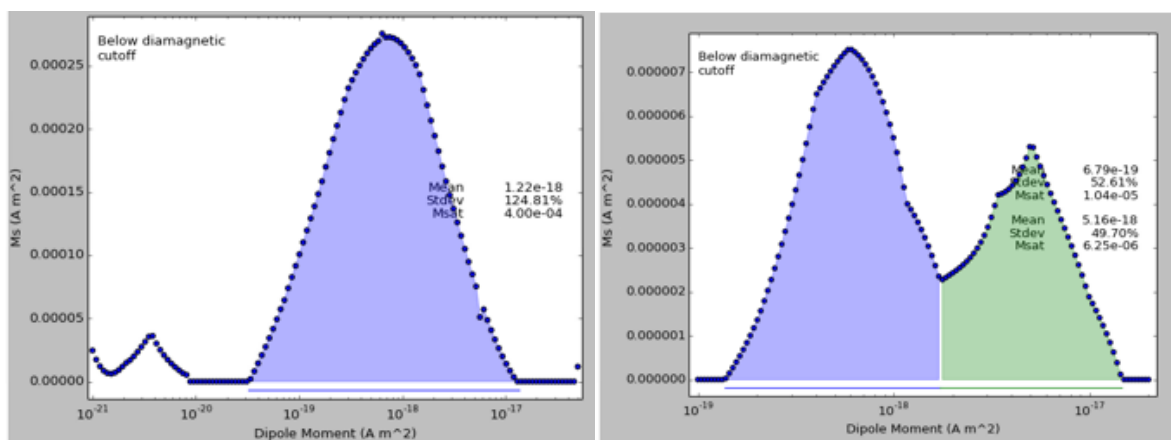
Figures 22 and 23: Magnetic particle distribution of both the ferrofluid (left) and the dry nanoparticles (right)

The magnetization of all the other ferrofluid samples can be calculated according to the same principle. The weight fraction of the nanoparticles in the ferrofluid was determined through drying of the sample (see table 11).

Table 11: ion of YIG in ferrofluid, Saturation magnetization and the calculated magnetization (in emu/g)

Ferrofluid Sample name*	Nanoparticle weight in ferrofluid (%)	Saturation magnetization ($\mu A*m^2$)	Magnetization (emu/g)
Maghemite	4.88	138	46.52
YAG 5 mg	1.39	1.6	1.87
YAG 10 mg	0.65	2.67	6.58
YAG 15 mg	1.03	1.26	2.06
Pre-heated**	1.51	16.7	16.6
Non pre-heated**	1.58	21.8	23.69

Magnetite is not shown here is due to the solvent (mineral oil has an evaporation point far above its flashpoint)
**taken as average*

The results show for the YAG amounts added, the magnetization seem to increase slightly except for the YAG sample of 10 mg, (which discussed in section 4.1). The magnetization values are slightly above the literature values. This is mostly likely due to the presence of magnetic material such as unseeded YIG being present in the ferrofluid. However the magnetization is substantially lower than for maghemite, this means that it is important to determine if the decrease in absorbance is proportionally better than the decrease in magnetization. This will be discussed in section 4.6

4.5 Calculation the order of magnitude of the aggregates and size ratio to particles with MSV

This section will discuss the optimization of the magnetic sedimentation velocimetry (MSV) setup as well as the calculated aggregate sizes. Lastly these aggregate sizes are compared to the calculated particle sizes from 4.4.

The MSV setup was made in order to calculate the highest possible absorbance profile for a chosen color channel. The ferrofluid in the capillary has an orange tint (see appendix G). The most intense color channel was red followed by green and blue (see figure 24). Blue was chosen as red was too close to oversaturation and the green channel value had less contrast between the blank and sample meaning a lower absorbance profile.
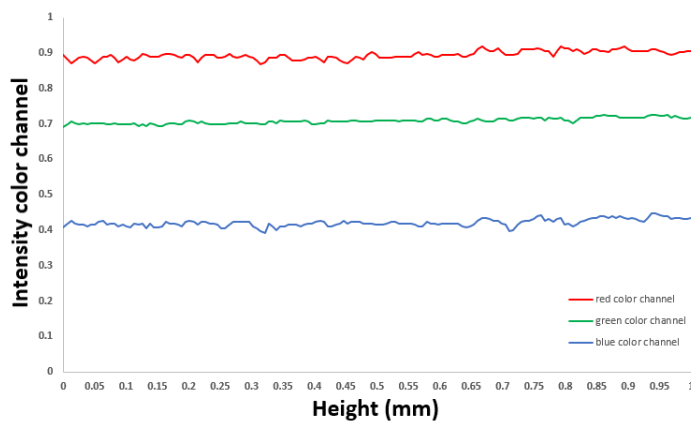
Figure 24: Intensity of each color channel over height at $t_{0 \text{ (converted)}}$ from 0-255 to 0-100% scale)

A conventional ferrofluid (maghemite) was measured over a period of 60 minutes with 10 minute intervals (see figure 25).
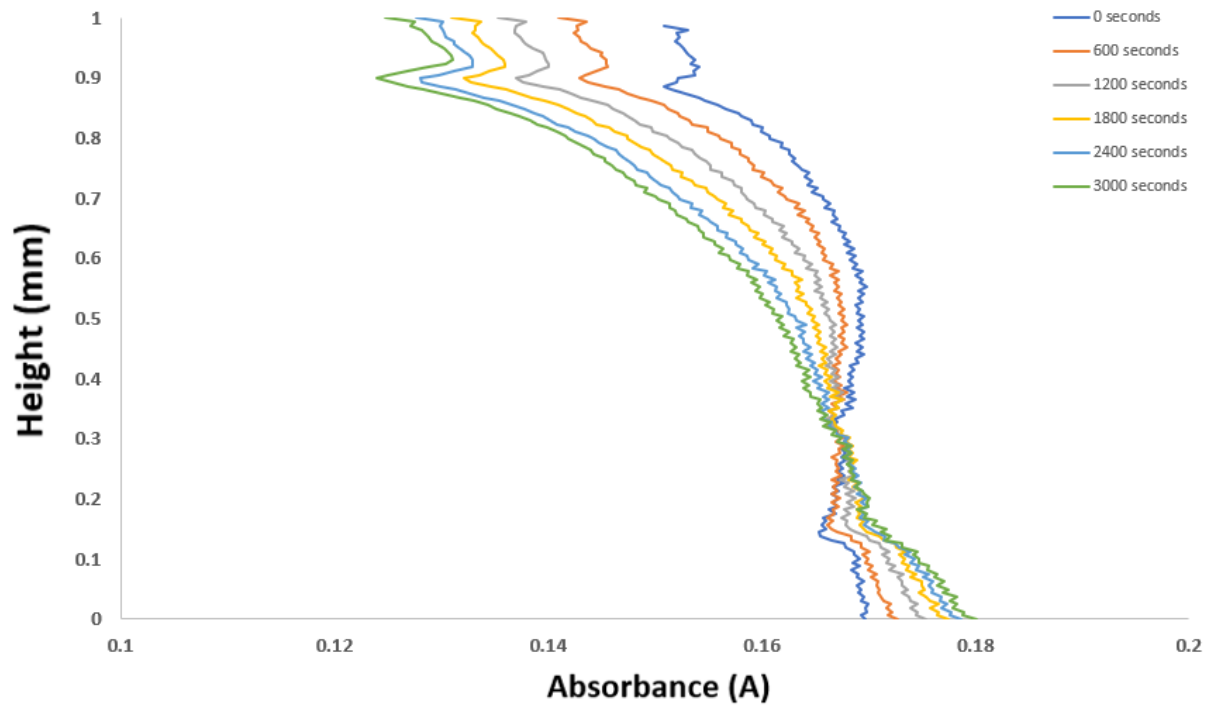
Figure 25: Absorbance of maghemite over a period of 60 minutes

The absorbance profile in figure 25 was converted into relative absorbance profile (see figure 26).
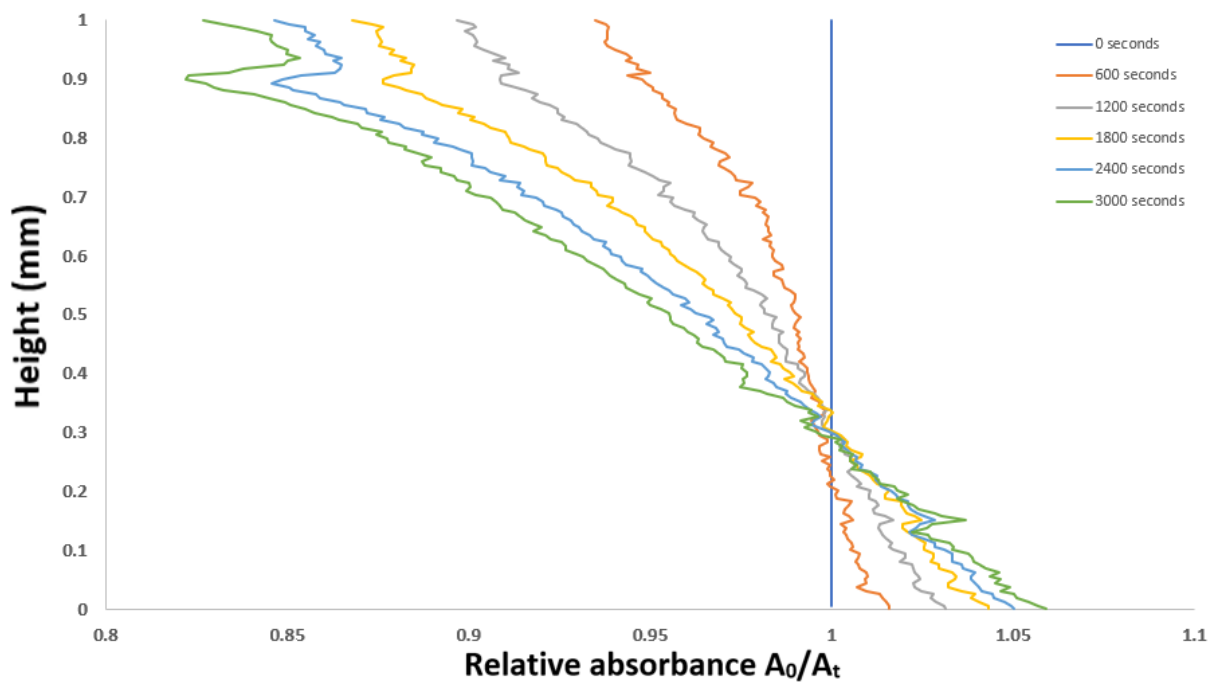
Figure 26: Relative absorbance of maghemite over a period of 60 minutes.

The relative absorbance profile at 0.95 height was taken for every measurement in time. This value was chosen as it encompassed the most amount of measuring points from A_0 and plotted in figure 27.
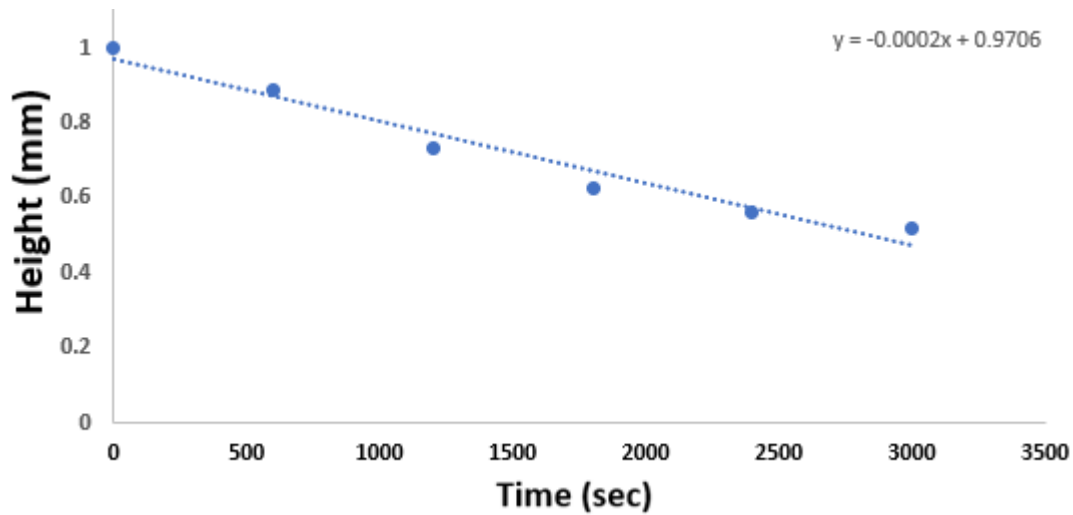
Figure 27: Graph the height at 0.95 relative absorbance over time.

The height of the capillary is 1 mm and the slope taken from figure 26 it can be calculated that the magnetophoretic velocity (v) results into $1.66*10^{-7}$ m/s. The radius of the particle can be determined according to formula 4.

$$\sqrt{\frac{6*(0.001*1.66*10^{-7})}{430000*\left(\frac{4}{3}\right)*(20)}} = 18 \text{ nm}$$

The calculated radius of 18 nm is above the calculated value from the VSM measurement (see section 4.2) and the expected literature value (A. van Silfhout et al. 2020). This could possibly be due to the reflection at the top row pixels of the capillary disturbing the absorbance profile.

When the same was performed for a YIG ferrofluid optical effects already showed after 10 minutes instead of 60 minutes. This is very likely due to the inhomogeneous particle sizes. To correct for it the absorbance was calculated by taking a 10 minute profile with 2 minute intervals (see figure 28).
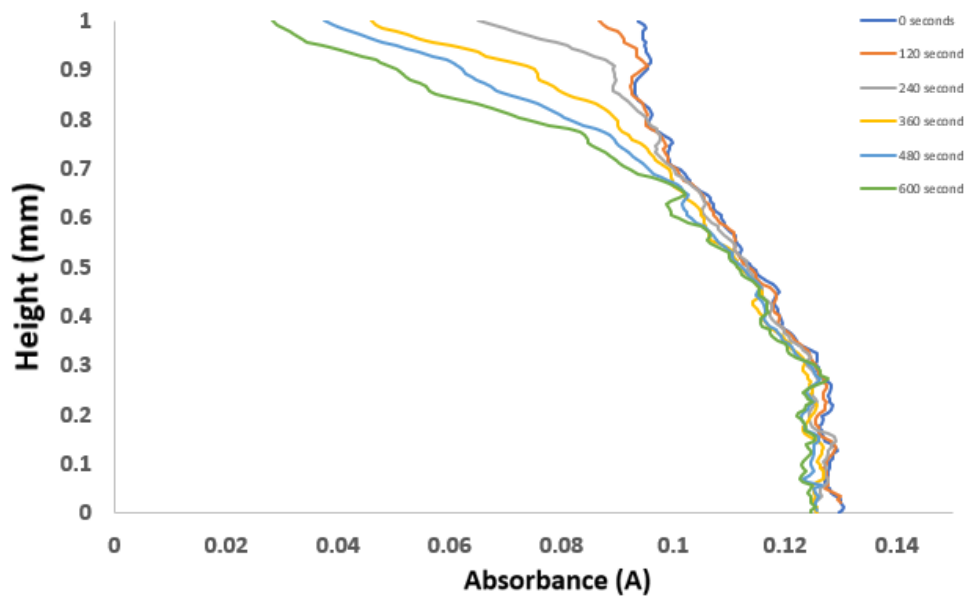
Figure 28: Absorption graph of YIG ferrofluid with 15 mg YAG added over 10 minutes

The absorbance value can the transformed into the relative absorbance profile (see figure 29).
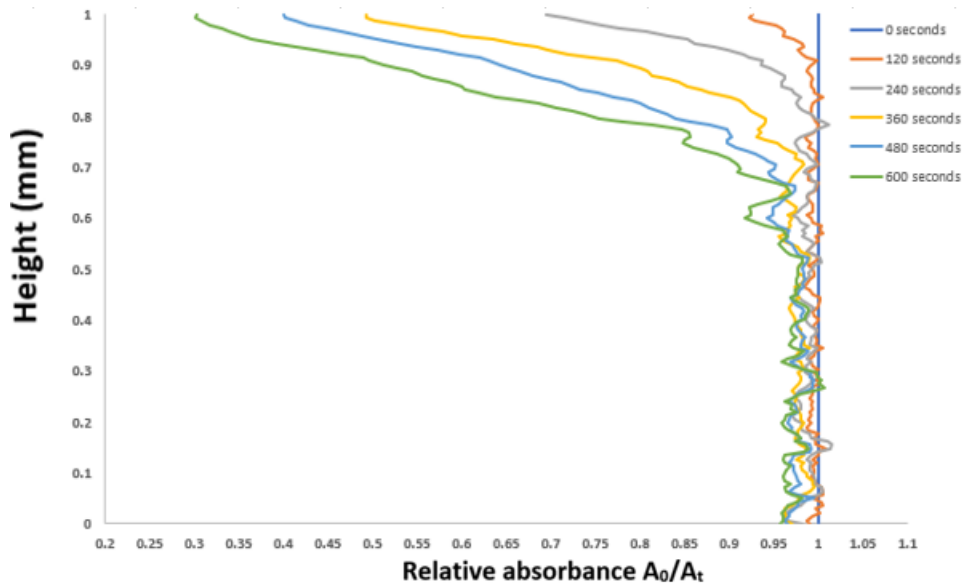
Figure 29: Relative absorbance of YIG ferrofluid 15 mg YAG added over a period of 10 minutes.
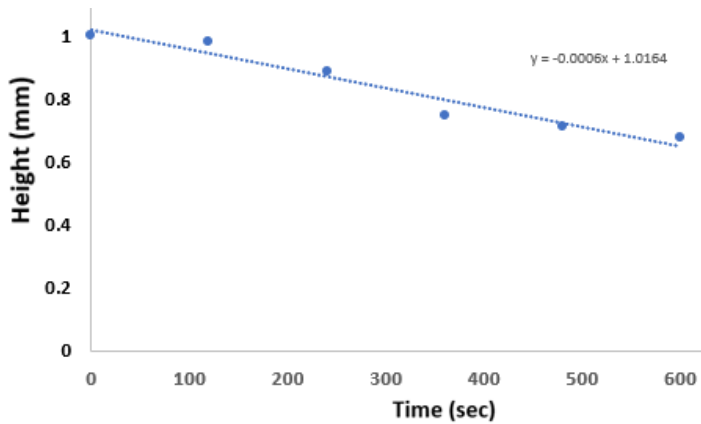
Figure 30: slope of the height of the relative absorption value in time.

From this graph the velocity can be taken as the slope of the graph which is $6.1*10^{-7}$ m*s, which can then further be used to determine the radius of aggregate with formula 3:

$$\sqrt{\frac{6*8.49*10^{-2}*(6.1*10^{-7})}{140000*\left(\frac{4}{3}\right)*20}} = 288 \text{ nm radius particles}$$

The calculated size of the aggregates is larger than the particle size by more than one order of magnitude. This seems to confirm that the synthesized nanoparticles in the ferrofluid are unstable in the present of an external field resulting in aggregation. This means that further synthesis of these YIG particles must increase the repulsion forces between the particles.

MSV was also done on the both a preheated and non-preheated sample (see E-1 to E-6) which both showed the same difference in the order of magnitude of the size of the aggregates (see table 12).

Table 12: Calculated aggregate sizes of preheated and non-preheated YIG sample.

Ferrofluid Sample name	Calculated particle size VSM	Calculated aggregate size	Ratio
Preheated	10.50 20.64	309.051	29.4 14.97
Non-preheated	2.86 13.0	412.30	144.1 31.71

The potential drawback of the MSV setup is the precision of the positions of both the blank and the ferrofluid as there taken at different points in time. If the positions of both are not exactly equal it causes a deviation from a pixel perfect situation. It should be noted with the measurements of YIG shown at t_0 already shows sedimentation this problem is present in several other measurement and be prescribed to the fact the beginning of the measurement is difficult to capture.

Determining the pixel size of larger aggregates causes another difficulty within the MSV setup. In order to capture the larger aggregates the setup needs to run for a longer time. As the bottom pixel rows cannot be observed due to capillary reflection it causes the entire absorbance profile to shift to the left. Making it impossible to capture all the absorbance profiles with only one relative absorbance value (see figures 31 and 32). This could possible resolved by further optimizing the camera setup so it can capture lower pixel lines without distortion from the bottom of the capillary.
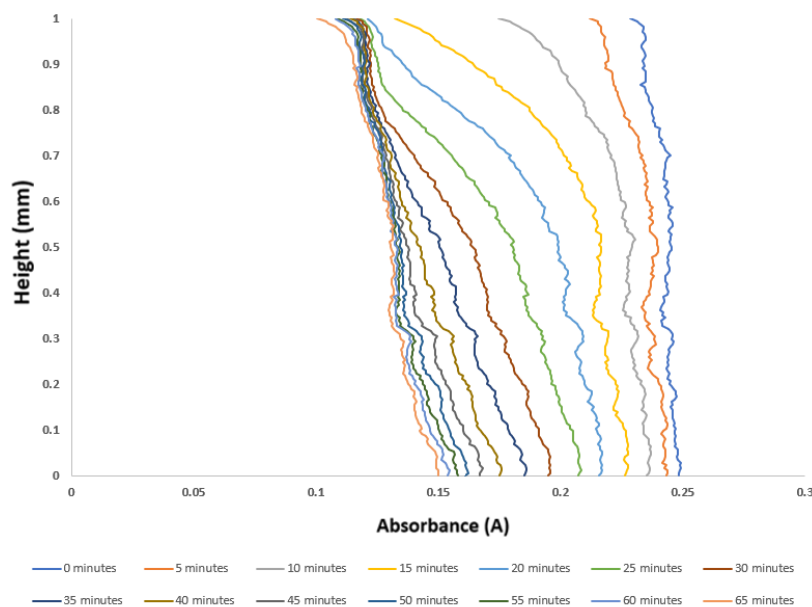
Figure 31: absorbance over 60 mins

The absorbance value can the transformed into the relative absorbance profile (see figure 32).
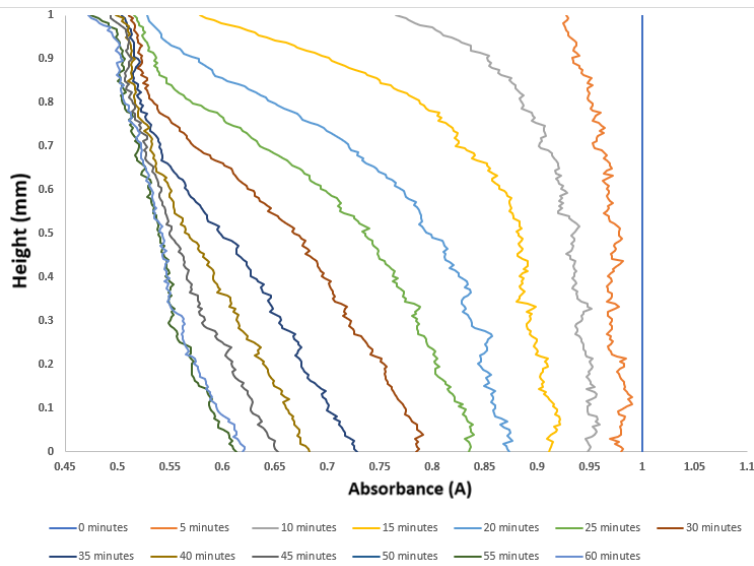
Figure 32: Relative absorbance over 60 mins

4.6 Determine the optical absorbance of the YIG ferrofluid with UV-VIS

Lastly this section will discuss the optical absorbance of the YIG ferrofluid normalized for the volume fraction. This was determined via UV-VIS analysis for both a pre-heated and non-preheated YIG sample as well as the maghemite sample (magnetite is not included as volume fraction could not established). All samples needed a factor of dilution in order to be measured with the UV-VIS. The results of the UV-VIS measurement can be seen in figure 33.
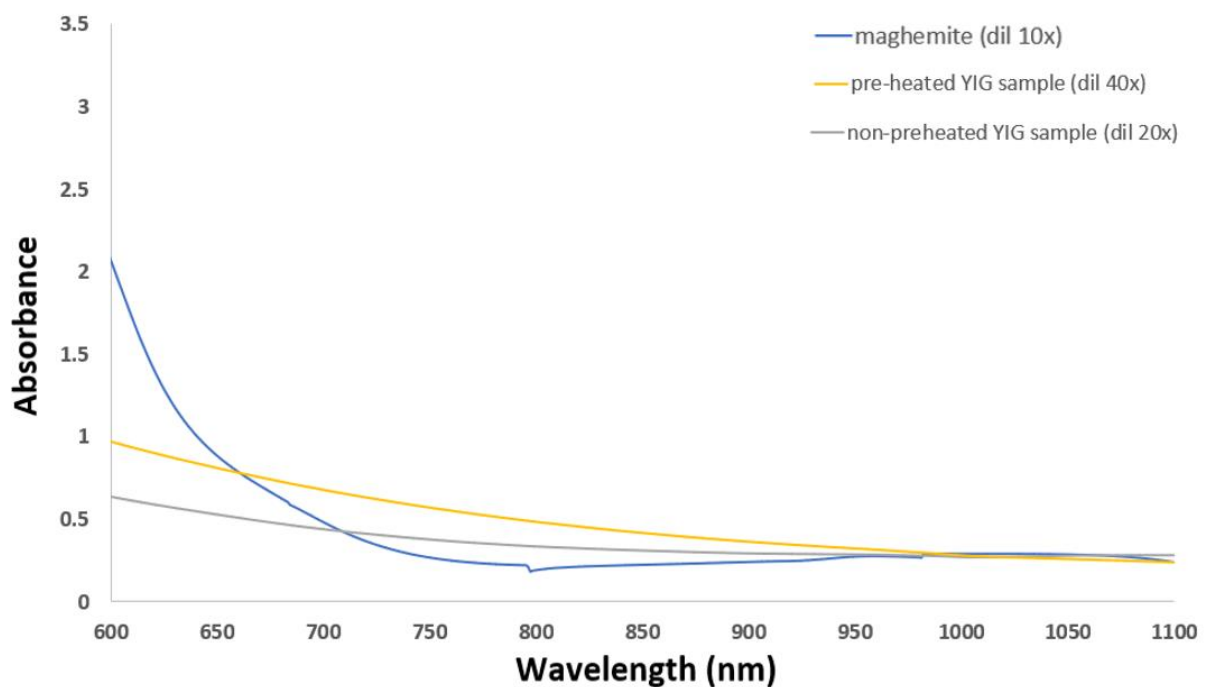
Figure 33: UV-VIS spectrum of maghemite a non-preheated and preheated YIG ferrofluid samples

The absorbance values can then be adjusted for the volume fraction (see table 11) and the dilution factor according to formula 9.

$$\text{Abs. co. per volume fraction (cm}^{-1}) = \frac{(\text{weight fraction/denisty/dil. factor})}{\text{absorbance}}$$

Formula 9: Calculation of the absorbance per volume fraction in cm^{-1}.
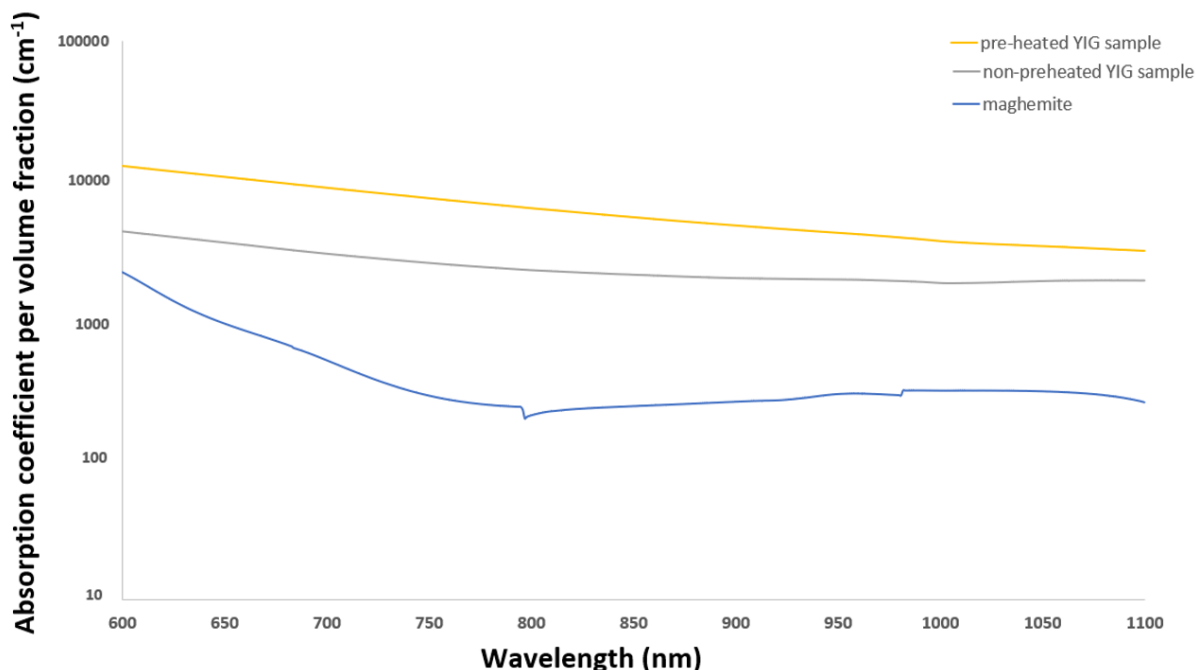
Figure 34: UV-VIS spectrum normalized over the volume fraction.

Figure 34 shows that YIG ferrofluid samples have absorption coefficient which is at least order of magnitude higher than the maghemite sample. This most likely do to large aggregate formation in the ferrofluid which causes light scattering which distored the absorption coefficient. The mesurments show that under current conditions the synthesized ferrofluids does not exhibit a lower optical absorbance. However monocrystal YIG particles have a lower optical absorption than maghemite particles (see figure 1) this still might mean that a synthezied stable ferrofluid with uniform size distrubtion has (in the abcence of light scattering effects) a lower optical absorbance than conventional ferrofluids.

5. Conclusions

The synthesis produces nanoparticles with a size which is below 50 nm, that are superparamagnetic and have composition with is consistent with yttrium iron garnet. However these particles are not uniform is size or shape indicating non-optimal crystallization. The particles also form aggregates when exposed to an external field indicating weak surface functionalization. Both these factors mean that the synthesized YIG ferrofluid does not have stable nanoparticles. The synthesized YIG ferrofluid also exhibited higher optical absorbance than the maghemite ferrofluid when adjusted for volume fraction which is most likely do to scattering effects of larger aggregates. This means that the synthesized ferrofluid is not an alternative to the conventional ferrofluids.

6. Recommendations

The most important improvement to the synthesis is preventing the aggregation the nanoparticles when exposed to an external field. This could be done looking at the stabilization process seen in the synthesis of maghemite in which citrate is used to give further surface functionalization to the particles, The increase surface functionalization means an increase in repulsion forces which increases stabilization and therefore preventing aggregation (A. van Silfhout 2020). Other stabilization techniques that could be of note are polymetric stabilizers as polymer coating could increase the steric repulsion. Furthermore the crystal structures might be improved if the YIG reaction mixture in no longer stirred in the autoclave as this causes the seed crystals to sediment towards the bottom which could improve the crystallization process.

Further optimization can also be one on the MSV setup. The current setup requires a degree of precision and timing for the measurements which is difficult to achieve due to the non-uniform thickness and length of the printed capillary holder and the optimal fit on the capillary holder onto the frame. So in order to improve the SVM setup samples holder could be printed with a more precise printer. The frame of the capillary holder could also be changed so that the holder can be clicked into position which eliminates margin error in the position of the capillary. It would also best to make the capillary holder single use as residual glue residue can make optimally positioning of new capillary difficult.

# 7. Acknowledgements

References

-J.H. Adair, E. Suvaci, J. Sindel. (2001), DLVO theory ,*Encyclopedia of materials : Science and technology,* -
-Mitsubishi chemical group,1,4-Butanediol,
https://www.m-chemical.co.jp/en/products/departments/mcc/c4/product/1201001_7922.html (accessed 1-2-2023)
-NIST chemistry WebBook, 1,4 Butandiol,
https://webbook.nist.gov/cgi/cbook.cgi?ID=C110634&Mask=4 (assessed 2-10-2022)

A. Z. Arsad, A.W.M. Zuhdi, N.B. Ibrahim, M.A. Hannan (2023), Recent Advances in Yttrium Iron Garnet Films: Methodologies, Characterization, Properties, Applications, and Bibliometric Analysis for Future Research Directions, Journal of Applied Sciences, Vol. 13, Issue 2, 1218

-S. Chikazumi, Physics of Magnetism; Wiley: New York, 1964.

-K. Kim, H. Seung Lee, M. Hee Lee and S. Ho Lee (2002). Comparative magneto-optical investigation of d-d charge-transfer transitions Fe_3O_4, $CoFe_2O_4$, and $NiFe_2O_4$*, Journal of Applied Physics 91*, p. 9974

-E.J, Bakker, P.C. Rem and N. Fraunholcz (2009) Upgrading Mixed Polyolefin Waste with Magnetic Density Separation. *Upgrading Mixed Polyolefin Waste with Magnetic Density Separation. Waste Manage. 29,* 1712-1717

-M. Inoue, T. Nishikawa, and T. Inui (1998) Glycothermal synthesis of rare earth iron garnets, Journal of Materials research, Vol. 13, No. 4, 856-860

Laboratory of colloid and surface chemistry (LCSC). *Overview of DLVO theory*, University of Geneva
https://colloid.ch/index.php?name=dlvo (accessed 13-3-2023)

-R. E. Rosensweig. Ferrohydrodynamics (2014). Dover Publishers, New York, 2nd edition,

-R. E. Rosensweig (1987). Magnetic fluids. *Annual Review of Fluid Mechanics 19,* 437-463

-W Fontijn. W.F.J. Fontijn, P.J. Zaag, van der, M.A.C. Devillers, V.A.M. Brabers, R. Metselaar (1997). Optical and magneto-optical polar Kerr spectra of Fe_3O_4 and Mg^{2+} - or Al^{3+} -substituted Fe_3O_4*, Physical Review B 56,* No. 9, 5432-5441

-M. Friàk, A. Schindlmayr, M. Scheffler (2007). Ab initio study of the half-metal to metal transition in strained magnetite. *New Journal of Physics 7, pp. 5*

-D. Jiles. (2015) Introduction to Magnetism and Magnetic Materials. *CRC press*

-R. M. Cornell, U. Schwertmann (2003), The Iron Oxides: Structure, Properties, Reactions, Occurences and Uses, Wiley-VCH Verlag GmbH & Co. KGaA,Weinheim,2nd Edition

-Liquids Research Limited, Role of a Ferrofluid in a Loudspeaker System.
https://www.liquidsresearch.com/en-GB/for_loudspeaker_applications-53.aspx
(accessed on 12-2-2022)

-J. van Rijssel, B. Kuipers (2014). "Minorim inversion program"

-D. Nguyet, N. Duong, T. Satoh, L.N. Anh, T.D Hein (2012). Temperature-dependent magnetic properties of yttrium iron garnet nanoparticles prepared by citrate sol–gel, Journal of Alloys and Compounds, Volume 541, p18-22

-J. Rongjin, Y. Wenhui, F. Caixiang, and Z. Yanwei (2013). Glycothermal synthesis of heavily Ce-doped YIG nanocrystals and their microstructures and magnetic properties. *Journal of Materials Chemistry C 1,* 1763

-A. van Silfhout. B. Erné(2019). Magnetic detection of nanoparticle sedimentation in magnetized ferrofluids. *Journal of magnetism and magnetic materials 472*, 53-58

-A. van Silfhout, H. Engelkamp, B. Erné (2020). Colloidal Stability of Aqueous Ferrofluids at 10 T. *The Journal of Physical Chemistry Letters 11*, 5908-5912

-Technical University Braunschweig, Institute for Electrical Measurement Science and Fundamental Electrical Engineering
https://www.emg.tu-bs.de/forschung/material/maghemite_e.html (accessed on 5-12-2022)

-Y.Mos. (2018) X-ray Diffraction of Iron containing samples: The importance of a Suitable Configuration. Geomicrobiology Journal 35, no 6 511-517.

-Y. Xiaowei, Z. Yanwei, M. Leiqing, H. Longxiang (2011) *Oleic acid assisted glycothermal synthesis of cuboidal $Ba_{0.6}Sr_{0.4}TiO_3$ nanocrystals and their ordered architectures via self-assembly, Journal of Colloid and Interface science 357,* 308-316

-W Fontijn et al. (1997). Optical and magneto-optical polar Kerr spectra of Fe_3O_4 and Mg^{2+} - or Al^{3+} -substituted Fe_3O_4, *Physical Review B 56,* No. 9, 5432-5441

-A. Prabhaker, Daniel D. Stancil (2009). Spin Waves: Theory and applications; Appendix A Properties of Yttrium–Iron–Garnet (YIG), 333

-H. A. Shokrollahi, (2017). Review of the Magnetic Properties, Synthesis Methods and Applications of Maghemite. *Journal of Magnetism and Magnetic Materials 426,* 74-81.

-L. Oliver, I. Brown, (1951).The Clausius-Clapeyron equation, Syracuse University , *Journal of Chemical Education 28 no. 8,*428 ,Syracause, New York

-D.Swinehart (1964). The Beer-Lambert law, *Journal of chemical education 39, no 7*, 333

Appendices

Appendix A: TEM samples of synthesized nanoparticles
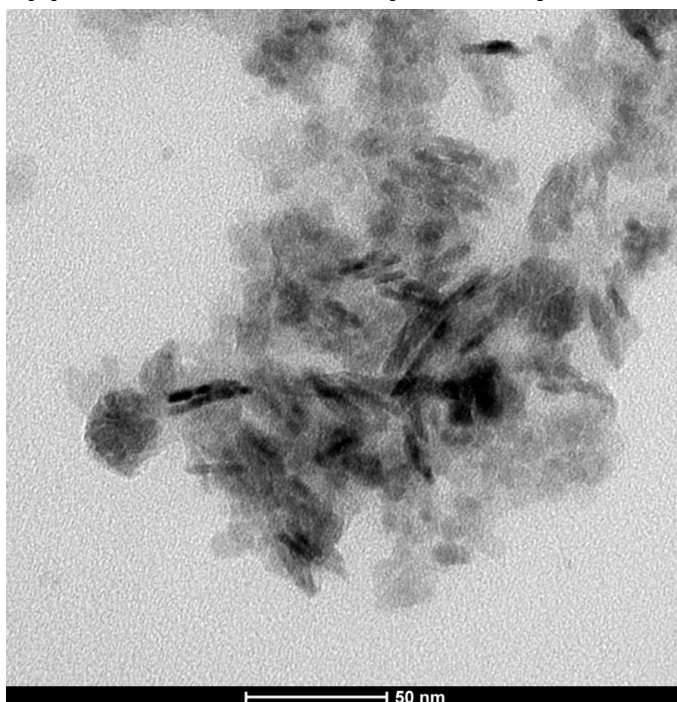
Figure A.1: TEM picture of 3 hour synthesized nanoparticles with 5 mg of YAG added
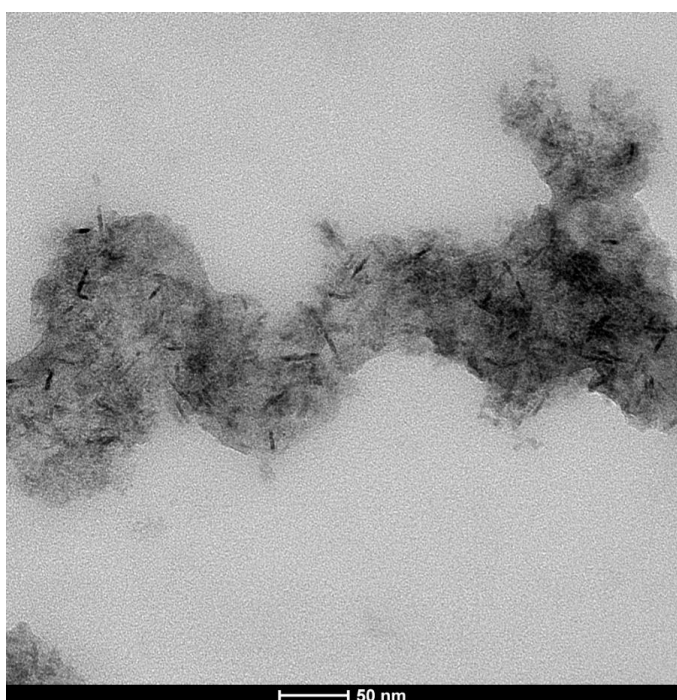
Figure A.2: TEM picture of 3 hour synthesized nanoparticles with 10 mg of YAG added
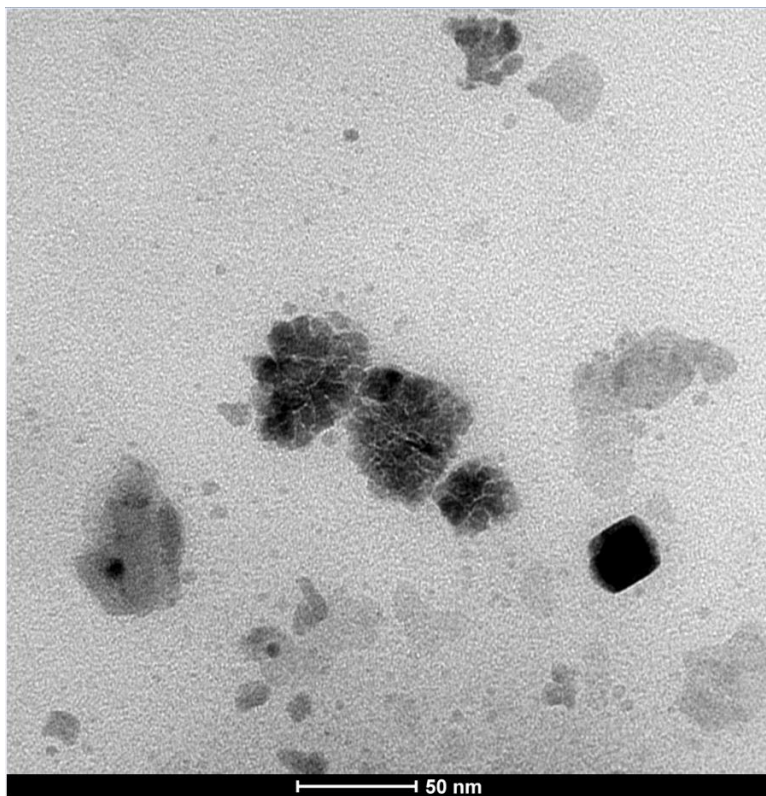
Figure A.3: TEM picture of 3 hour synthesized nanoparticles with 15 mg of YAG added
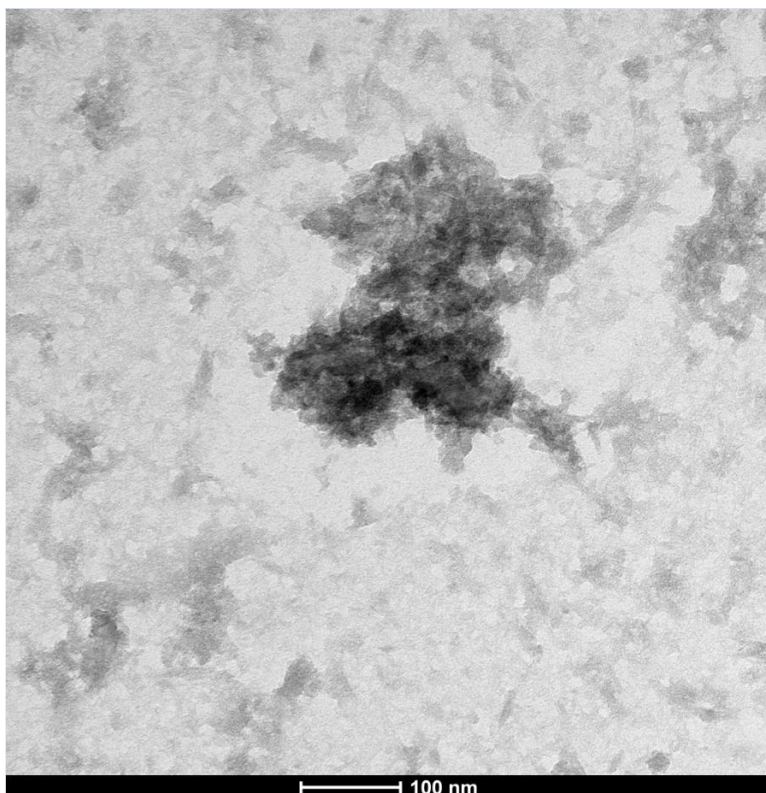
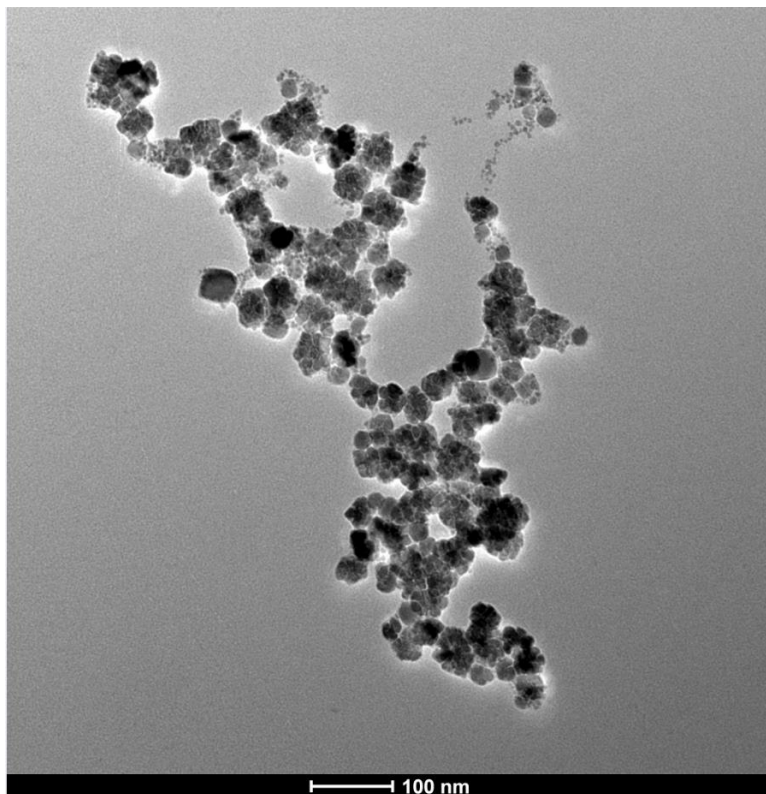**Figure A.4:** TEM picture of 8 hour synthesized nanoparticles with 15 mg of YAG added (without pre heated reaction vessel)

Figure A.5: TEM picture of 8 hour synthesized nanoparticles with 15 mg of YAG added (without heated reaction vessel.
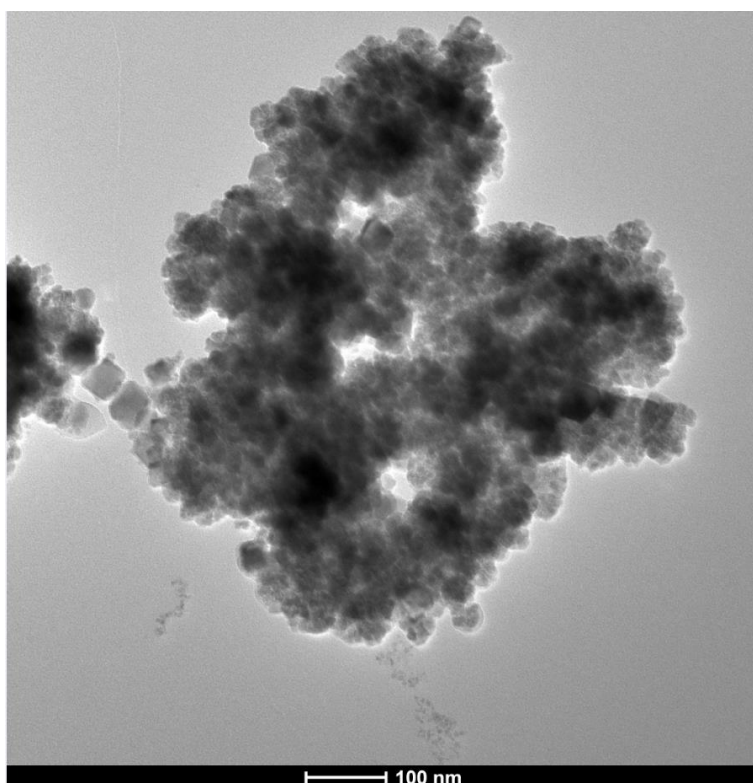
Figure A.6: TEM picture of 8 hour synthesized nanoparticles with 15 mg of YAG added (without heated) (repeat synthesis) reaction vessel.
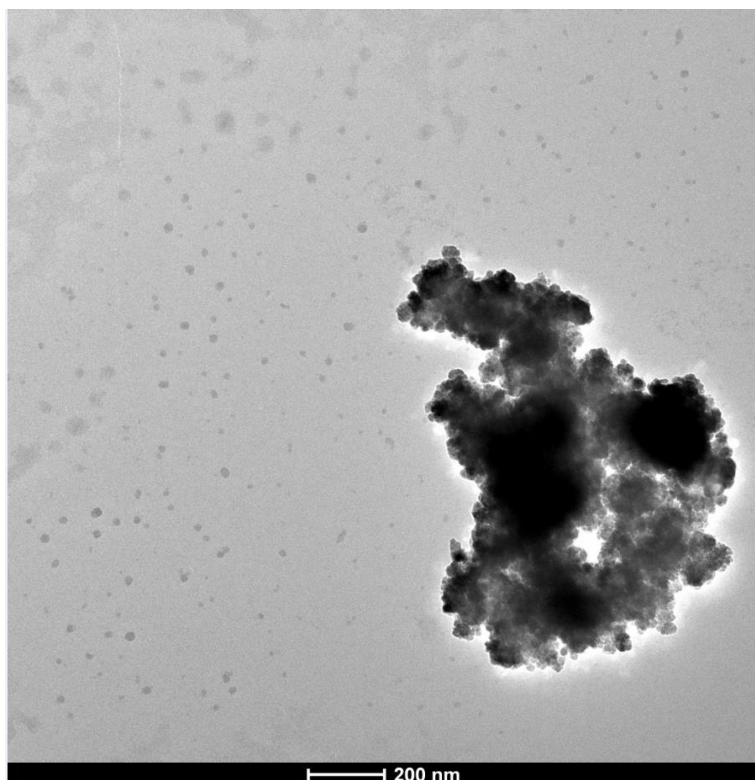
Figure A.7: TEM picture of 8 hour synthesized nanoparticles with 15 mg of YAG added (heated) synthesis) reaction vessel.
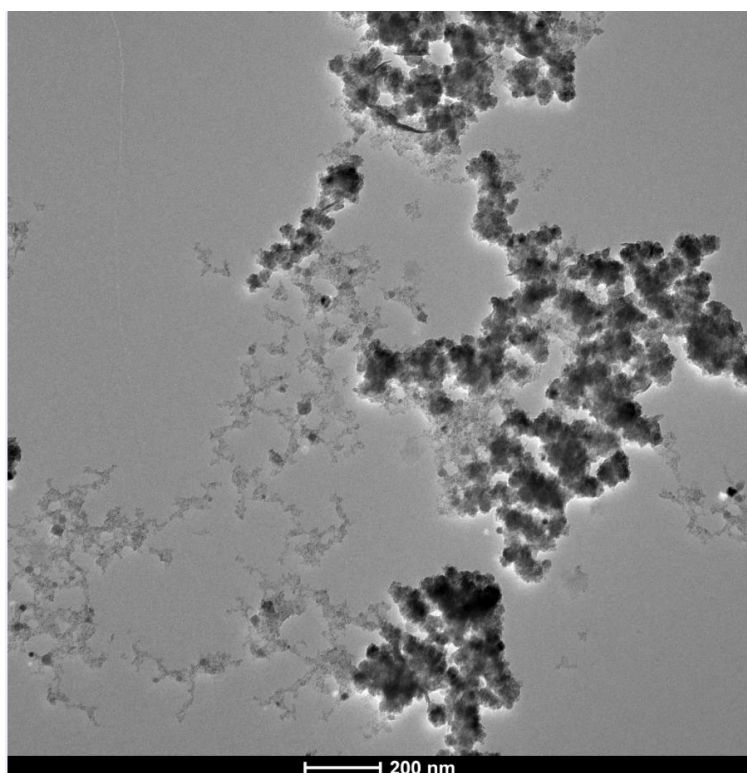
Sample A.8: TEM picture of 8 hour synthesized nanoparticles with 15 mg of YAG added (heated) synthesis) reaction vessel without ultra-sonication/centrifugation

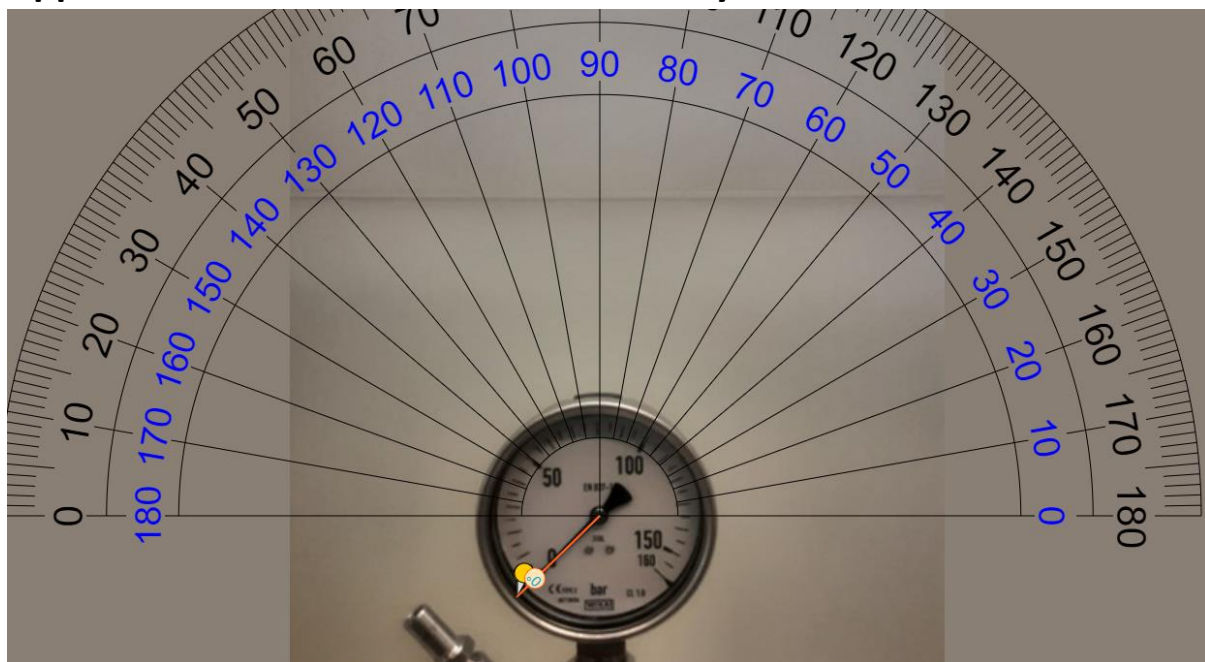## Appendix B: Pressure measurement of synthesis

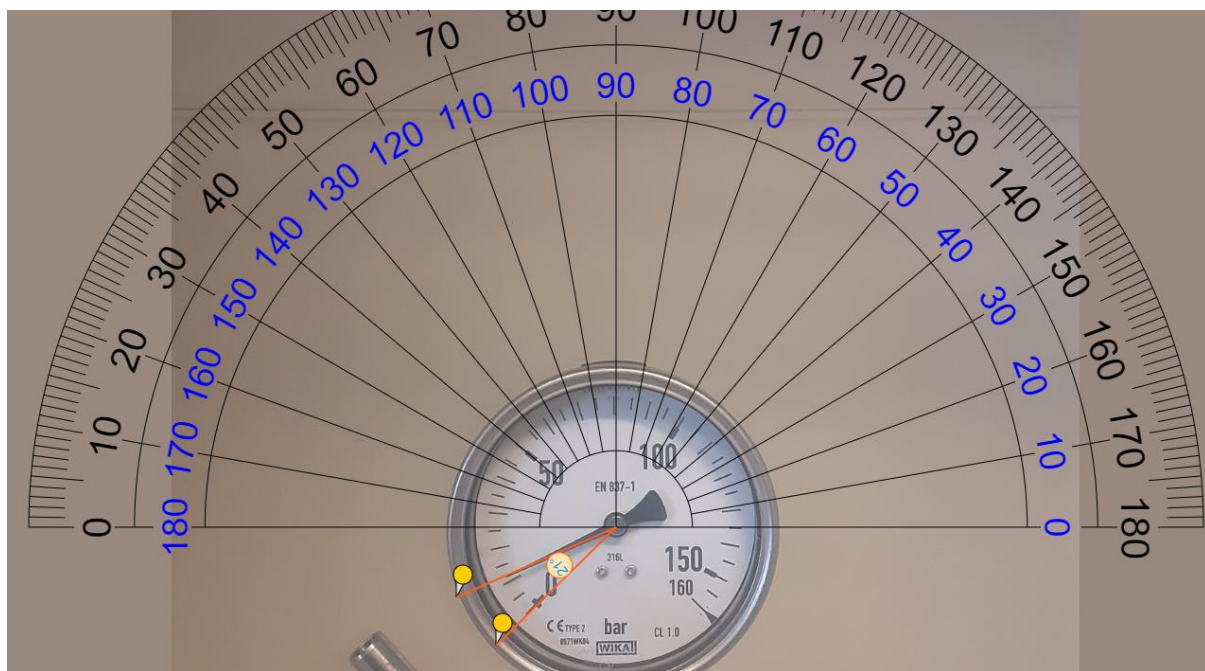**Figure B.1:** Pressure measurement of non-preheated blank at t_0

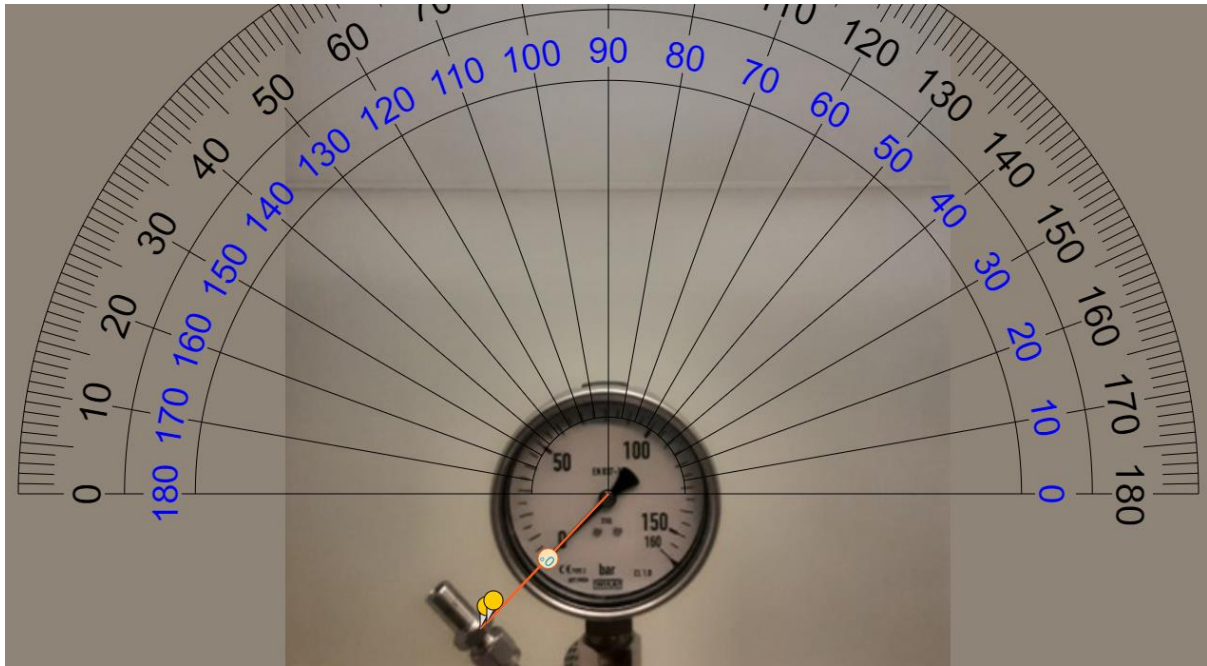**Figure B.2:** Pressure measurement of non-preheated sample at t_{410min}

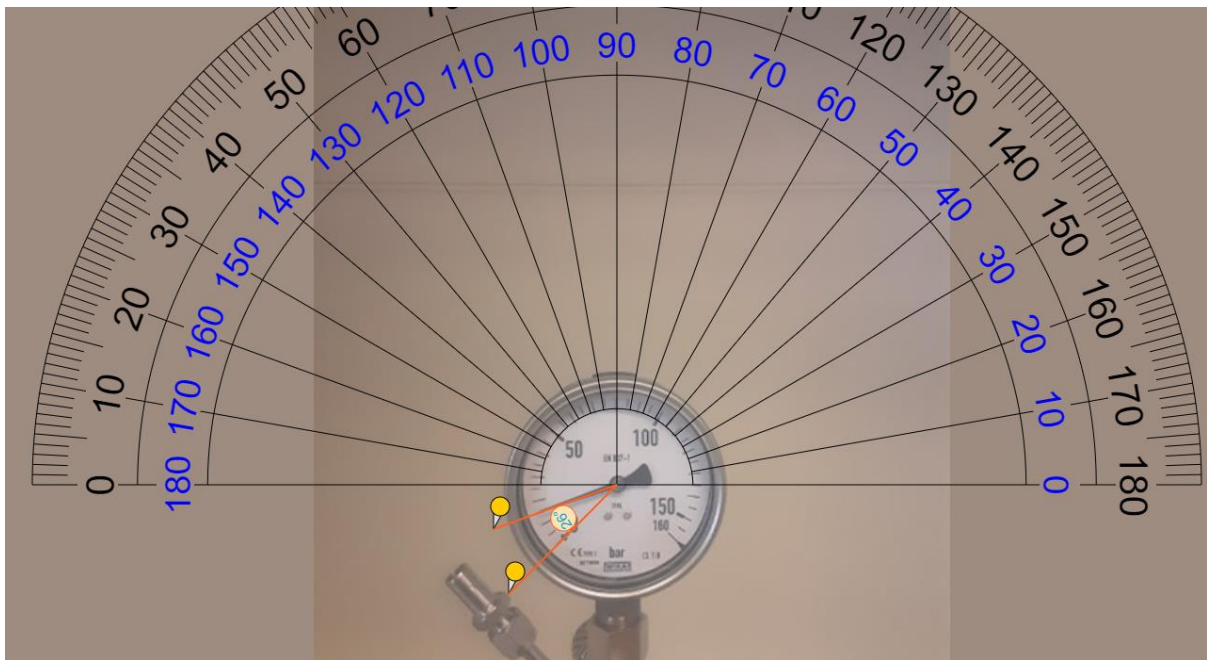**Figure B.3:** Pressure measurement of preheated blank at t_0

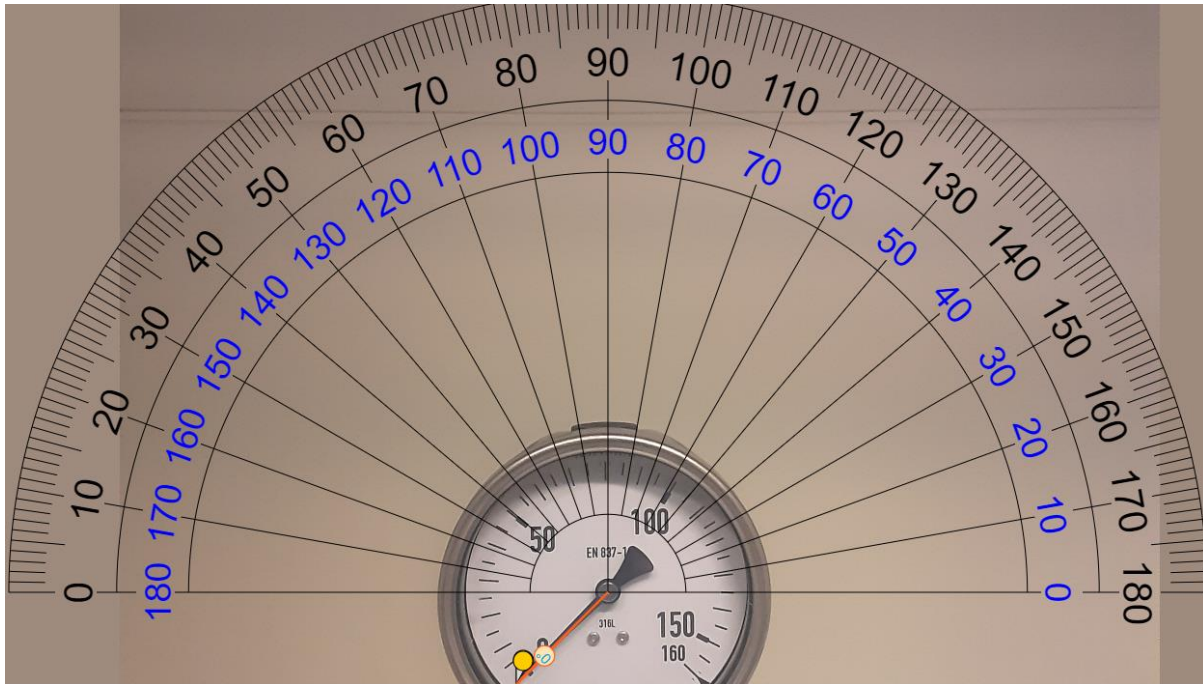**Figure B.4:** Pressure measurement of preheated blank at t_{450min}

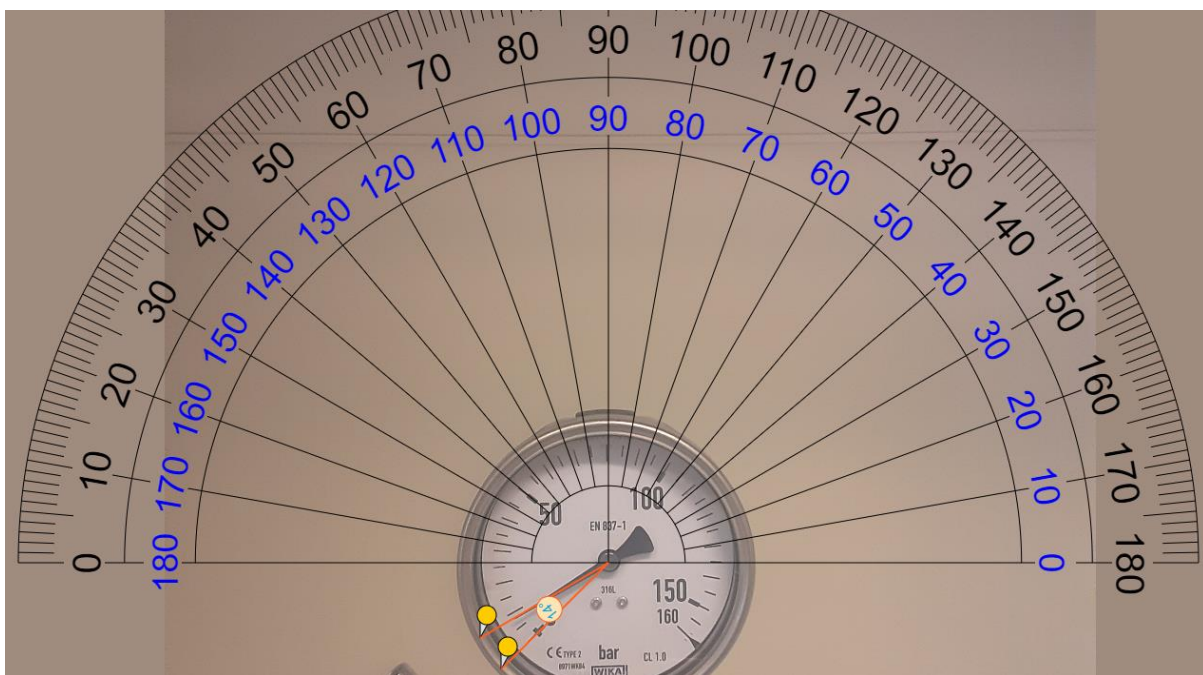**Figure B.5:** Pressure measurement of non-preheated sample at t_0

Figure B.6: Pressure measurement of non-preheated sample at t_{450min}
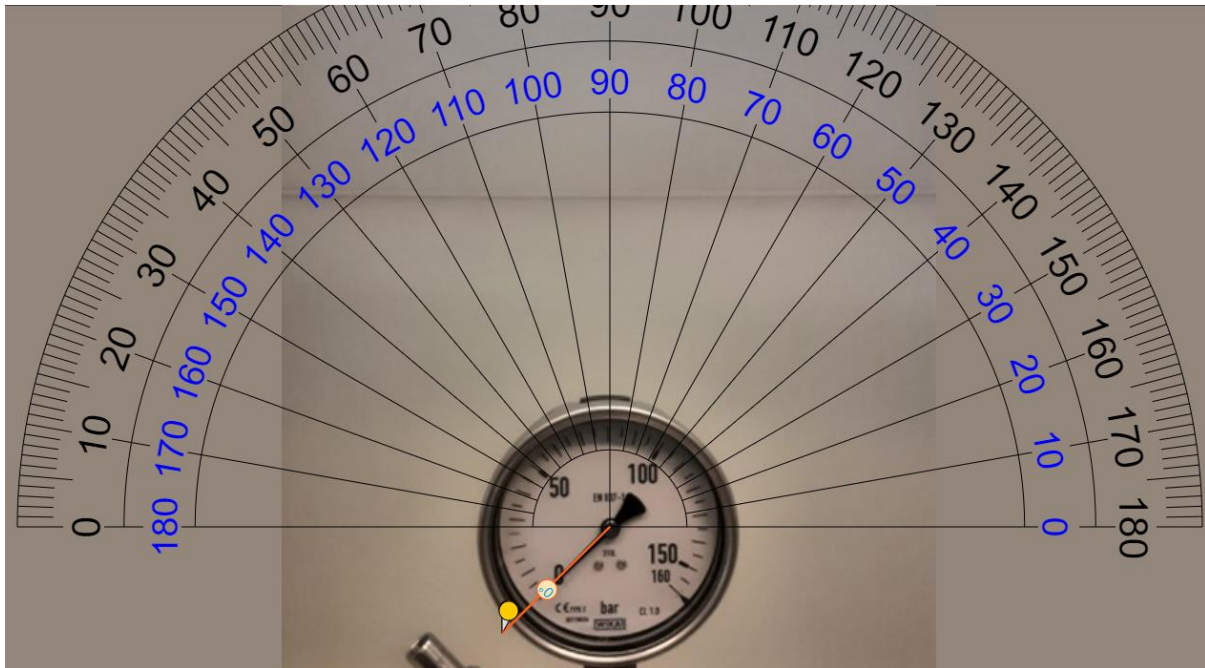
Figure B.7: Pressure measurement of preheated sample at t_0
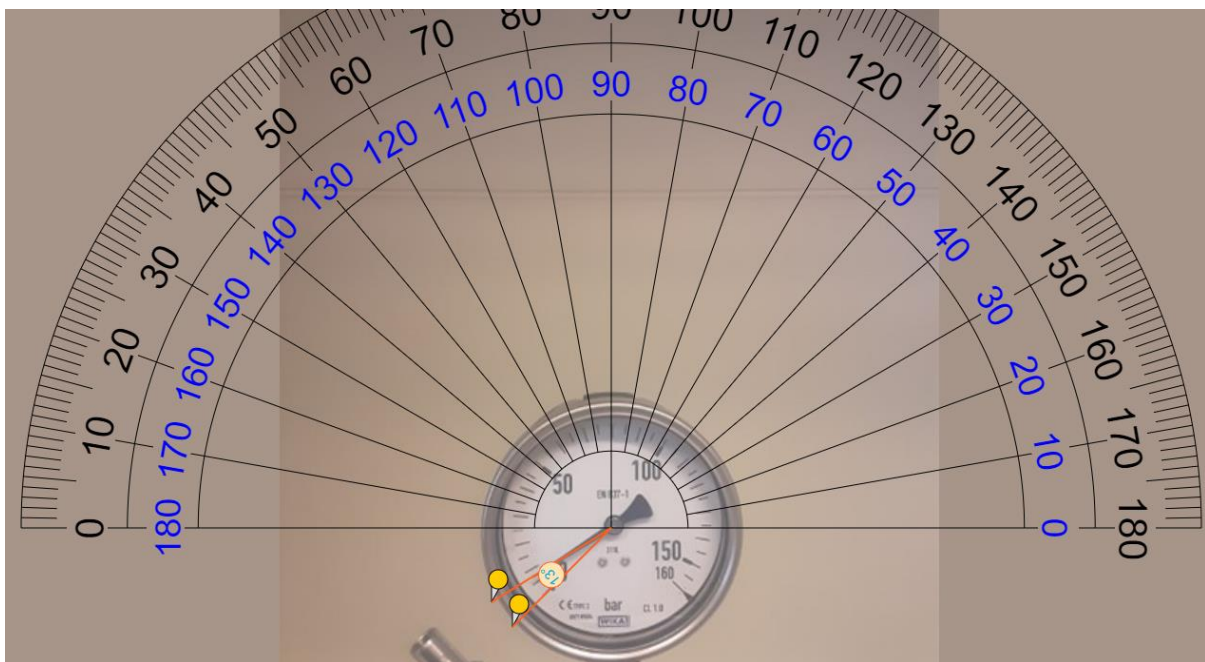

Figure B.8: Pressure measurement of preheated sample at t_0

Appendix C: VSM of synthesized ferrofluids

Figure C.1: VSM of maghemite
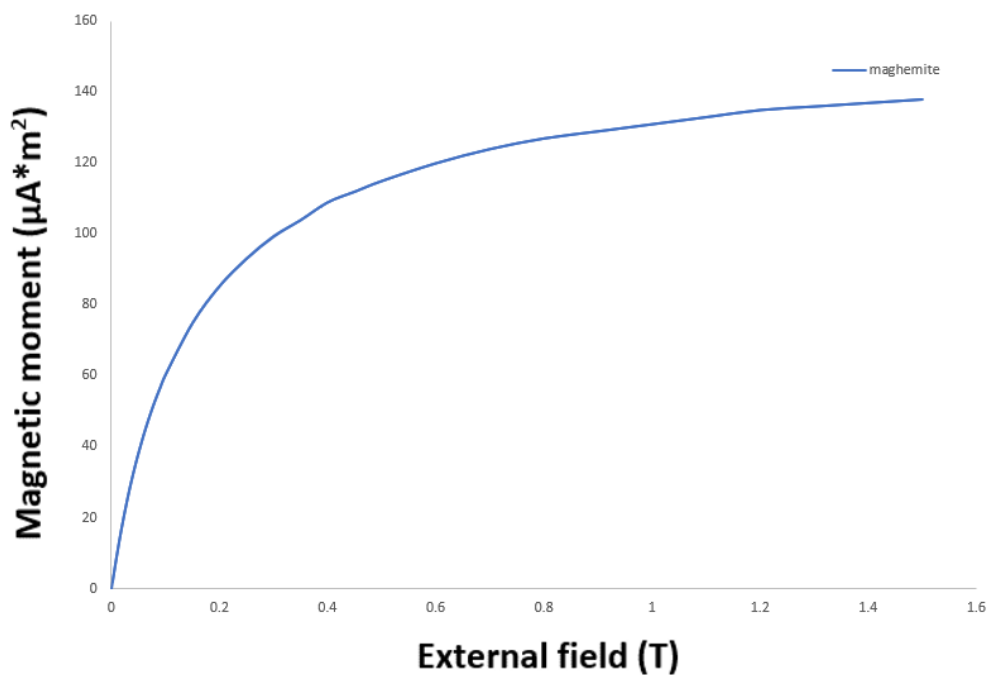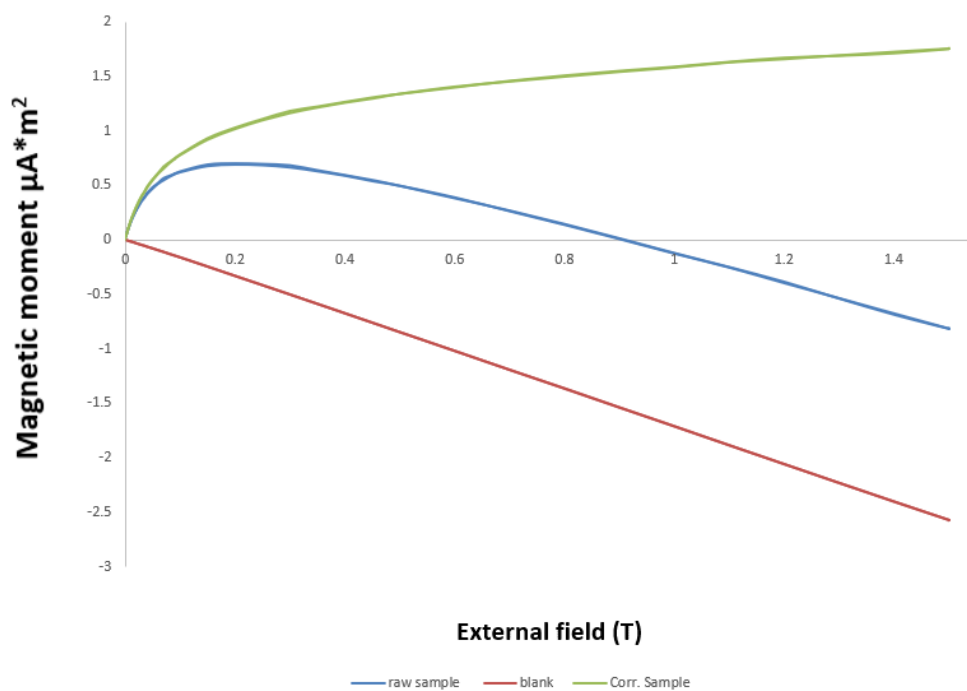

Figure C.2 VSM of magnetite
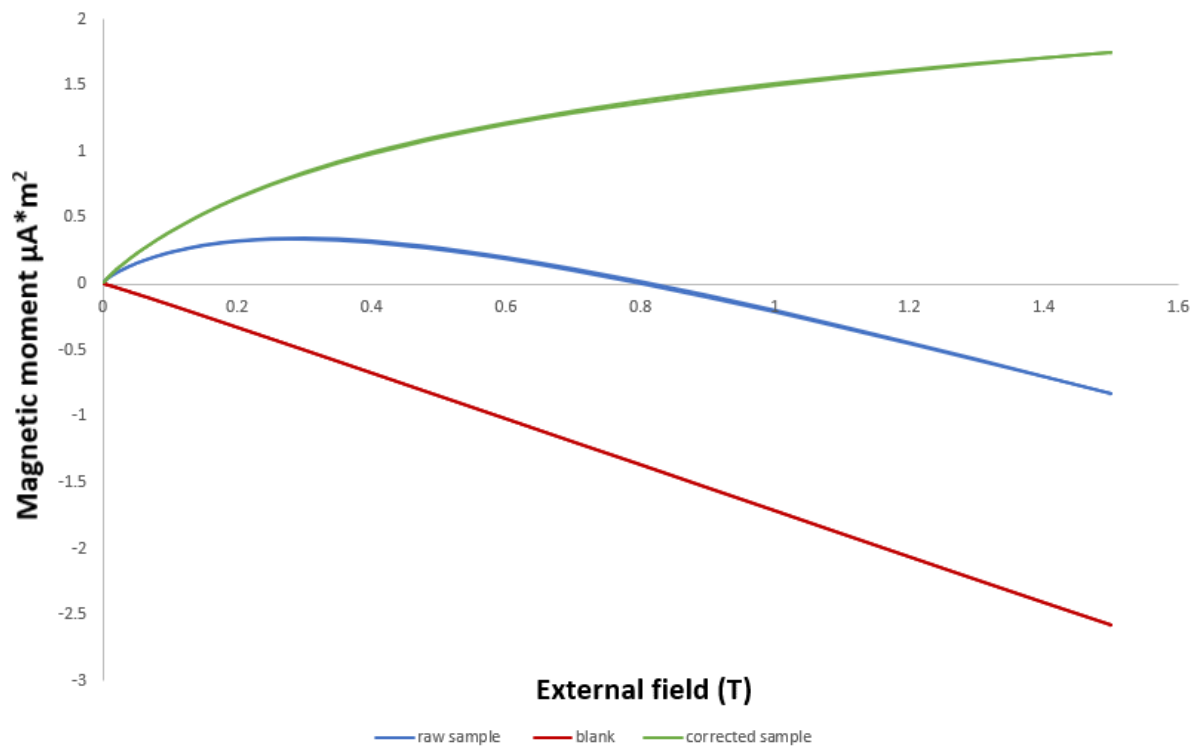
Figure C.3: VSM results of YIG sample with 5 mg YAG added 4 hour synthesis
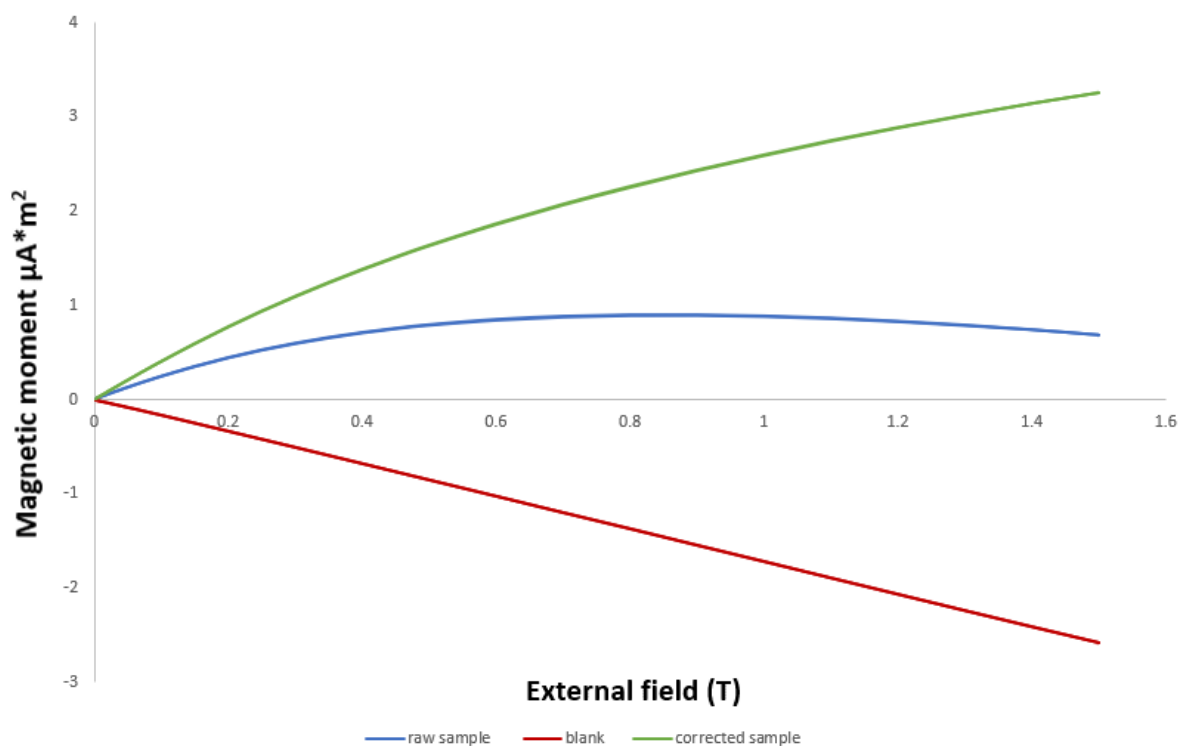
Figure C.4: VSM results of YIG sample with 10 mg YAG added 4 hour synthesis
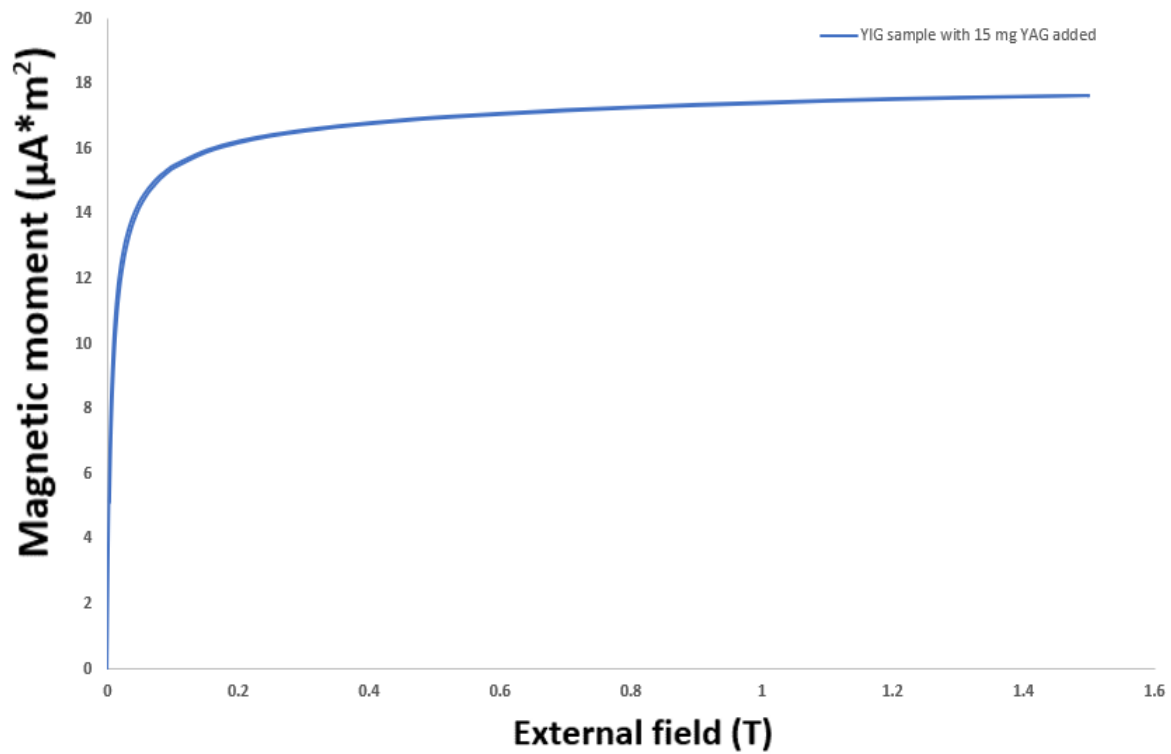
Figure C.5: VSM results of YIG sample with 15 mg YAG added 7-8 hour synthesis pre heated
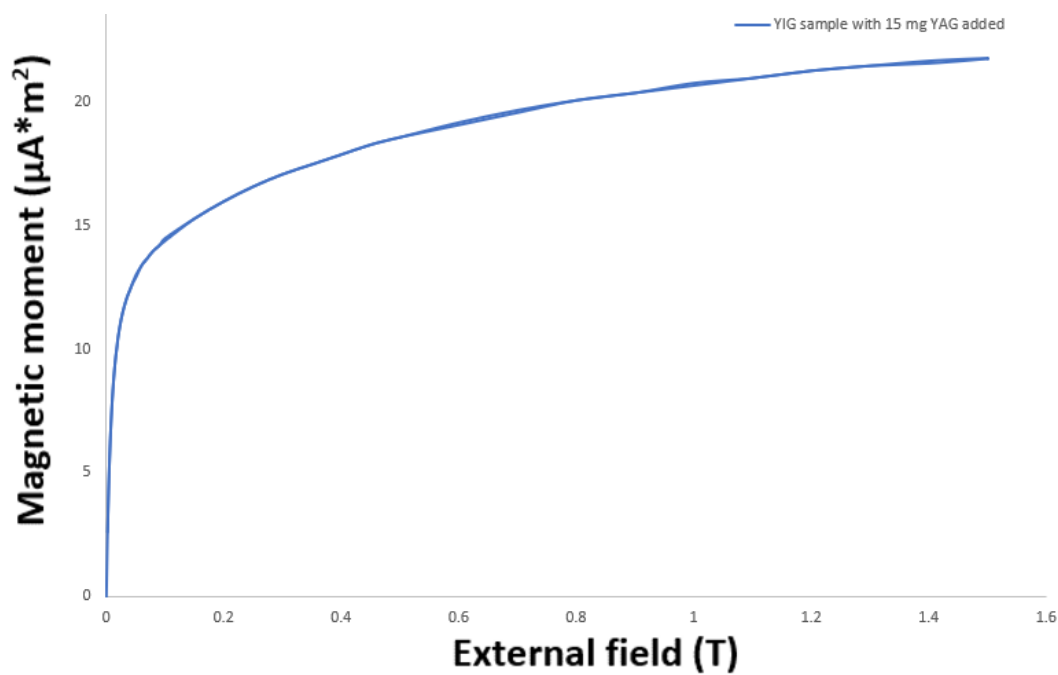
Figure C.6: VSM results of YIG sample with 15 mg YAG added 7-8 hour synthesis non-preheated
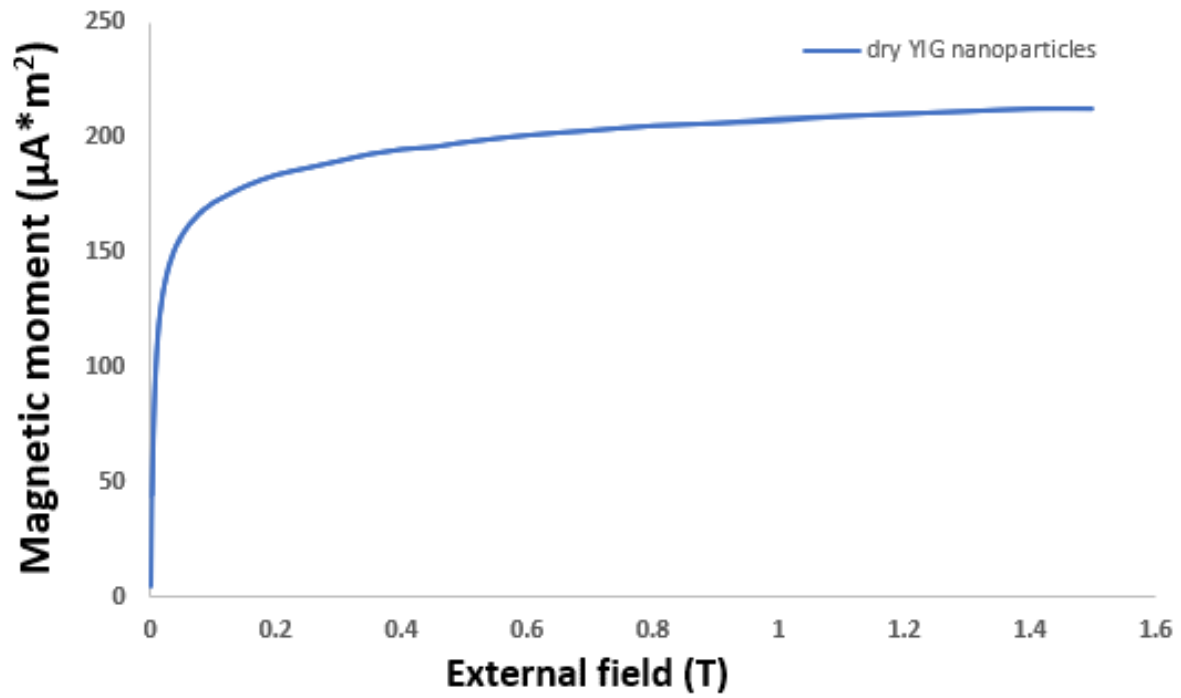
Figure C.7: VSM results of dry nanoparticles of from ferrofluid seen in C.5
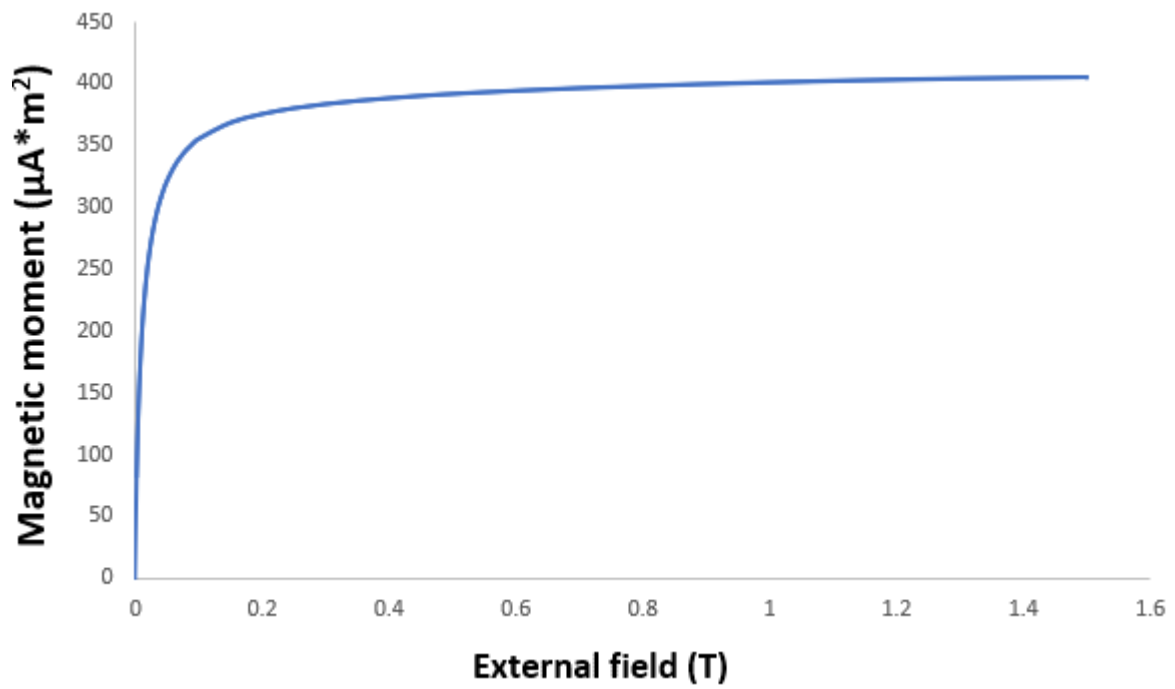
Figure C.8: VSM results of nanoparticles of from ferrofluid seen in C.6

Appendix D: Magnetic dipole moment distribution of ferrofluids
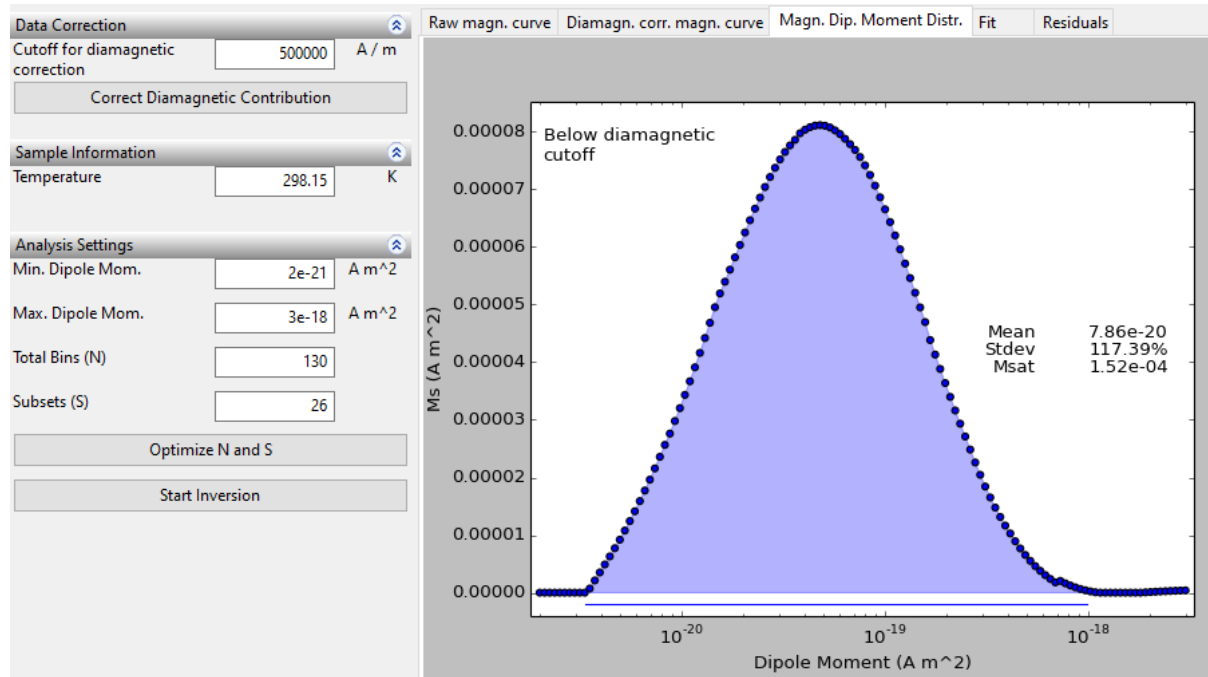
Figure D.1: Magnetic dipole moment distribution of maghemite
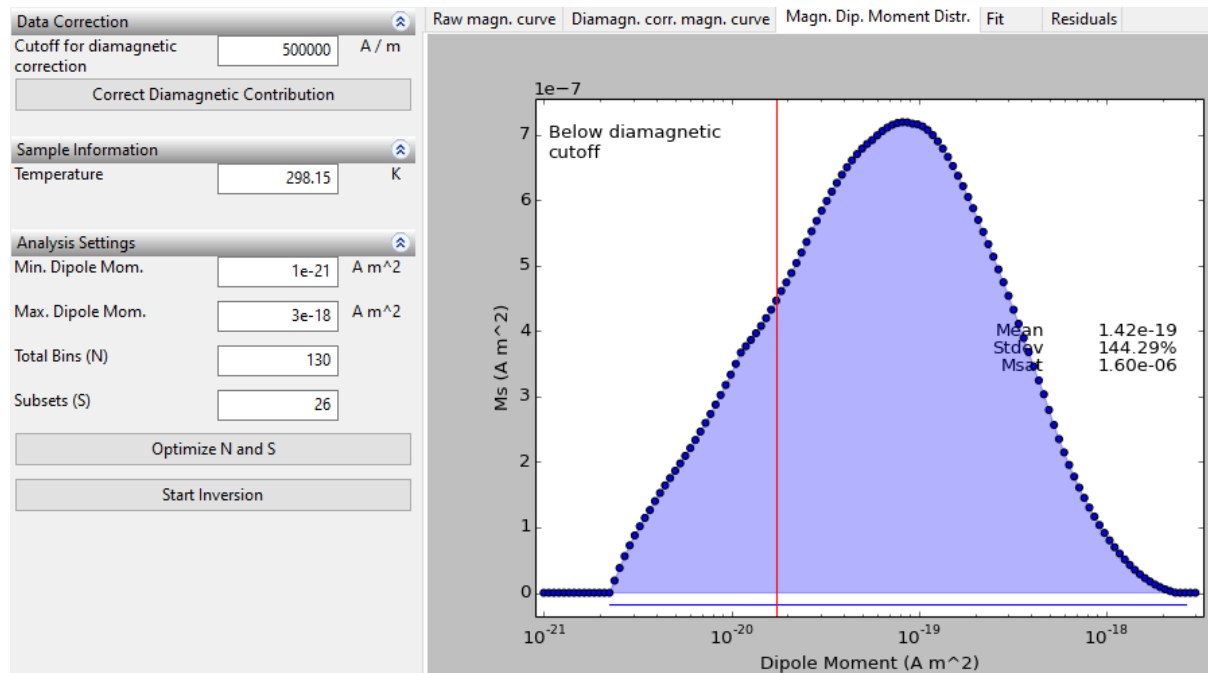
Figure D.2: Magnetic dipole moment distribution of magnetite
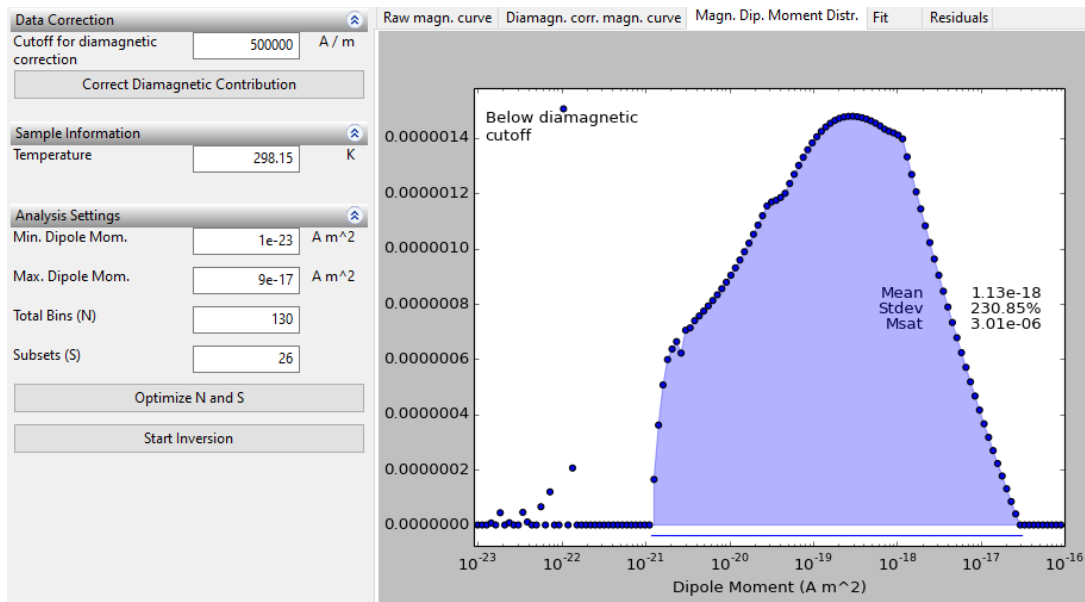
Figure D.3: Magnetic dipole moment distribution of YIG sample with 5 mg YAG added 4 hour synthesis
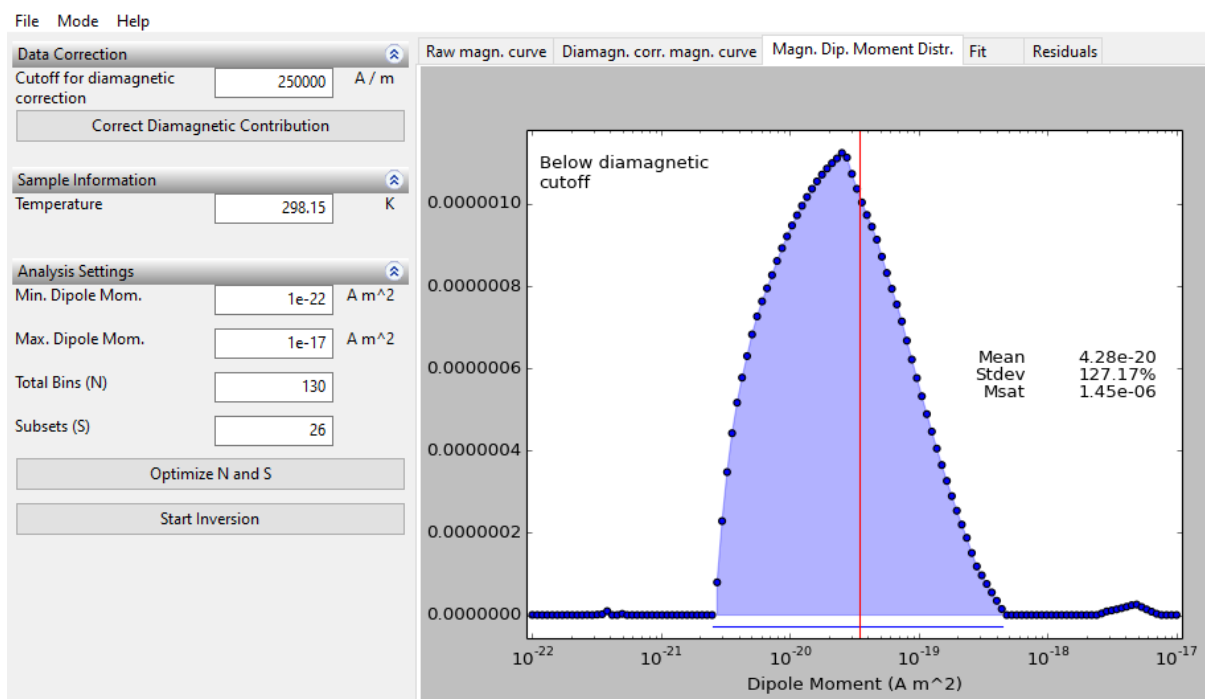
Figure D.4: Magnetic dipole moment distribution of 10 mg YAG added 4 hour synthesis
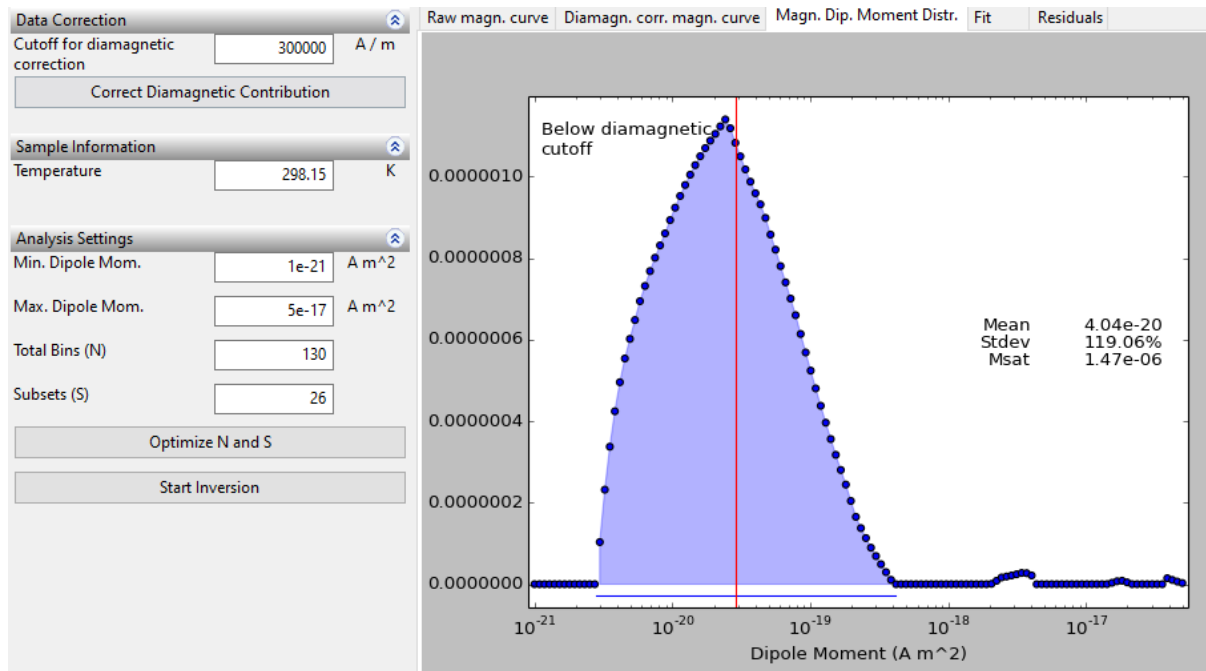
Figure D.4: Magnetic dipole moment distribution of YIG sample with 15 mg YAG added
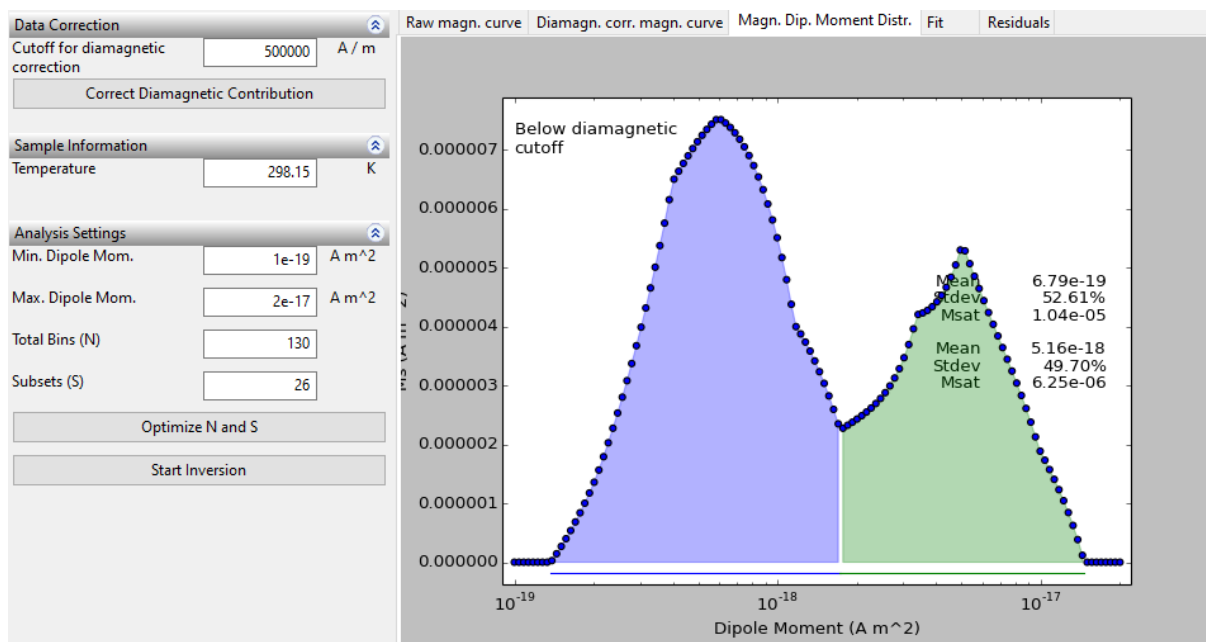
Figure D.5: Magnetic dipole moment distribution of YIG sample with 15 mg YAG added 7-8 hour synthesis preheated
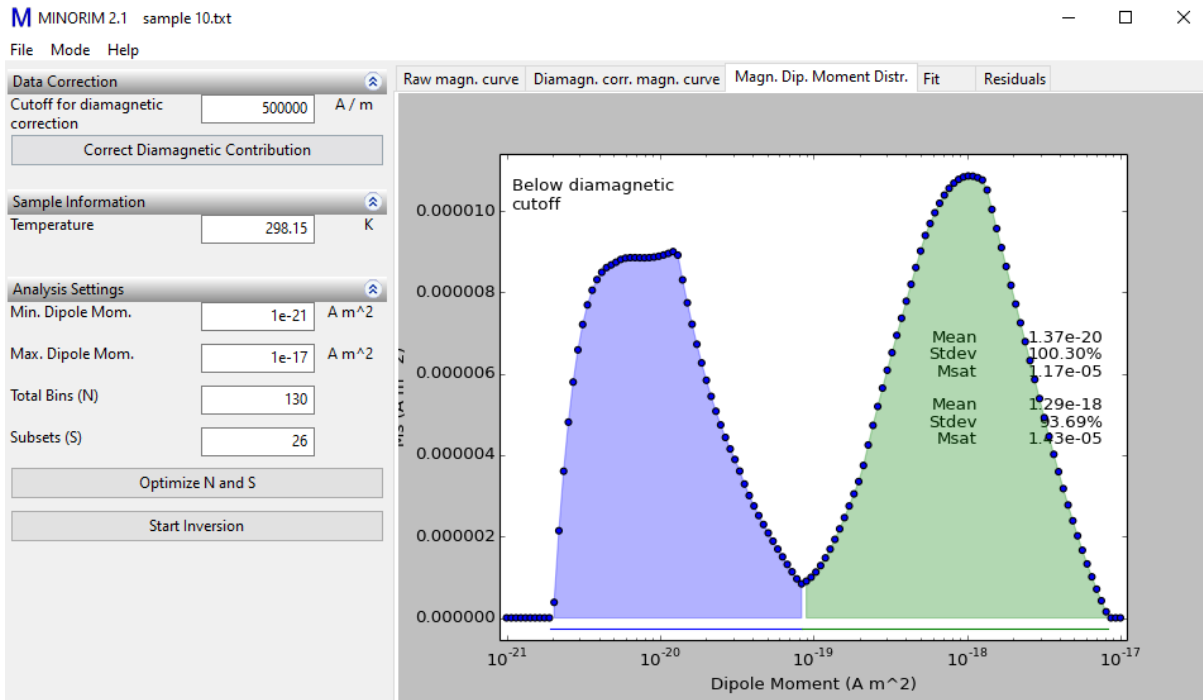
Figure D.6: Magnetic dipole moment distribution of YIG sample with 15 mg YAG added 7-8 hour synthesis non-preheated
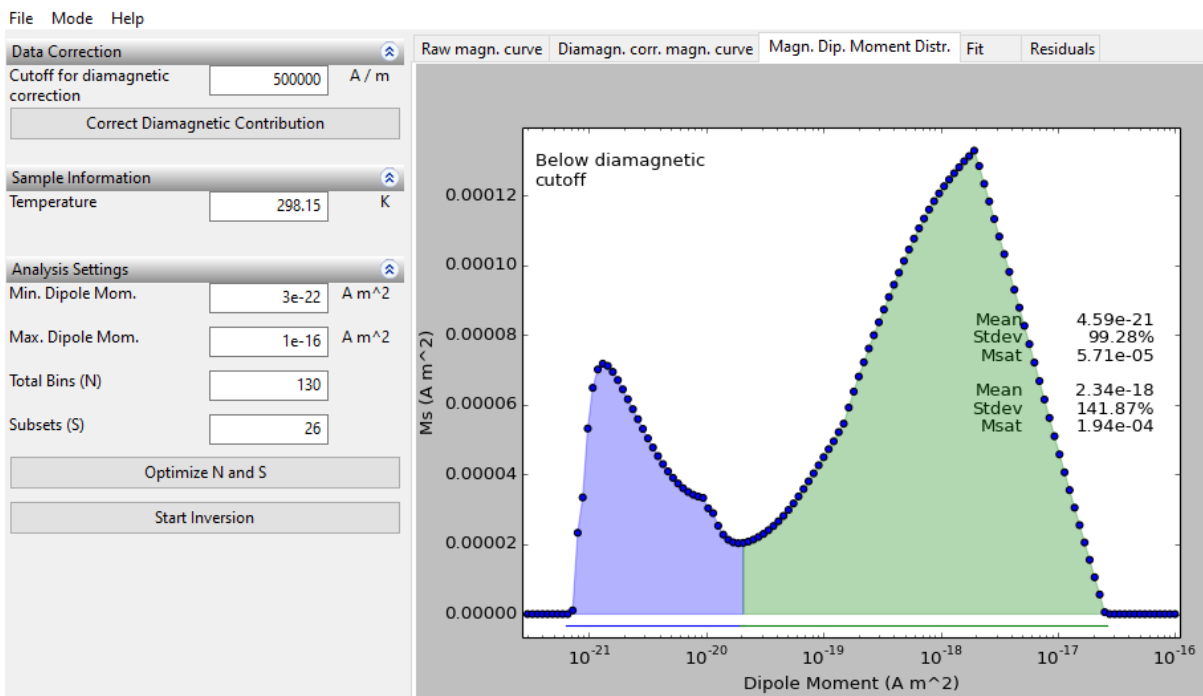
Figure D.7: Magnetic dipole moment distribution of the dry nanoparticles of the YIG sample with 15 mg YAG added 7-8 hour synthesis pre-heated
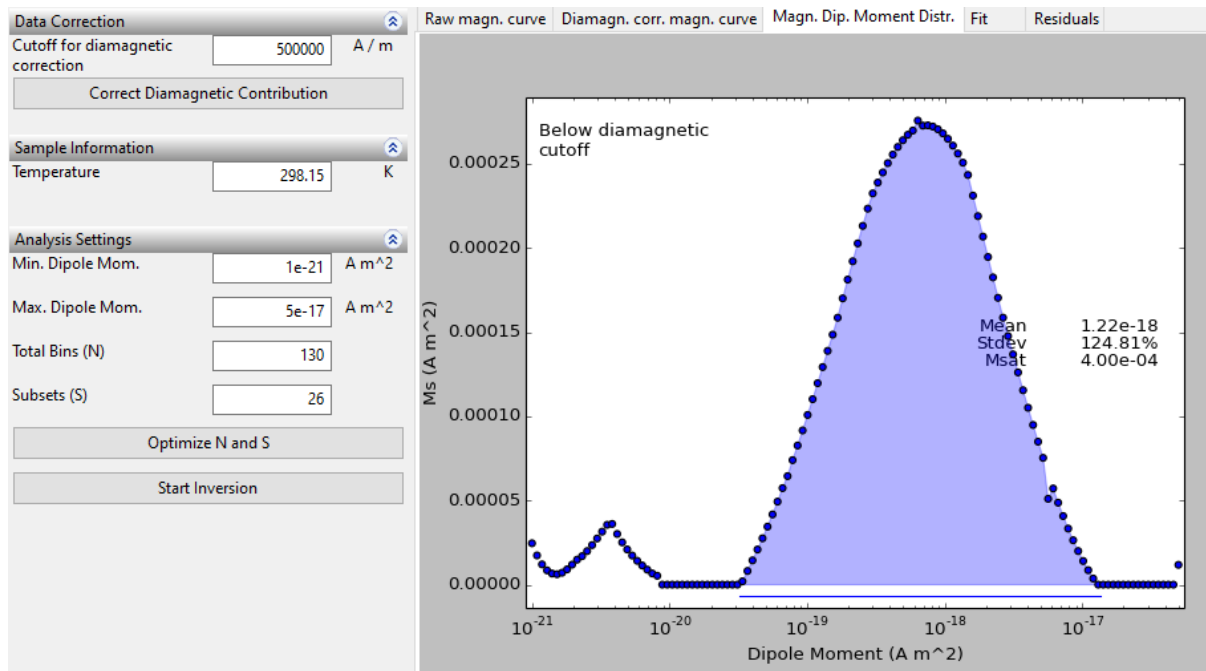
Figure D.8: Magnetic dipole moment distribution of dry nanoparticles of the YIG sample with 15 mg YAG added 7-8 hour synthesis non pre-heated

Appendix E: Sedimentation profiles, relative profiles of synthesized ferrofluids
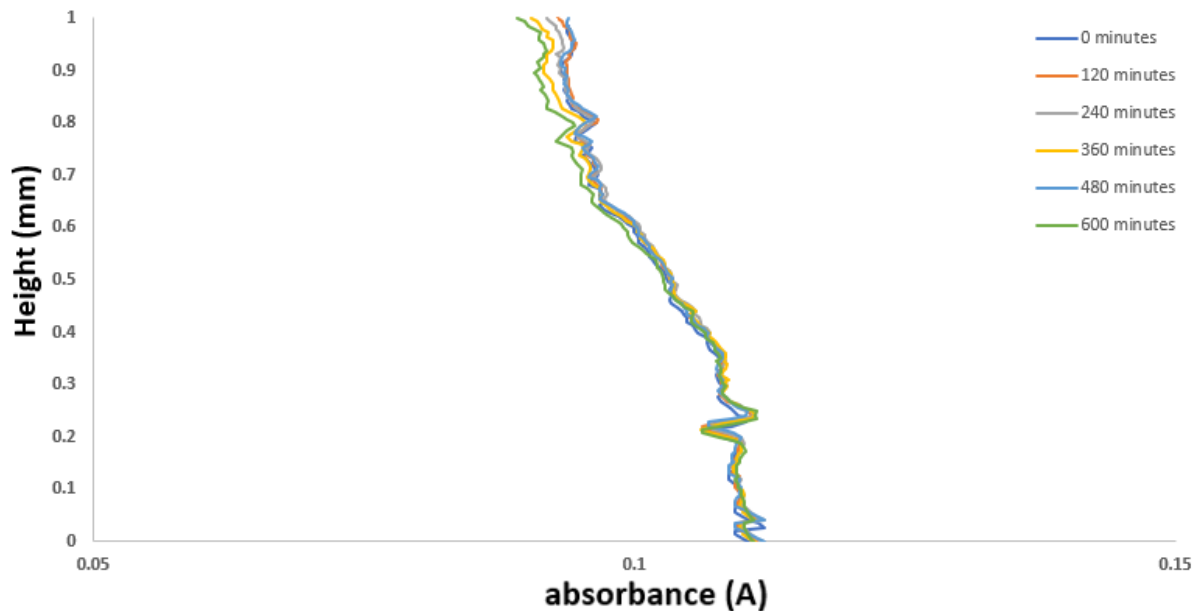
Figure E.1: Absorbance profile of YIG sample with 15 mg YAG added 7-8 hour synthesis pre-heated
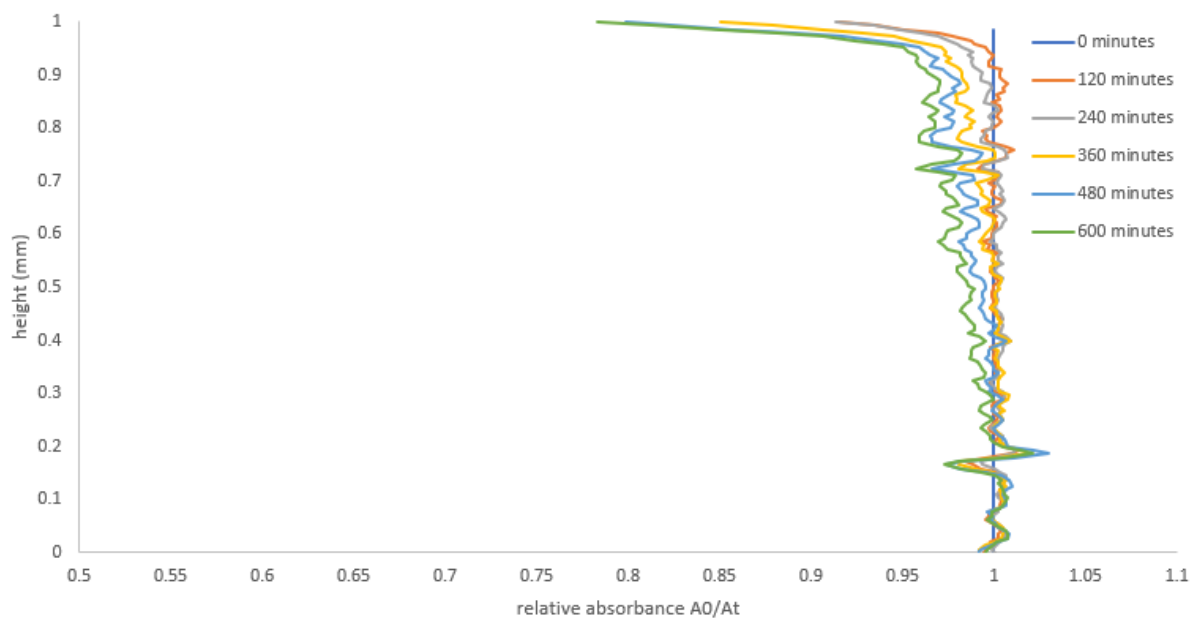
Figure E.2: Relative absorbance profile of YIG sample with 15 mg YAG added 7-8 hour synthesis preheated

The trendline equation shown on the chart: $y = -0.0007x + 1.0356$
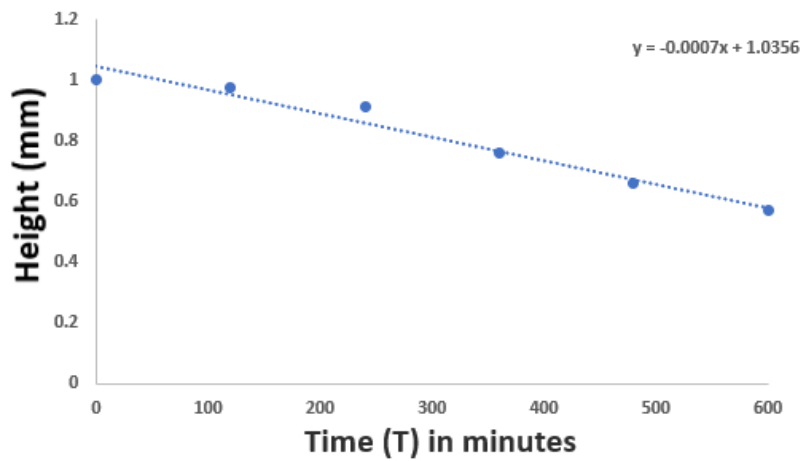
Figure E.3: Time of height at which the relative absorption is 95% of a_0 of YIG sample with 15 mg YAG added 7-8 hour synthesis preheated
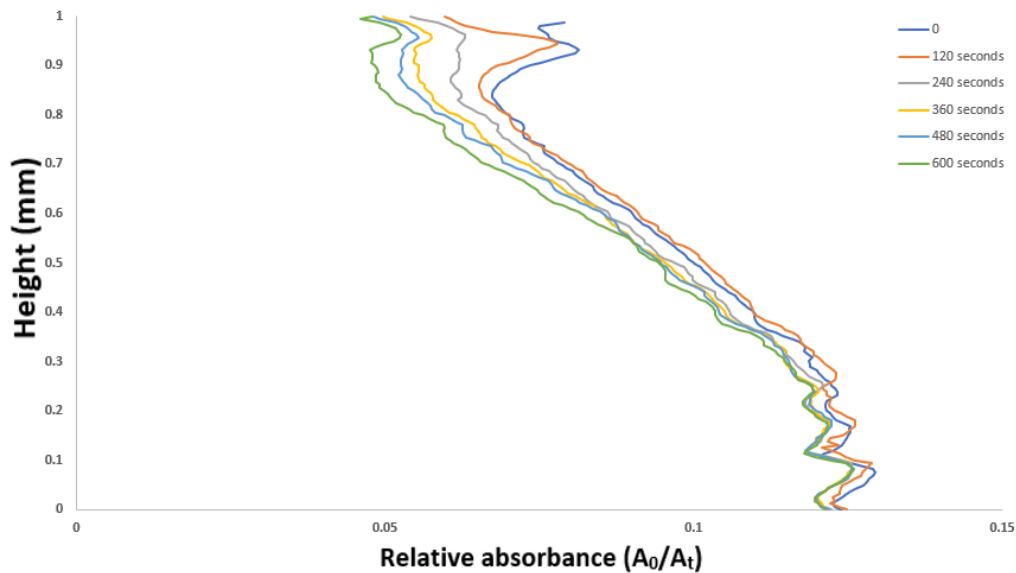
**Figure E.4:** Absorbance profile of YIG sample with 15 mg YAG added 7-8 hour synthesis non preheated
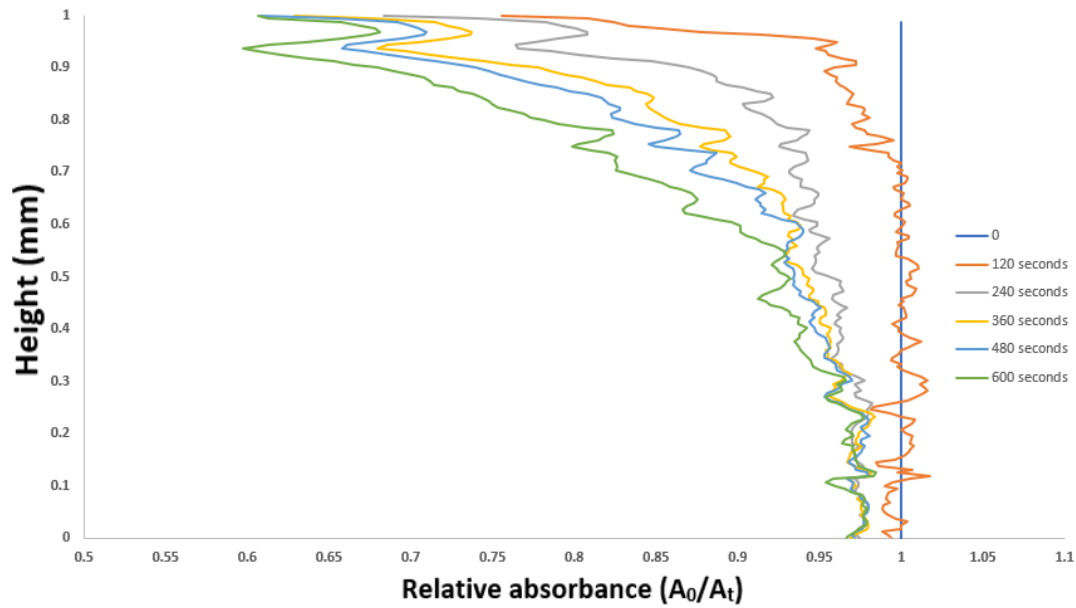
Figure E.5: relative absorbance profile of YIG sample with 15 mg YAG added 7-8 hour synthesis non preheated

$$y = -0.0012x + 0.9859$$

Figure E.6: Time of height at which the relative absorption is 95% of a_0 of YIG sample with 15 mg YAG added 7-8 hour synthesis non-preheated

Appendix F: Python scripts for Magnetic sedimentation velocimetry

```python
import rawpy                          # processes the raw NEF  file image data
import math                          # modules to do the calculation for absorption
import numpy as np                   # processes the color data into a array
import os                            # allows us to run a command in the Python script


def image_processeing(f,h_pix):      # defines the function used to calculate the concentration profile
    location_blank = 'C:/Users/blanco/DSC_0079.NEF'     # blank sample
    raw1 = rawpy.imread(f)                        # opens RAW  sample picture
    rgb1 = raw1.postprocess()                     # extracts pixel data
    raw_blank = rawpy.imread(location_blank)      # opens RAW blank picture
    rgb_blank = raw_blank.postprocess()           # extracts pixel data

  K = (3720/2490)      #divides total number of vertical pixel lines over the first line of the capillary
  G = (3720/2283)      #divides total number of vertical pixel lines over the first line of the capillary for blank

top_row1 = int(len(rgb1)/K)            # sets top row of pixels sample
height = np.zeros(h_pix)               # generates a list of zeros equal to the amount of pixels used
for i in range(len(height)):           # sets the value total height of the vertical axis to 1
  height[i] = 1 - (i / h_pix)

top_rowb = int(len(rgb_blank)/G)       # does the same but for blank image
  height = np.zeros(h_pix)

for i in range(len(height)):
  height[i] = 1 - (i / h_pix)
h=2500                                 # sets horizontal boundary left side
w=2600                                 # sets horizontal boundary right side          # part 1
```
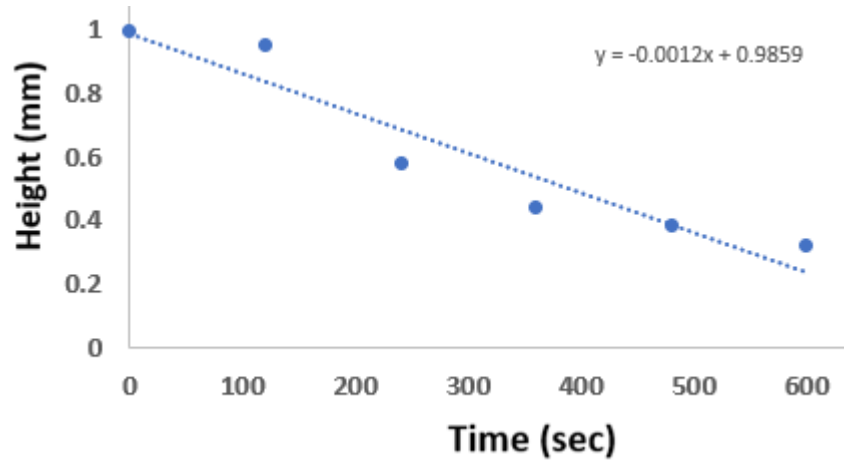
```python
rgb1_2 = rgb1[top_row1:top_row1 + h_pix,h:w]   #extracts color data form every pixel in matrix
rgb2_blank = rgb_blank[top_rowb:top_rowb + h_pix,h:w]   #extracts color data form every pixel in matrix for blank
av_abs = np.zeros(h_pix)               # generates a list of zeros equal to the amount of pixels used


c = 2
c2 = 2                                  # sets the color channel used (0=red,1=green,2=blue)

for i in range(len(av_abs)):           # used to iterate over each pixel row
    sum_gr = 0                          # sets the value of the sum to zero
    for j in range(len(rgb1_2[i])):     # used to iterate over each pixel in the row
        if rgb1_2[i][j][c]==0:          # check if value is zero set to 1 prevents divide by zero
            rgb1_2[i][j][c] = 1
        if rgb2_blank[i][j][c2]==0:     # check if value is zero set to 1 prevents divide by zero blank
            rgb2_blank[i][j][c2] = 1

    pix_abs = -math.log(rgb1_2[i][j][c]/rgb2_blank[i][j][c2] ,10) # calculates the absorbance of each pixel corrected for background
    sum_gr += pix_abs               # adds the absorbance value to the sum_gr(which is zero)
av_abs[i] = sum_gr / len(rgb1_2[i]) # divides the sum of the absorbance data of a pixel row over the number of pixels in row creating the-
                                    #  average value of each pixel row
    return av_abs                       # return the absorbance data as variable          # part 2
```

```python
directory ='C:/Users/user_local/Desktop/Data/kevin YIG 3% particles/8h/2nd measurement/small particles'
                                    # sets the dir path
filename = '*.NEF'                  # sets the extension each file need to have to be processed
h_pix = (160)                       # sets the total number of pixel rows
filelist = os.listdir(directory)       # opens dir path
data = np.zeros([len(filelist),h_pix]) # generates a list of zero equal to the amount of files processed and the total number of pixel rows

for n in range(len(filelist)):             # used to iterate over every file in dir
    f = os.path.join(directory, filelist[n])   # joins dir path with the file list and sets
    data[n,:] = image_processeing(f,h_pix)  # gets absorbance profile for every file in dir          # part 3
```

Figure F.1: Calculating concentration profile without loop

```
import rawpy                    # processes the raw NEF file image data
import math                     # modules to do the calculation for absorption
import numpy as np              # processes the color data into a array
from PIL import Image           # displays image in matrix
import matplotlib.pyplot as plt # used to create graph

location_1 = 'C:/Users/sample t=0/DSC_0452.NEF' # location of the .NEF image of the sample
location_2 = 'C:/Users/sample t=2 minutes/DSC_0453.NEF' # location of the .NEF image of the sample
location_3 = 'C:/Users /sample t=4 minutes/DSC_0454.NEF' # location of the .NEF image of the sample
location_4 = 'C:/Users/sample t=6 minutes/DSC_0455.NEF' # location of the .NEF image of the sample
location_5 = 'C:/Users/sample t=8 minutes/DSC_0456.NEF' # location of the .NEF image of the sample
location_6 = 'C:/Users/sample t=8 minutes/DSC_0457.NEF' # location of the .NEF image of the sample
location_blank = 'C:/Users/blanco/DSC_0451.NEF' # location of the .NEF image of the capillary with 1,4 butadiol

raw1 = rawpy.imread(location_1)           # opens RAW  sample picture
rgb1 = raw1.postprocess()                  # extracts pixel data
raw2 = rawpy.imread(location_2)           # opens RAW  sample picture
rgb2 = raw2.postprocess()                  # extracts pixel data
raw3 = rawpy.imread(location_3)           # opens RAW  sample picture
rgb3 = raw3.postprocess()                  # extracts pixel data
raw4 = rawpy.imread(location_4)           # opens RAW  sample picture
rgb4 = raw4.postprocess()                  # extracts pixel data
raw5 = rawpy.imread(location_5)           # opens RAW  sample picture
rgb5 = raw5.postprocess()                  # extracts pixel data
raw6 = rawpy.imread(location_6)           # opens RAW  sample picture
rgb6 = raw6.postprocess()                  # extracts pixel data
raw_blank = rawpy.imread(location_blank)  # opens RAW  sample picture
rgb_blank = raw_blank.postprocess()        # extracts pixel data

h_pix = (160)                             # sets the total number of pixel rows
H = (3720/2080)            # divides total number of vertical pixel lines over the first line of the capillary
I = (3720/2300)            # divides total number of vertical pixel lines over the first line of the capillary
J = (3720/2275)            # divides total number of vertical pixel lines over the first line of the capillary
K = (3720/2304)            # divides total number of vertical pixel lines over the first line of the capillary
L = (3720/2305)            # divides total number of vertical pixel lines over the first line of the capillary
M = (3720/2300)            # divides total number of vertical pixel lines over the first line of the capillary
G = (3720/2321)            # divides total number of vertical pixel lines over the first line of the capillary for blank

top_row = int(len(rgb1)/H)      # select the pixel line on the top of the capillary (now set to exactly half of the picture)
height = np.zeros(h_pix)
for i in range(len(height)):    # generate a list of heights (in mm) from 0 to 1
    height[i] = 1 - (i / h_pix)
h = 2000                        # sets left boundary
w = 3000                        # sets right boundary

rgb1_2 = rgb1[top_row1:top_row1 + h_pix,h:w]  # cut tuple in only the pixel matrix
rgb2_2 = rgb2[top_row2:top_row2 + h_pix,h:w]  # cut tuple in only the pixel matrix
rgb3_2 = rgb3[top_row3:top_row3 + h_pix,h:w]  # cut tuple in only the pixel matrix
rgb4_2 = rgb4[top_row4:top_row4 + h_pix,h:w]  # cut tuple in only the pixel matrix
rgb5_2 = rgb5[top_row5:top_row5 + h_pix,h:w]  # cut tuple in only the pixel matrix
rgb6_2 = rgb6[top_row6:top_row6 + h_pix,h:w]  # cut tuple in only the pixel matrix
rgb2_blank = rgb_blank[top_rowb:top_rowb + h_pix,h:w]  # Same for blank              # part 1
```

```
av_abs = np.zeros(h_pix)   # make a list of zeroes in the correct size
c = 2                      # sets the color channel used (0=red,1=green,2=blue)
for i in range(len(av_abs)):        # run a for-loop over each row of pixels
    sum_gr = 0                      # set sum value to zero
    for j in  range(len(rgb1_2[i])): # run a for-loop over each individual pixel in the row
        if rgb1_2[i][j][1]==0:       # quick check if the blank is zero; prevents division by 0 (python error
            rgb1_2[i][j][1] = 1
        if rgb2_blank[i][j][1]==0:   # quick check if the blank is zero; prevents division by 0 (python error)
            rgb2_blank[i][j][1] = 1

        pix_abs = -math.log(rgb1_2[i][j][c]/rgb2_blank[i][j][c] ,10) # calculate the absorbance for the specific pixel (corrects background
for each pixel individually)
```

```python
            sum_gr += pix_abs
        av_abs[i] = sum_gr / len(rgb1_2[i])     # average the absorbance for the row and adds it to the av_abs list

av_abs = np.zeros(h_pix)   # make a list of zeroes in the correct size
c = 2                      # sets the color channel used (0=red,1=green,2=blue)


for i in range(len(av_abs)):             # run a for-loop over each row of pixels
    sum_gr = 0                           # set sum value to zero
    for j in  range(len(rgb1_2[i])):     # run a for-loop over each individual pixel in the row
        if rgb1_2[i][j][1]==0:           # quick check if the blank is zero; prevents division by 0 (python error
            rgb1_2[i][j][1] = 1
        if rgb2_blank[i][j][1]==0:       # quick check if the blank is zero; prevents division by 0 (python error)
            rgb2_blank[i][j][1] = 1

        pix_abs = -math.log(rgb1_2[i][j][c]/rgb2_blank[i][j][c] ,10) # calculate the absorbance for the specific pixel (corrects background
for each pixel individually)
        sum_gr += pix_abs
    av_abs[i] = sum_gr / len(rgb1_2[i])     # average the absorbance for the row and adds it to the av_abs list

for i in range(len(av_abs2)):            # run a for-loop over each row of pixels
    sum_gr = 0                           # set sum value to zero
    for j in  range(len(rgb2_2[i])):     # run a for-loop over each individual pixel in the row
        if rgb1_2[i][j][1]==0:           # quick check if the blank is zero; prevents division by 0 (python error
            rgb1_2[i][j][1] = 1
        if rgb2_blank[i][j][1]==0:       # quick check if the blank is zero; prevents division by 0 (python error)
            rgb2_blank[i][j][1] = 1

        pix_abs2 = -math.log(rgb2_2[i][j][c]/rgb2_blank[i][j][c] ,10) # calculate the absorbance for the specific pixel (corrects background
for each pixel individually)
        sum_gr2 += pix_abs2
    av_abs2[i] = sum_gr2 / len(rgb2_2[i])     # average the absorbance for the row and adds it to the av_abs list

for i in range(len(av_abs3)):            # run a for-loop over each row of pixels
    sum_gr = 0                           # set sum value to zero
    for j in  range(len(rgb3_2[i])):     # run a for-loop over each individual pixel in the row
        if rgb3_2[i][j][1]==0:           # quick check if the blank is zero; prevents division by 0 (python error
            rgb3_2[i][j][1] = 1
        if rgb2_blank[i][j][1]==0:       # quick check if the blank is zero; prevents division by 0 (python error)
            rgb2_blank[i][j][1] = 1

        pix_abs3 = -math.log(rgb3_2[i][j][c]/rgb2_blank[i][j][c] ,10) # calculate the absorbance for the specific pixel (corrects background
for each pixel individually)
        sum_gr3 += pix_abs3
    av_abs3[i] = sum_gr3 / len(rgb3_2[i])     # average the absorbance for the row and adds it to the av_abs list

for i in range(len(av_abs4)):            # run a for-loop over each row of pixels
    sum_gr = 0                           # set sum value to zero
    for j in  range(len(rgb4_2[i])):     # run a for-loop over each individual pixel in the row
        if rgb4_2[i][j][1]==0:           # quick check if the blank is zero; prevents division by 0 (python error
            rgb4_2[i][j][1] = 1
        if rgb2_blank[i][j][1]==0:       # quick check if the blank is zero; prevents division by 0 (python error)
            rgb2_blank[i][j][1] = 1

        pix_abs4 = -math.log(rgb4_2[i][j][c]/rgb2_blank[i][j][c] ,10) # calculate the absorbance for the specific pixel (corrects background
for each pixel individually)
        sum_gr4 += pix_abs4
    av_abs4[i] = sum_gr4 / len(rgb4_2[i])     # average the absorbance for the row and adds it to the av_abs list

for i in range(len(av_abs5)):            # run a for-loop over each row of pixels
    sum_gr = 0                           # set sum value to zero
    for j in  range(len(rgb5_2[i])):     # run a for-loop over each individual pixel in the row
        if rgb5_2[i][j][1]==0:           # quick check if the blank is zero; prevents division by 0 (python error
            rgb5_2[i][j][1] = 1
        if rgb2_blank[i][j][1]==0:       # quick check if the blank is zero; prevents division by 0 (python error)
            rgb2_blank[i][j][1] = 1
```

```
        pix_abs5 = -math.log(rgb5_2[i][j][c]/rgb2_blank[i][j][c] ,10) # calculate the absorbance for the specific pixel (corrects background
for each pixel individually)
        sum_gr5 += pix_abs5
    av_abs5[i] = sum_gr5 / len(rgb5_2[i])     # average the absorbance for the row and adds it to the av_abs list


for i in range(len(av_abs6)):          # run a for-loop over each row of pixels
    sum_gr = 0                         # set sum value to zero
    for j in  range(len(rgb6_2[i])): # run a for-loop over each individual pixel in the row
        if rgb6_2[i][j][1]==0:         # quick check if the blank is zero; prevents division by 0 (python error
            rgb6_2[i][j][1] = 1
        if rgb2_blank[i][j][1]==0:    # quick check if the blank is zero; prevents division by 0 (python error)
            rgb2_blank[i][j][1] = 1

        pix_abs6 = -math.log(rgb6_2[i][j][c]/rgb2_blank[i][j][c] ,10) # calculate the absorbance for the specific pixel (corrects background
for each pixel individually)
        sum_gr6 += pix_abs6
    av_abs6[i] = sum_gr6 / len(rgb6_2[i])     # average the absorbance for the row and adds it to the av_abs list               #part 2
```

```
# plots absorbance profile (optional, this part can be done in excel)
plt.figure(figsize=(6,4))                              # make a figure with size specified (in inches)
plt.subplots_adjust(left=0.10, bottom=0.15, right=0.96, top=0.99, wspace=None, hspace=None) # adjust some variables for alignment
inside the figure
plt.plot(av_abs, height, label = 't=0')    # plots absorbance profile
plt.plot(av_abs2, height, label = 't=2')   # plots absorbance profile
plt.plot(av_abs3, height, label = 't=4')   # plots absorbance profile
plt.plot(av_abs4, height, label = 't=6')   # plots absorbance profile
plt.plot(av_abs5, height, label = 't=8')    # plots absorbance profile
plt.plot(av_abs6, height, label = 't=10')  # plots absorbance profile
plt.ylabel('Height (mm)')                   # axis titles
plt.xlabel('Concentration (A/m)')
plt.ylim([0,1])                             # axis limits
plt.xlim([-0.2,0.30])
plt.grid()                                  # add gridlines to the figure
plt.legend()                                # add legend to the figure
plt.show()                                  # shows figure                                    #part 3
```

Figure F.2: Calculating concentration profile without loop

YIG sample t=0 (left) t= 5 min (center), t=10 min (right)

YIG sample t=15 min (left) t= 20 min (center), t=25 min (right)

YIG sample t=30 min (left) t=35 min (center), t=40 min (right)

YIG sample t=45 min (left) t= 50 min (center), t=55 min (right)

Figure G-1: Image sequence of a YIG sample over 60 minutes over the blue color channel

(see section 4.5)